

Copyright Warning & Restrictions

The copyright law of the United States (Title 17, United States Code) governs the making of photocopies or other reproductions of copyrighted material.

Under certain conditions specified in the law, libraries and archives are authorized to furnish a photocopy or other reproduction. One of these specified conditions is that the photocopy or reproduction is not to be “used for any purpose other than private study, scholarship, or research.” If a user makes a request for, or later uses, a photocopy or reproduction for purposes in excess of “fair use” that user may be liable for copyright infringement,

This institution reserves the right to refuse to accept a copying order if, in its judgment, fulfillment of the order would involve violation of copyright law.

Please Note: The author retains the copyright while the New Jersey Institute of Technology reserves the right to distribute this thesis or dissertation

Printing note: If you do not wish to print this page, then select “Pages from: first page # to: last page #” on the print dialog screen

The Van Houten library has removed some of the personal information and all signatures from the approval page and biographical sketches of theses and dissertations in order to protect the identity of NJIT graduates and faculty.

INFORMATION TO USERS

The most advanced technology has been used to photograph and reproduce this manuscript from the microfilm master. UMI films the text directly from the original or copy submitted. Thus, some thesis and dissertation copies are in typewriter face, while others may be from any type of computer printer.

The quality of this reproduction is dependent upon the quality of the copy submitted. Broken or indistinct print, colored or poor quality illustrations and photographs, print bleedthrough, substandard margins, and improper alignment can adversely affect reproduction.

In the unlikely event that the author did not send UMI a complete manuscript and there are missing pages, these will be noted. Also, if unauthorized copyright material had to be removed, a note will indicate the deletion.

Oversize materials (e.g., maps, drawings, charts) are reproduced by sectioning the original, beginning at the upper left-hand corner and continuing from left to right in equal sections with small overlaps. Each original is also photographed in one exposure and is included in reduced form at the back of the book.

Photographs included in the original manuscript have been reproduced xerographically in this copy. Higher quality 6" x 9" black and white photographic prints are available for any photographs or illustrations appearing in this copy for an additional charge. Contact UMI directly to order.

U·M·I

University Microfilms International
A Bell & Howell Information Company
300 North Zeeb Road, Ann Arbor, MI 48106-1346 USA
313/761-4700 800/521-0600

Order Number 9021163

**Propagation of millimeter wave signals in forests using the
equation of radiative transfer with strong forward scattering
phase functions**

Cho, Nack Yang, D.Eng.Sc.

New Jersey Institute of Technology, 1990

U·M·I
300 N. Zeeb Rd.
Ann Arbor, MI 48106

**Propagation of Millimeter Wave Signals in Forests
Using the Equation of Radiative Transfer
with Strong Forward Scattering Phase Functions**

**By
Nack Y. Cho**

**Dissertation submitted to the Faculty of the Graduate School
of the New Jersey Institute of Technology in partial
fulfillment of the requirements for the degree of
Doctor of Engineering Science
November, 1989**

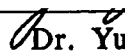
Approval of Dissertation

Title of Dissertation : Propagation of Millimeter Wave Signals in Forests
 Using the Equation of Radiative Transfer
 with Strong Forward Scattering Phase Functions

Name of Candidate : Nack Y. Cho
 Doctor of Engineering Science, 1989

Dissertation and Abstract Approved :

_____	_____
Dr. Gerald M. Whitman	Date

_____	_____
 Dr. Yunjin Kim	Date

_____	_____
Dr. Felix Schwering	Date

_____	_____
Dr. Edip Niver	Date

VITA

Name: Nack Y. Cho

Degree and date to be conferred : D. Eng. Sc., 1990

Secondary education : Seoul Senior High School, Seoul, Korea ;
February, 1974

Collegiate institutions attended	Date	Degree	Date of degree
Seoul National Univ.	3/74 - 2/78	BS(EE)	1978
N.J.I.T.	9/80 - 12/82	MS(EE)	1983
N.J.I.T.	9/86 - 12/89	D.Eng.Sc.(EE)	1990

Major : Electrical Engineering

Publications : "Parametric Inverse Radiative Transfer Using a Strong Forward Model," N. Cho, Y. Kim, G. Whitman, Presented at Benjamin Franklin Symposium, Cherry Hill, NJ, 1989.

"Verification of a Strong Forward Model Using Parametric Inverse Radiative Transfer," N. Cho, Y. Kim, G. Whitman Presented at the IEEE AP-S/URSI Meeting, San Jose, Ca, 1989.

"Time-domain Inverse Scattering Using a Nonlinear Renormalization Technique," Y. Kim, D. Jaggard, N. Cho, to appear in J. of Electromagnetic Waves and Applications, 1989.

"Transients in a Fractal Slab," D. Jaggard, Y. Kim, N. Cho, submitted for publication.

"Time-domain Approach for one-dimensional Inverse Scattering Using a Nonlinear Renormalization technique," presented at the IEEE AP-S/URSI Meeting, Syracuse, NY, 1988

"Transients in a Fractal Slab," Y. Kim, D. Jaggard, N. Cho, presented as Invited Paper at the IEEE AP-S/URSI Meeting, San Jose, Ca, 1989.

"Moment Method Solution of the Time-dependent Transport Equation," G. Whitman, F. Schwering, N. Cho, Proceedings of International Symposium on Antennas and Propagation, pp. 687-690, Kyoto, Japan, 1985.

Positions Held :

**Jan. 1987 - Special Instructor in Electrical Engineering, N.J.I.T.
July 1987**

**June 1985 - Microwave Engineer, RCA Astro Electronics, East
June 1987 Windsor, N.J.**

**Jan. 1983 - Design Engineer, Westinghouse Electric Co. Whippany,
May 1985 N.J.**

**Sept. 1982 - Special Instructor in Electrical Engineering, N.J.I.T.
Dec. 1982**

ABSTRACT

Title of dissertation : Propagation of Millimeter Wave Signals in Forests
 Using the Equation of Radiative Transfer
 with Strong Forward Scattering Phase Functions

Nack Y. Cho, Doctor of Engineering Science, 1989

Dissertation directed by : Dr. Gerald M. Whitman and Dr. Yunjin Kim

A forest is a highly scattering medium at millimeter wave frequencies. The propagation of cw millimeter wave signals in forests has been studied previously, both theoretically and experimentally. Published experimental data verified that continuous wave transmission is possible over lengths of the order of a few hundred meters and that a forest acts to strongly scatter energy in the forward direction. The cw studies yielded the determination of the range dependence, beam broadening effects and depolarization effects of millimeter wave signals in a forest. However, pulse broadening effects, which are of importance particularly in the case of digital signal transmission, remained to be studied. The main purpose of this dissertation is to provide a theory of these effects applicable to the millimeter wave region. A second purpose of the dissertation is to refine the previously developed cw theory by linking it to the experimental cw data by an optimization scheme. In Part I of this study a periodic sequence of gaussian plane wave pulses is assumed to impinge upon a forest half-space. The forest is taken to be statistically homogeneous and to consist of a random distribution of particles which scatter and absorb radiation. A theory of millimeter wave pulse propagation in a forest is developed using the scalar time-dependent equation of radiative transfer. The forest is assumed to be described by a scatter function which consists of a strong narrow forward lobe superimposed over an isotropic background. The power intercepted by a receiving antenna in the forest is computed as a function of path length and travel time. It is demonstrated through numerical computations that the detection of a transmitted signal is

indeed feasible and that pulse broadening occurs at large penetration depths. In Part II a parametric inversion scheme is developed which permits the determination of forest parameters at millimeter wave frequencies. Using the available experimental data for the cw case, the inversion scheme is applied to the time-independent equation of radiative transfer. By initially choosing values for the unknown parameters, and then judiciously varying parameters using an optimization technique similar in concept to "simulated annealing" and requiring that the difference between the experimentally and theoretically determined values of received power be minimal, the desired unknown forest parameters are found. The method appears to provide meaningful parameter characterization of the forest despite the limited available experimental data.

ACKNOWLEDGEMENT

To complete this dissertation I owe a debt of gratitude to several individuals. To begin with, I would like to express my sincere appreciation to my advisors, Dr. Gerald M. Whitman and Dr. Yunjin Kim who guided and inspired me in so many ways. In addition and equally important, I wish to thank Dr. Felix Schwering of the US Army CECOM, Fort Monmouth, N.J. for leading this collaborative research effort and contributing significantly to its theoretical development in Part I. Finally, my wife Susan and both her and my parents who supported and encouraged me for so many years.

TABLE OF CONTENTS

	Page
ABSTRACT	i
ACKNOWLEDGEMENT	iii
TABLE OF CONTENTS	iv
LIST OF TABLES	vi
LIST OF FIGURES	vii
I. Pulsed Millimeter Wave Propagation in Forests using the Time-Dependent Transport Equation with Strong Forward Scatter Profiles	
I.1 Introduction	1
I.2 General Formulation	4
I.3 Strong Forward Diffuse Intensity	11
I.4 Omnidirectional Diffuse Intensity	18
I.5 Power Received by Highly Directive Antenna	24
I.6 Numerical Results for Normal Incidence	29
I.7 Conclusions and Suggestions	34
II. Determination of Forest Parameters using the Capturing Technique and the Time-Independent Transport Equation	
II.1 Introduction	35
II.2 Power Calculations	37
II.3 Experimental Results	41
II.4 Parametric Inversion (Capturing Technique)	45
II.5 Optimization Results	48
II.6 Conclusions and Suggestions	52

APPENDICES	A. Time-Dependent Transport Equation	100
	B. Recursion Relations	104
	C. Narrow Lobe Diffuse Intensity and Power in the Zero Order Approximation	107
	D. Isotropic Background Diffuse Intensity	112
	E. Total Received Power in The First Order Approximation	115
	F. Discussion of Simulated Annealing	119
	G. Computer Programs	123
REFERENCES		138

LIST OF TABLES

	Page
Table 1-1	Summary of parameters for Fig. 1-6 through Fig. 1-30.
	Set A : First order approximation
	Set B : Zero order approximation
	30
Table 2-1	Optimized parameter values for two angular ranges in the one tree case
	50
Table 2-2	Optimized parameter values and their averages
	51

LIST OF FIGURES

	Page
Fig.1-1 Coordinate geometry used in the definition of specific intensity $I(r,t;s)$	55
Fig.1-2 Forest half-space	56
Fig.1-3 Gaussian pulse train	57
Fig.1-4 Triangular basis functions	58
Fig.1-5 Receiving antenna in the forest	59
Fig.1-6 Relative power in dB for $T'=2.$, $z'=1.$, $W=0.75$, $\alpha=0.2$ (first order approximation case)	60
Fig.1-7 Relative power in dB for $T'=2.$, $z'=10.$, $W=0.75$, $\alpha=0.2$ (first order approximation case)	61
Fig.1-8 Relative power in dB for $T'=2.$, $z'=20.$, $W=0.75$, $\alpha=0.2$ (first order approximation case)	62
Fig.1-9 Relative power in dB for $T'=2.$, $z'=30.$, $W=0.75$, $\alpha=0.2$ (first order approximation case)	63
Fig.1-10 Relative power in dB for $T'=2.$, $z'=1.$, $W=0.75$, $\alpha=0.8$ (first order approximation case)	64
Fig.1-11 Relative power in dB for $T'=2.$, $z'=10.$, $W=0.75$, $\alpha=0.8$ (first order approximation case)	65
Fig.1-12 Relative power in dB for $T'=2.$, $z'=20.$, $W=0.75$, $\alpha=0.8$ (first order approximation case)	66
Fig.1-13 Relative power in dB for $T'=2.$, $z'=30.$, $W=0.75$, $\alpha=0.8$ (first order approximation case)	67
Fig.1-14 Relative power in dB for $T'=2.$, $z'=1.$, $W=0.95$, $\alpha=0.2$ (first order approximation case)	68
Fig.1-15 Relative power in dB for $T'=2.$, $z'=10.$, $W=0.95$, $\alpha=0.2$ (first order approximation case)	69
Fig.1-16 Relative power in dB for $T'=2.$, $z'=20.$, $W=0.95$, $\alpha=0.2$ (first order approximation case)	70
Fig.1-17 Relative power in dB for $T'=2.$, $z'=30.$, $W=0.95$, $\alpha=0.2$ (first order approximation case)	71
Fig.1-18 Relative power in dB for $T'=2.$, $z'=1.$, $W=0.95$, $\alpha=0.8$ (first order approximation case)	72

Fig.1-19	Relative power in dB for $T'=2.$, $z'=10.$, $W=0.95$, $\alpha=0.8$ (first order approximation case)	73
Fig.1-20	Relative power in dB for $T'=2.$, $z'=20.$, $W=0.95$, $\alpha=0.8$ (first order approximation case)	74
Fig.1-21	Relative power in dB for $T'=2.$, $z'=30.$, $W=0.95$, $\alpha=0.8$ (first order approximation case)	75
Fig.1-22	Relative power in dB for $T'=10.$, $z'=30.$, $W=0.95$, $\alpha=0.8$ (first order approximation case)	76
Fig.1-23	Relative power in dB for $T'=2.$, $z'=1.$, $W=0.75$, $\alpha=0.2$ (zero order approximation case)	77
Fig.1-24	Relative power in dB for $T'=2.$, $z'=10.$, $W=0.75$, $\alpha=0.2$ (zero order approximation case)	78
Fig.1-25	Relative power in dB for $T'=2.$, $z'=20.$, $W=0.75$, $\alpha=0.2$ (zero order approximation case)	79
Fig.1-26	Relative power in dB for $T'=2.$, $z'=30.$, $W=0.75$, $\alpha=0.2$ (zero order approximation case)	80
Fig.1-27	Relative power in dB for $T'=2.$, $z'=1.$, $W=0.95$, $\alpha=0.8$ (zero order approximation case)	81
Fig.1-28	Relative power in dB for $T'=2.$, $z'=10.$, $W=0.95$, $\alpha=0.8$ (zero order approximation case)	82
Fig.1-29	Relative power in dB for $T'=2.$, $z'=20.$, $W=0.95$, $\alpha=0.8$ (zero order approximation case)	83
Fig.1-30	Relative power in dB for $T'=2.$, $z'=30.$, $W=0.95$, $\alpha=0.8$ (zero order approximation case)	84
Fig.2-1	Numerically calculated data for various z' (0.1, 1.0 and 10.0) with W (0.5) and α (0.2) fixed	85
Fig.2-2	Numerically calculated data for various W (0.5, 0.75 and 0.9) with z' (1.0) and α (0.2) fixed	86
Fig.2-3	Numerically calculated data for various α (0.2, 0.5 and 0.8) with z' (1.0) and W (0.5) fixed	87
Fig.2-4	Geometry of the experiment in a forest	88
Fig.2-5	Experimentally measured power data	89
Fig.2-6	Convergence of the parameter z' during the optimization processing using synthetic data	90

Fig.2-7	Convergence of the parameter W during the optimization processing using synthetic data	91
Fig.2-8	Convergence of the parameter α during the optimization processing using synthetic data	92
Fig.2-9	Total error during a optimization using synthetic data	93
Fig.2-10	Comparison between theoretical and experimental received power (3 tree case)	94
Fig.2-11	Comparison between theoretical and experimental received power (8 tree case)	95
Fig.2-12	Comparison between theoretical and experimental received power (1 tree case)	96
Fig.A1	Differential cylindrical volume element for derivation of transport equation	97
Fig.B1	Local linear coordinate system for evaluation of double integrals	98
Fig.B2	Angles measured in spherical coordinate system	99

I. Pulsed Millimeter Wave Propagation in Forests using the Time-Dependent Transport Equation with Strong Forward Scatter Profiles

I.1 Introduction

The US Army is currently developing millimeter wave radio systems for tactical communication and data transmission purposes. Under battlefield conditions, millimeter wave radios may have to transmit through a forest environment. Transmitters as well as receivers might even have to be placed in a wooded area for camouflage purposes. Recent experimental and theoretical studies [1,2,3] have confirmed the feasibility of millimeter wave communication through such a medium. These studies, however, treated only the time-independent case. Since digital signals most likely will be used, information on pulse broadening and permissible data transmission rate, are needed. To obtain this information and to provide further understanding, this analytical study was undertaken. As a result, a theory of millimeter wave pulse propagation in forests using the scalar time-dependent equation of radiative transfer (transport equation) evolved. The theory takes multiple scattering phenomena into account but ignores the consequences of interference, which is justified by the experimental results provided one is not interested in very local effects.

A periodic sequence of gaussian plane wave pulses is assumed to be incident from free-space into a forest. The forest is characterized as a random distribution of particles which scatter and absorb radiation. To a first approximation, the forest is assumed to be statistically homogeneous, *i.e.*, spatially independent, and to be characterized by

four parameters, two of which are the absorption and scatter cross sections per unit volume, σ_A and σ_s , respectively, whose dimensions are m^{-1} .

On entering the forest, energy gets scattered in all directions. In the millimeter wave region all scatter objects in the forest, be they tree trunks or twigs, have dimensions which are large compared to wavelength. Consequently, the forest can be described by a scatter or phase function that consists of a strong narrow forward lobe superimposed over an isotropic background ; the latter portion accounts for the scattering of energy in all directions. Such a scatter profile was experimentally reported in [2] at the millimeter wave frequency of 57.6 GHz. It is assumed that the scatter function depends only on the angle γ , measured between the incident direction and the scattered direction. The phase function is characterized by two additional parameters, namely, $\Delta\gamma$, the beamwidth of the forward scatter lobe and α , the probability of intensity being scattered in the forward direction. Note that a forest physically consists of a great variety of large and small objects with innumerable random orientations. As such, its true scatter profile is extremely complicated and spatially dependent. Therefore, characterizing the forest by the four constant parameters σ_A , σ_s , $\Delta\gamma$ and α implies a certain averaging process which is assumed without proof.

In transport theory, the basic equation is called the "equation of radiative transfer" or the "transport equation" [4,5,6]. It is an integro-differential equation which is derived from the principle of conservation of energy ; see Appendix A. This equation's dependent variable is called specific intensity $I(r,t;s)$, which is defined at position r at time t as the power per unit area, crossing a surface da

normal to the direction of travel s , per unit solid angle $d\Omega$, *i.e.*, $I(r,t;s) = dP(r,t;s) / dad\Omega$ in units of watts per square meter per steradian; s is a unit vector; see Fig. 1.

In Section I.2, the general scalar time-dependent transport equation is presented. Specific intensity is decomposed into three components, namely, the coherent intensity I_c and two components of incoherent or diffuse intensity I_1 and I_2 . Appropriate boundary conditions are also specified. Equations for I_1 and I_2 are solved in Sections I.3 and I.4, respectively. Section I.5 discusses the power received by a highly directive antenna placed in the forest. Section I.6 presents numerical results. Of particular importance is the depiction of pulse broadening at relatively large penetration depths in the forest. Lastly, Section I.7 gives conclusions and suggestions for further inquiries.

I.2 General Formulation

A plane wave pulse train is assumed to be obliquely incident¹ in the unit vector direction s_p onto a planar interface separating free-space from a statistically homogeneous, strongly forward scattering medium (a forest); see Fig. 2. At the origin $s_p = 0$, the incident signal is taken to be a periodic sequence of gaussian plane wave pulses having an instantaneous Poynting vector magnitude

$$S(0, t) = 2S_p F(0, t) \cos^2 2\pi f_c t, \quad (1-1)$$

where

$$F(0, t) = \frac{a}{\sqrt{\pi}} e^{-(at/T)^2}, \quad -T/2 \leq t \leq T/2 \quad (1-1a)$$

and S_p is essentially the time-averaged power per unit area which flows in the s_p direction in a time period of T seconds. The millimeter wave carrier frequency f_c has a time period $T_c \ll T$. The gaussian envelope function in (1) is normalized such that

$$\frac{1}{T} \int_{-T/2}^{T/2} F(0, t) dt = 1. \quad (1-2)$$

The constant " a " is chosen sufficiently large so that the $F(0, t)$ goes to zero as t approaches $\pm T/2$. The limits of integration in (2) can then be replaced by $\pm \infty$ and the integral evaluated. This is done in Section I.6.

Since the incident plane wave pulse train is an even periodic

¹Two theories will be presented. A zero order solution for oblique incidence and a first order solution for normal incidence. To permit both developments, oblique incidence is initially considered.

function of time t with pulse repetition rate T seconds, it can be represented at $s_p = 0$ by the even Fourier series

$$F(0,t) = -\frac{1}{2} b_0 + \sum_{\nu=1}^{\infty} b_{\nu} \cos \nu \omega t = \Re \left[\sum_{\nu=0}^{\infty} F_{\nu}^{\circ} e^{j\nu \omega t} \right], \quad (1-3)$$

where

$$\omega = \frac{2\pi}{T}, \quad b_{\nu} = \frac{2}{T} \int_{-T/2}^{T/2} F(0,t) \cos \nu \omega t \, dt, \quad (1-3a)$$

" \Re " stands for "the real part of", F_{ν}° is a real constant and ω is angular frequency. By choosing α sufficiently large so that the gaussian function in (1a) goes to zero as t approaches $\pm T/2$, the limits of integration in (3a) can be replaced by $\pm \infty$ to yield

$$F_{\nu}^{\circ} = \frac{\varepsilon_{\nu} b_{\nu}}{2} = \varepsilon_{\nu} e^{-(\pi \nu / \alpha)^2}, \quad \varepsilon_{\nu} = \begin{cases} 1, & \nu = 0 \\ 2, & \nu \neq 0 \end{cases}. \quad (1-3b)$$

Considering only that portion of the signal in the baseband, the intensity of the incident plane wave pulse train, in unit of watts per square meter per steradian, which travels in free-space at the speed of light c in the unit vector direction s , is given by the expression

$$I_p = S_p F(t - s \cdot r/c) \delta(s - s_p), \quad (1-4)$$

where

$$F(t - s \cdot r/c) = \Re \sum_{\nu=0}^{\infty} F_{\nu}^{\circ} e^{j\nu \omega(t-s \cdot r/c)}, \quad (1-4a)$$

$$\delta(s-s_p) = \delta(\theta-\theta_p) \delta(\phi-\phi_p) / \sin \theta = \delta(\mu-\mu_p) \delta(\phi-\phi_p) \quad (1-4b)$$

and

$$\mu = \cos\theta, \quad \mu_p = \cos\theta_p. \quad (1-4c)$$

Note that $z = s \cos\theta$ for planar geometry. In (4), $\delta(x)$ is a Dirac delta function and angles (θ, ϕ) represent an arbitrary direction in a spherical coordinate system while (θ_p, ϕ_p) are used to designate the direction of the incident radiation.

Specific intensity is governed by the equation of radiative transfer, which for planar geometries takes the form

$$-\frac{1}{c} \frac{\partial I}{\partial t} + \cos\theta \frac{\partial I}{\partial z} + \sigma_t I = \frac{\sigma_s}{4\pi} \iint p(s, s') I(z, t; \theta', \phi') \sin\theta' d\theta' d\phi'. \quad (1-5)$$

In the derivation of (5) in Appendix A, the medium is assumed to be free of dispersion. Since at millimeter wave frequencies all forest parameters are assumed to be independent of frequency, (5) applies. The parameter $\sigma_t = \sigma_A + \sigma_s$ is the total or extinction cross-section per unit volume and $p(s, s')$ is the scatter or phase function. It is assumed to depend only on γ and to be given by

$$p(\gamma) = p_1(\gamma) + p_0, \quad (1-5a)$$

where

$$p_0 = 1 - \alpha, \quad p_1(\gamma) = \alpha q(\gamma) = \alpha \left(\frac{2}{\Delta\gamma}\right)^2 e^{-(\frac{\gamma}{\Delta\gamma})^2}, \quad \Delta\gamma \ll \pi, \quad (1-5b)$$

with normalization

$$\frac{1}{4\pi} \iint p(s, s') d\Omega' = 1, \quad d\Omega' = \sin\theta' d\theta' d\phi'. \quad (1-5c)$$

The angle γ is measured between the incident direction s' or equivalently (θ', ϕ') and the scatter direction s or (θ, ϕ) . It is specified by the relation

$$\cos\gamma = \mathbf{s} \cdot \mathbf{s}' = \cos(\phi - \phi')\sin\theta\sin\theta' + \cos\theta\cos\theta' . \quad (1-5d)$$

The differential solid angle $d\Omega$ about the scatter direction \mathbf{s} is depicted in Fig 1. The phase function in (5a,b) consists of a narrow gaussian shaped lobe (p_1) superimposed on a uniform omnidirection background (p_0). The parameter $\Delta\gamma$ is the beamwidth of the forward lobe and α is the ratio of the probability of intensity being scattered in the forward direction to the probability of intensity being scattered in all directions (which is unity).

Introducing normalized variables

$$z' = \sigma_t z , \quad t' = \sigma_t c t \quad (1-6a)$$

and the parameter albedo

$$W = \sigma_s / \sigma_t , \quad (1-6b)$$

allows us to rewrite (5), using $\mu = \cos\theta$, as

$$\frac{\partial I}{\partial t'} + \mu \frac{\partial I}{\partial z'} + I = \frac{W}{4\pi} \int_0^\pi \int_0^{2\pi} p(\gamma) I(z', t'; \mu', \phi') d\mu' d\phi', \quad z' \geq 0. \quad (1-7)$$

The intensity I has two components, namely, the coherent intensity I_c and the incoherent or diffuse intensity I_d :

$$I = I_c + I_d . \quad (1-8)$$

Substituting (8) into (7) and defining the coherent component to satisfy the equation

$$\frac{\partial I_c}{\partial t'} + \mu \frac{\partial I_c}{\partial z'} + I_c = 0 \quad (1-9)$$

yield for the incoherent component the equation

$$\frac{\partial I_d}{\partial t'} + \mu \frac{\partial I_d}{\partial z'} + I_d = -\frac{W}{4\pi} \iint_{\mathcal{H}} p(\gamma) (I_d + I_c) d\mu' d\phi' . \quad (1-10)$$

To solve (9) and (10) it is convenient to introduce Fourier series representations for the incident, coherent and diffuse intensities

$$I_i(z', t'; \mu, \phi) = \Re \left[\sum_{v=-\infty}^{\infty} I_{iv}(z'; \mu, \phi) e^{jv\omega' t'} \right] , \quad i = p, c, d , \quad (1-11)$$

where

$$T' = \sigma_i cT, \quad \omega' = 2\pi / T'. \quad (1-11a)$$

Note that because equation (5) is linear, the frequency parameter in (11) is the normalized version of the angular frequency encountered in (4a). Observe also that (9) dictates that I_c depends only on z' , t' and μ .

Substituting (11) into (9) and (10) yields the two equations

$$jv\omega' I_{cv} + \mu \frac{dI_{cv}}{dz'} + I_{cv} = 0 , \quad (1-12a)$$

$$jv\omega' I_{dv} + \mu \frac{dI_{dv}}{dz'} + I_{dv} = -\frac{W}{4\pi} \iint_{\mathcal{H}} p(\gamma) (I_{dv} + I_{cv}) d\mu' d\phi' . \quad (1-12b)$$

Solving (12a) by direct integration yields

$$I_{cv}(z'; \mu) = A_{cv} e^{-(1+jv\omega')z'/\mu} . \quad (1-13)$$

To determine the unknown constant A_{cv} , recognize that the incoherent intensity I_d is a consequence of multiple scattering effects in the forest. Since the scatter radiation is generated inside the forest and, therefore, can only leave the forest at $z' = 0$, the only intensity which flows in the same direction as the incident radiation at $s = 0$ or $z' = 0$ is I_c . Hence, the boundary conditions which must be satisfied are

$$I_c = I_p, I_d = 0 \quad \text{at } z' = 0 \quad \text{for } 0 \leq \mu \leq 1. \quad (1-14a)$$

In addition, since the medium (the forest) is lossy ($\sigma_A \neq 0$), the intensity must vanish at infinity, *i.e.*,

$$I_c \rightarrow 0, I_d \rightarrow 0 \quad \text{as } z' \rightarrow \infty. \quad (1-14b)$$

From (4),(11),(13),(14a) and using the normalized coordinates introduced in (6a), it follows that

$$A_{cv} = S_p F_v^0 \delta(\mu - \mu_p) \delta(\phi - \phi_p). \quad (1-15)$$

Hence, the time-dependent coherent intensity becomes

$$I_c(z', t'; \mu, \phi) = S_p F(t' - z'/\mu_p) e^{-z'/\mu_p} \delta(\mu - \mu_p) \delta(\phi - \phi_p), \quad (1-16)$$

where

$$F(t' - z'/\mu_p) = \Re \sum_{v=0}^{\infty} F_v(z'/\mu_p) e^{jv\omega' t'} \quad (1-16a)$$

with

$$F_v(z'/\mu_p) = F_v^0 e^{-jv\omega' z'/\mu_p}. \quad (1-16b)$$

Physically, the coherent intensity describes the attenuation of the intensity in the forest due to absorption and outscattering along the direction of the entering signal.

After using the coherent intensity I_{cv} found above in (13) and (15), the equation for the diffuse intensity (12b) is solved by first separating the diffuse intensity into two parts [3]

$$I_{dv}(z'; \mu, \phi) = I_{1v}(z'; \mu, \phi) + I_{2v}(z'; \mu), \quad (1-17)$$

such that the "strong forward" diffuse intensity I_{1v} , which depends on

z' , μ and ϕ , satisfies

$$\mu \frac{dI_{1v}}{dz'} + (1 + jv\omega') I_{1v} = \frac{W\alpha}{4\pi} \int_0^\pi \int_0^{2\pi} q(\gamma) I_{1v} d\mu' d\phi' + \frac{S}{4\pi} \frac{W\alpha}{p} F_v(z'/\mu_p) e^{-z'/\mu_p} q(\gamma_p) \quad (1-18)$$

and the "omnidirectional" diffuse intensity I_{2v} , which does not have a preference direction in the scattering process, satisfies

$$\begin{aligned} \mu \frac{dI_{2v}}{dz'} + (1 + jv\omega') I_{2v} = & \frac{W\alpha}{4\pi} \int_0^\pi \int_0^{2\pi} q(\gamma) I_{2v} d\mu' d\phi' \\ & + \frac{W(1-\alpha)}{4\pi} \int_0^\pi \int_0^{2\pi} (I_{1v} + I_{2v}) d\mu' d\phi' + \frac{S}{4\pi} \frac{W(1-\alpha)}{p} F_v(z'/\mu_p) e^{-z'/\mu_p} \end{aligned} \quad (1-19)$$

where

$$\cos\gamma = \cos(\phi - \phi') [(1 - \mu^2)(1 - \mu'^2)]^{1/2} + \mu\mu' \quad , \quad (1-19a)$$

$$\cos\gamma_p = \cos(\phi - \phi_p) [(1 - \mu^2)(1 - \mu_p^2)]^{1/2} + \mu\mu_p \quad . \quad (1-19b)$$

For convenience, I_1 and its transform I_{1v} are designated "strong forward" diffuse intensities while I_2 and its transform I_{2v} are called "omnidirectional" diffuse intensities. Their designations are inferred from the defining equations which determine the significant nature of the scattering process. As can be seen from (18), I_{1v} is generated by scattering into the strong forward lobe $q(\gamma)$ of the phase function. Meanwhile, I_{2v} , as defined by (19), is primarily generated by scattering into the isotropic background portion of the scatter function, namely, $p_0 = 1 - \alpha$. To satisfy (14), I_{1v} and I_{2v} are taken to obey the boundary conditions

$$I_{1v} = 0, I_{2v} = 0 \quad \text{for } z' = 0, 0 \leq \mu \leq 1 \quad (1-20a)$$

$$I_{1v} \rightarrow 0, I_{2v} \rightarrow 0 \quad \text{as } z' \rightarrow \infty \quad . \quad (1-20b)$$

I.3 Strong Forward Diffuse Intensity

To determine the strong forward diffuse intensity I_1 , the solution to (18) for I_{10} is needed. To simplify the analysis without loss of physical understanding, the normal incidence case is considered, *i.e.*, $\mu_p = \cos\theta_p = 1$. Since scattering in the forest takes place symmetrically about the forward direction $\theta = 0^\circ$, I_{10} is independent of ϕ . Furthermore, because the scatter profile is characterized by a strong forward lobe $q(\gamma)$, scattering takes place essentially in a small angular domain about the θ equal to zero direction; hence, a perturbation solution to (18) for I_{10} will be developed which remains valid only for small values of θ different from zero and limited penetration depths; the $\theta = 0^\circ$ or zero order solution will be shown to agree with results derived by an alternative method which involves setting $\mu = 1$ in (18); see Appendix C.

Let

$$I_{10}(z'; \mu) = S_p F_p^0 e^{-(1+j\nu\omega')z'} g_v(z'; \mu) \quad (1-21)$$

Substitution of (21) into (18) and (20) yields

$$\begin{aligned} (1+j\nu\omega')(1-\mu)g_v(z'; \mu) + \mu \frac{dg_v(z'; \mu)}{dz'} \\ = \frac{W\alpha}{4\pi} \int_0^{2\pi} \int_{-1}^1 q(\gamma) g_v(z'; \mu') d\mu' d\phi' + \frac{W\alpha}{4\pi} q(\gamma_p) \end{aligned} \quad (1-22)$$

where $\gamma = \theta$ and $\gamma_p = \theta_p$, subject to boundary conditions

$$g_v(0; \mu) = 0 \quad \text{and} \quad g_v(z'; \mu) e^{-z'} \rightarrow 0 \quad \text{for } z' \rightarrow \infty. \quad (1-23)$$

Assume the series expansion

$$g_v(z'; \mu) = \sum_{m=1}^M a_{v,m}(\mu) z'^m, \quad M \text{ large}. \quad (1-24)$$

This ansatz satisfies both boundary conditions in (23). Substituting (24) into (22) and setting the coefficients of all powers z'^m to zero yield the following explicit equations for the coefficients $a_{v,m}(\mu)$ which can be solved in sequence.

$$\begin{aligned} z'^0 : \quad \mu a_{v,1} &= -\frac{W\alpha}{4\pi} q(\gamma) \\ &\vdots \\ &\vdots \end{aligned} \quad (1-25)$$

$$z'^m : (1+jv\omega')(1-\mu)a_{v,m} + (m+1)\mu a_{v,m+1} = -\frac{W\alpha}{4\pi} \int_0^{2\pi} \int_0^1 q(\gamma) a_{v,m}(\mu') d\mu' d\phi'.$$

$$m = 1, 2, \dots, M-1$$

By adding and subtracting appropriate factors, the above equations can be rewritten as

$$\begin{aligned} a_{v,1} &= -\frac{W\alpha}{4\pi} q(\gamma) + (1-\mu)a_{v,1} \\ &\vdots \\ &\vdots \end{aligned} \quad (1-26)$$

$$(m+1)a_{v,m+1} = \frac{W\alpha}{4\pi} \int_0^{2\pi} \int_0^1 q(\gamma) a_{v,m}(\mu') d\mu' d\phi' + (1-\mu)[(m+1)a_{v,m+1} - (1+jv\omega')a_{v,m}]$$

$$m = 1, 2, \dots, M-1$$

Note that $(1-\mu)$ is a small parameter.

In Appendix B, two recursion relations are derived; for $\gamma = \theta$ these are

$$\frac{1}{4\pi} \int_0^{2\pi} \int_0^\pi q(\gamma) q_m(\theta') \sin\theta' d\theta' d\phi' = q_{m+1}(\theta) \quad (1-27a)$$

and

$$\frac{1}{4\pi} \int_0^{2\pi} \int_0^\pi q(\gamma) q_m(\theta') \theta'^2 \sin\theta' d\theta' d\phi' = \frac{m}{m+1} (\Delta\gamma^2 + \frac{m}{m+1} \theta^2) q_{m+1}(\theta). \quad (1-27b)$$

Making use of (27) and setting $\mu = 1$ permits the system of equations (26) to be written for the zero order approximation as

$$a_{v,m}^0 = \frac{(W\alpha)^m}{4\pi m!} q_m(\gamma) \quad , \quad m = 1, 2, \dots, M \quad , \quad (1-28)$$

where $q(\gamma) = q_1(\gamma)$, $\gamma = \theta$, and

$$q(\gamma) = \frac{4}{\Delta\gamma^2} e^{-\left(\frac{\gamma}{\Delta\gamma}\right)^2} , \quad q_m(\gamma) = \frac{4}{m\Delta\gamma^2} e^{-\frac{1}{m}\left(\frac{\gamma}{\Delta\gamma}\right)^2} . \quad (1-29)$$

A first order solution, assuming $(1 - \mu)$ is small, is obtained by inserting the above zero order solution into the right hand side of (26). This yields

$$\begin{aligned} a_{v,1}^1 &= \frac{W\alpha}{4\pi} q(\gamma) + (1-\mu) \frac{W\alpha}{4\pi} q_1(\gamma) = \frac{W\alpha}{4\pi} (2-\mu) q_1(\gamma) \\ &\vdots \\ &\vdots \end{aligned} \quad (1-30)$$

$$a_{v,m+1}^1 = \frac{1}{4\pi} \frac{W\alpha}{m+1} \int_0^{2\pi} \int_0^\pi q(\gamma) a_{v,m}^1 d\mu' d\phi' + (1-\mu) \left[a_{v,m+1}^0 - \frac{1}{m+1} (1+jv\omega') a_{v,m}^0 \right] ,$$

$$m = 1, 2, \dots, M-1.$$

Integrals in (30) are evaluated by approximating $(1-\mu)$ by $\theta^2/2$ since θ is small and by using the recursion relations (27). Hence,

$$a_{v,1}^1 = \frac{W\alpha}{4\pi} (2-\mu) q_1(\gamma) \quad (1-31a)$$

$$\begin{aligned} a_{v,2}^1 &= \frac{1}{4\pi} \frac{(W\alpha)^2}{2!} \left\{ \frac{1}{4\pi} \iint q(\gamma) [q_1(\theta') + \frac{1}{2} \theta'^2 q_1(\theta')] \sin\theta' d\theta' d\phi' \right\} \\ &\quad + \frac{1}{4\pi} \frac{(W\alpha)^2}{2!} (1-\mu) q_2(\theta) - \frac{1}{4\pi} \frac{W\alpha}{2!} (1+jv\omega')(1-\mu) q_1(\theta) \\ &= \frac{1}{4\pi} \frac{(W\alpha)^2}{2!} \left[1 + \frac{1}{4} \Delta\gamma^2 + \frac{5}{4} (1-\mu) \right] q_2(\theta) - \frac{1}{4\pi} \frac{W\alpha}{2!} (1+jv\omega')(1-\mu) q_1(\theta) \end{aligned} \quad (1-31b)$$

$$\begin{aligned} a_{v,3}^1 &= \frac{1}{4\pi} \frac{(W\alpha)^3}{3!} \left\{ \frac{1}{4\pi} \iint q(\gamma) \left[1 + \frac{1}{4} \Delta\gamma^2 + \frac{5}{8} \theta'^2 \right] q_2(\theta') \sin\theta' d\theta' d\phi' \right\} \\ &\quad - \frac{1}{4\pi} \frac{(W\alpha)^2}{3!} (1+jv\omega') \left\{ \frac{1}{4\pi} \iint q(\gamma) - \frac{1}{2} \theta'^2 q_1(\theta') \sin\theta' d\theta' d\phi' \right\} \\ &\quad + \frac{1}{4\pi} \frac{(W\alpha)^3}{3!} (1-\mu) q_3(\theta) - \frac{1}{4\pi} \frac{(W\alpha)^2}{3!} (1+jv\omega')(1-\mu) q_2(\theta) \\ &= \frac{(W\alpha)^3}{4\pi 3!} \left[1 + \frac{2}{3} \Delta\gamma^2 + \frac{14}{9} (1-\mu) \right] q_3(\theta) - \frac{(W\alpha)^2}{4\pi 3!} (1+jv\omega') \left[\frac{1}{4} \Delta\gamma^2 + \frac{5}{4} (1-\mu) \right] q_2(\theta) \end{aligned} \quad (1-31c)$$

·
·
·

From (31), the (m) and (m+1) terms are inferred to be

$$a_{v,m}^1 = \frac{(W\alpha)^m}{4\pi m!} \left[1 + A_m \Delta\gamma^2 + B_m (1-\mu) \right] q_m(\theta) - \frac{(W\alpha)^{m-1}}{4\pi m!} (1+jv\omega') \left[C_m \Delta\gamma^2 + D_m (1-\mu) \right] q_{m-1}(\theta) \quad (1-32a)$$

and

$$\begin{aligned}
a_{v,m+1}^1 = & \frac{(W\alpha)^{m+1}}{4\pi(m+1)!} \left\{ \frac{1}{4\pi} \int_0^{2\pi} \int_0^\pi q(\gamma) \left[1 + A_m \Delta \gamma^2 + \frac{B_m}{2} \theta'^2 \right] q_m(\theta') \sin \theta' d\theta' d\phi' \right\} \\
& - \frac{(W\alpha)^m}{4\pi(m+1)!} (1+jv\omega') \left\{ \frac{1}{4\pi} \int_0^{2\pi} \int_0^\pi q(\gamma) \left[C_m \Delta \gamma^2 + \frac{D_m}{2} \theta'^2 \right] q_{m-1}(\theta') \sin \theta' d\theta' d\phi' \right\} \\
& + \frac{(W\alpha)^{m+1}}{4\pi(m+1)!} (1-\mu) q_{m+1}(\theta) - \frac{(W\alpha)^m}{4\pi(m+1)!} (1+jv\omega') (1-\mu) q_m(\theta) , (1-32b)
\end{aligned}$$

where $1 - \mu \approx \theta^2/2$ is used in the integrands and A_m , B_m , C_m and D_m remain to be determined. Evaluating the integrals in (32a) using the recursion relations (27) yields

$$\begin{aligned}
a_{v,m+1}^1 = & \frac{(W\alpha)^{m+1}}{4\pi(m+1)!} \left[1 + \left(A_m + \frac{1}{2} \frac{m}{m+1} B_m \right) \Delta \gamma^2 + \left(1 + \frac{m^2}{(m+1)^2} B_m \right) (1-\mu) \right] q_{m+1}(\theta) \\
& - \frac{(W\alpha)^m}{4\pi(m+1)!} (1+jv\omega') \left[\left(C_m + \frac{1}{2} \frac{m-1}{m} D_m \right) \Delta \gamma^2 + \left(1 + \frac{(m-1)^2}{m^2} D_m \right) (1-\mu) \right] q_m(\theta) .
\end{aligned} \quad (1-33)$$

Comparing (32a) with (33), it follows that

$$A_{m+1} = A_m + \frac{1}{2} \frac{m}{m+1} B_m \quad (1-34a)$$

$$B_{m+1} = 1 + \frac{m^2}{(m+1)^2} B_m \quad (1-34b)$$

$$C_{m+1} = C_m + \frac{1}{2} \frac{m-1}{m} D_m \quad (1-34c)$$

$$D_{m+1} = 1 + \frac{(m-1)^2}{m^2} D_m . \quad (1-34d)$$

Comparing (34a) to (34c) and (34b) to (34d) result in

$$C_{m+1} = A_m \quad \text{and} \quad D_{m+1} = B_m . \quad (1-35)$$

Making use of (34) in the comparison of (32a) to the first equation in (31a) gives $A_1 = 0$, $B_1 = 1$, $C_1 = 0$ and $D_1 = 0$. Recursion formulas (34) then show that

$$A_m = \frac{1}{6} \sum_{k=1}^m (k - \frac{1}{2}) - \frac{1}{12} = \frac{1}{12} (m^2 - 1) \quad (1-36a)$$

and

$$B_m = \frac{1}{m^2} \sum_{k=1}^m k^2 = \frac{1}{6} \frac{m+1}{m} (2m+1) \quad (1-36b)$$

Hence, (32a) becomes

$$\begin{aligned} a_{v,m}^1 = & \frac{(W\alpha)^m}{4\pi m!} \left[1 + \frac{1}{12} (m^2 - 1) \Delta \gamma^2 + \frac{1}{6} \frac{m+1}{m} (2m+1)(1-\mu) \right] q_m(\theta) \\ & - \frac{(W\alpha)^{m-1}}{4\pi m!} (1+j\nu\omega') \left[\frac{1}{12} [(m-1)^2 - 1] \Delta \gamma^2 + \frac{1}{6} \frac{m}{m-1} (2m-1)(1-\mu) \right] q_{m-1}(\theta) . \end{aligned} \quad (1-37)$$

To first approximation, (24) thus can be expressed as

$$g_v(z'; \mu) = \frac{1}{4\pi} \sum_{m=1}^M \frac{(W\alpha z')^m}{m!} q_m(\theta) \left\{ 1 + \xi_m(\theta) \left[1 - \frac{z'}{m+1} (1+j\nu\omega') \right] \right\} \quad (1-38)$$

denoting

$$\xi_m(\theta) = \frac{1}{6} \left[(m^2 - 1) \frac{\Delta \gamma^2}{2} + \frac{m+1}{m} (2m+1)(1-\mu) \right] . \quad (1-38a)$$

Because of the factor $z'^m/m!$, it is anticipated that the series in (38) exhibits a maximum value at $z' \approx M$; hence, to ensure convergence M ought

to be chosen larger than z' .

By substituting (21) and (38) into (11), the strong forward diffuse intensity $I_1(z', t'; \mu)$ is finally obtained as

$$I_1(z', t'; \mu) = \Re \left[\sum_{v=0}^{\infty} I_{1v} e^{jv\omega' t'} \right] \quad (1-39a)$$

$$= \Re \left[\sum_{v=0}^{\infty} \frac{S_p F_v^0}{4\pi} e^{jv\omega' (t'-z')} e^{-z'} \sum_{m=1}^M \frac{(W\alpha z')^m}{m!} q_m(\theta) \cdot \left\{ 1 + \xi_m(\theta) \left[1 - \frac{z'}{m+1} (1+jv\omega') \right] \right\} \right] \quad (1-39b)$$

Rewriting this expression using (4a) gives

$$I_1(z', t'; \mu) = \frac{S_p}{4\pi} F(t'-z') e^{-z'} \sum_{m=1}^M \frac{(W\alpha z')^m}{m!} q_m(\theta) (1 + \xi_m(\theta)) - \frac{S_p}{4\pi} [F(t'-z') + F'(t'-z')] e^{-z'} \frac{1}{W\alpha} \sum_{m=1}^{M-1} \frac{(W\alpha z')^{m+1}}{(m+1)!} q_m(\theta) \xi_m(\theta), \quad (1-40)$$

where $F(t'-z')$ is the undistorted normally incident plane wave gaussian pulse (see (4)) and $F'(t'-z')$ is its first derivative with respect to time t' . Because of the appearance of the derivative term, pulse broadening occurs, which is observable when the term $(W\alpha z')$ is large. Hence, an input signal which sharply rises and falls will exhibit stronger pulse broadening.

An alternative analytic method based on [3] was used to find the zero order solution for the diffuse intensity I_1 . This solution agrees with (39) when $\xi_m(\theta)$ is set to zero; see Appendix C for details.

I.4 Omnidirectional Diffuse Intensity

The diffuse intensity I_{2v} , defined in (19) is primarily determined by the isotropic background portion of the scatter function, namely, $p_0 = 1 - \alpha$. This becomes more evident once the first integral on the right hand side of (19) is evaluated by approximating the narrow peaking function $q(\gamma)$ by a delta function in obtaining the following simpler equation for I_{2v} (see Appendix D for details)

$$\mu \frac{dI_{2v}}{d\tau_v} + I_{2v} = \frac{W_v}{2} \int_{-1}^1 I_{2v} d\mu' + \frac{S F_0^0 W_v}{4\pi} e^{-\tau_v/\mu_p}, \quad (1-41)$$

where

$$\tau_v = (1 + jv\omega' - W\alpha)z', \quad W_v = W(1 - \alpha)/(1 + jv\omega' - W\alpha), \quad (1-41a)$$

and boundary conditions (20) become

$$I_{2v} = 0 \quad \text{at} \quad \tau_v = 0, \quad 0 \leq \mu \leq 1 \quad (1-42a)$$

$$I_{2v} \rightarrow 0 \quad \text{as} \quad \tau_v \rightarrow \infty. \quad (1-42b)$$

Note that (41) has the same form as the time-independent transport equation for isotropic scattering except that W_v and τ_v are now complex. Hence, I_{2v} is expected to have a broad directional angular spectrum.

To solve (41) subject to boundary conditions (42), a number of solution methods are available in the literature for the time-independent isotropic transport equation in planar geometries [3-7]. The method of moments is used here [3,7].

Let $I_{2\nu}$ be represented by the following truncated series expansion with unknown expansion coefficients $I_n(\tau_\nu)$ and overlapping triangular bases functions $f_n(\mu)$

$$I_{2\nu}(\tau_\nu; \mu) = \sum_{n=0}^N I_n(\tau_\nu) f_n(\mu) \quad , \quad (1-43)$$

where

$$f_n(\mu) = \left\{ \begin{array}{ll} 0 & , \quad -1 \leq \mu \leq \mu_{n-1} \\ (\mu - \mu_{n-1}) / (\mu_n - \mu_{n-1}) & , \quad \mu_{n-1} \leq \mu \leq \mu_n \\ (\mu - \mu_{n+1}) / (\mu_n - \mu_{n+1}) & , \quad \mu_n \leq \mu \leq \mu_{n+1} \\ 0 & , \quad \mu_{n+1} \leq \mu \leq 1 \end{array} \right\} \quad , \quad n \neq 0, N, \quad (1-43a)$$

while boundary values, $f_0(\mu)$ and $f_N(\mu)$ have the shape of half-triangles

$$f_0(\mu) = \left\{ \begin{array}{ll} (\mu_1 - \mu) / (\mu_1 + 1) & , \quad -1 \leq \mu \leq \mu_1 \\ 0 & , \quad \mu_1 \leq \mu \leq +1 \end{array} \right\} \quad , \quad n = 0 \quad (1-43b)$$

$$f_N(\mu) = \left\{ \begin{array}{ll} 0 & , \quad -1 \leq \mu \leq \mu_{N-1} \\ (\mu - \mu_{N-1}) / (1 - \mu_{N-1}) & , \quad \mu_{N-1} \leq \mu \leq +1 \end{array} \right\} \quad , \quad n = N$$

and

$$\mu_n = \cos(1 - \frac{n}{N})\pi = -\cos(-\frac{n}{N}\pi), \quad n=0,1,\dots,N \quad . \quad (1-43c)$$

The functions $f_n(\mu)$ are shown in Fig. 4 for N assumed to be odd. With $f_n(\mu)$ defined as above, the diffuse intensity $I_{2\nu}(\tau_\nu; \mu)$ is given by the expansion coefficient at $\mu = \mu_n$, i.e., $I_{2\nu}(\tau_\nu; \mu_n) = I_n(\tau_\nu) f_n(\mu_n) = I_n(\tau_\nu)$ and at a value of μ in the interval $\mu_n \leq \mu \leq \mu_{n+1}$ by $I_{2\nu}(\tau_\nu; \mu) = I_n(\tau_\nu) f_n(\mu) + I_{n+1}(\tau_\nu) f_{n+1}(\mu)$.

Substituting (43) into (41) and restricting scatter angles to those specified by the relationships $\mu = \mu_n$, $n = 0, \dots, N$, give the following

system of $(N+1)$ equations for $(N+1)$ unknown expansion coefficients I_n

$$\mu_n \frac{dI_n}{d\tau_v} + I_n = -\frac{W_v}{2} \sum_{m=0}^N I_m P_m + \frac{W_v S_p F_v^0}{4\pi} e^{-\tau_v/\mu_p}, \quad n = 0, 1, 2, \dots, N, \quad (1-44)$$

where

$$P_m = \int_{-1}^{+1} f_m(\mu) d\mu = \begin{cases} (\mu_{m+1} - \mu_{m-1})/2, & m = 1, \dots, N-1 \\ (1 + \mu_1)/2 = (1 - \mu_{N-1})/2, & m = 0, N \end{cases} \quad (1-44a)$$

Using (43), boundary conditions (42) become

$$\sum_{n=0}^N I_n(0) f_n(\mu) = 0, \quad 0 \leq \mu \leq 1, \quad (1-45a)$$

and

$$\lim_{\tau_v \rightarrow \infty} \sum_{n=0}^N I_n(\tau_v) f_n(\mu) = 0. \quad (1-45b)$$

At values of $\mu = \mu_n$ such that $0 \leq \mu_n \leq 1$, (45a) reduces to

$$I_n(0) = 0, \quad n = (N+1)/2, (N+3)/2, \dots, N \quad (1-46a)$$

and (45b) becomes

$$\lim_{\tau_v \rightarrow \infty} \sum_{n=0}^N I_n(\tau_v) = 0. \quad (1-46b)$$

To solve (44) subject to boundary conditions (46) requires homogeneous and particular solutions.

A. Homogeneous Solution

The homogeneous solution to (44) is derived from the equation

$$\mu_n \frac{dI_n^h}{d\tau_v} + I_n^h = \frac{W_v}{2} \sum_{m=0}^N I_m^h P_m . \quad (1-47)$$

Assume

$$I_n^h(\tau_v) = A_{v_n}^h e^{-\tau_v/s_v} , \quad (1-48)$$

where $A_{v_n}^h$ is a complex constant which depends on n and v . Using (48), (47) becomes

$$A_{v_n}^h \left[-\frac{\mu_n}{s_v} + 1 \right] = -\frac{W_v}{2} \sum_{m=0}^N A_{v_m}^h P_m . \quad (1-49)$$

Setting the right hand side of (49) equal to Q_v , a quantity which is not a function of n , gives

$$A_{v_n}^h = \frac{Q_v}{1 - \mu_n / s_v} \quad (1-50a)$$

with

$$Q_v = -\frac{W_v}{2} \sum_{m=0}^N A_{v_m}^h P_m . \quad (1-50b)$$

Substituting (50a) into (50b) and canceling Q_v yield the eigenvalue equation

$$1 - \frac{W_v}{2} \sum_{m=0}^N \frac{P_m}{1 - \mu_m / s_v} = 0 . \quad (1-51)$$

Since (51) is a polynomial in s_v of order $(N+1)$, there are $(N+1)$ complex roots or eigenvalues s_{vk} , $k = 0, 1, \dots, N$, for each value of v . Using $\mu_{N-m} = -\mu_m$ and $P_{N-m} = P_m$, (51) can be shown to reduce to the simpler eigenvalue equation

$$1 - W_v \sum_{m=\frac{(N+1)}{2}}^N \frac{P_m}{1 - (\mu_m/s_v)^2} = 0. \quad (1-52)$$

This is a polynomial in s_v^2 of order $(N+1)/2$ and hence has $(N+1)/2$ complex roots or eigenvalues (s_{vk}^2) . Combining (43) with (48) and (50) and knowing that there are $(N+1)$ eigenvalues s_{vk} give $(N+1)$ possible eigen solutions. The homogeneous solution is then a linear combination of these eigen solutions which can be written as

$$I_n^h(\tau_v) = \sum_{k=0}^N A_{vnk}^h e^{-\tau_v/s_{vk}} = \sum_{k=0}^N \frac{Q_{vk}}{1 - \mu_n/s_{vk}} e^{-\tau_v/s_{vk}}. \quad (1-53)$$

Finally, from (43) the homogeneous solution is found to be

$$I_{2v}^h(\tau_v; \mu) = \sum_{n=0}^N I_n^h(\tau_v) f_n(\mu), \quad (1-54)$$

where $I_n^h(\tau_v)$ is given by (53).

B. Particular Solution

The particular solution is obtained by substituting an assumed solution of the form

$$I_n^p(\tau_v) = B_{v_n}^p e^{-\tau_v/\mu_p} \quad (1-55)$$

into (44). As a consequence,

$$(-\mu_n/\mu_p + 1) B_{v_n}^p = -\frac{W_v}{2} \sum_{k=0}^N B_{v_k}^p P_k + \frac{W_v S_p F_v^0}{4\pi}, \quad n=0,1,\dots,N, \quad (1-56)$$

where P_k is defined by (44a) with m replaced by k .

Assume that the subscript p on μ_p is an integer j lying in the range $0,1,\dots,N$. When $n = j$, the left hand side of (56) is zero. Therefore, the right hand side of (56), which does not depend on n , must always be zero, *i.e.*, even when $n \neq j$. Thus, for $n \neq j$, since the factor $(-\mu_n/\mu_p + 1) \neq 0$ then $B_{v_n}^p$ must be zero. Hence,

$$B_{v_n}^p = 0, \quad n \neq j, \quad (1-57)$$

and

$$0 = -\frac{W_v}{2} B_{v_j}^p P_j + \frac{W_v S_p F_v^0}{4\pi}, \quad n = j. \quad (1-58)$$

Combining (55), (57) and (58) gives the particular solution

$$I_n^p(\tau_v) = \begin{cases} -\frac{S_p F_v^0}{2\pi P_j} e^{-\tau_v/\mu_j}, & n = j \\ 0, & n \neq j \end{cases} \quad (1-59)$$

C. Total Solution

The total solution is the sum of the homogeneous and particular solutions

$$I_{2v} = I_{2v}^h + I_{2v}^p = \sum_{n=0}^N I_n(\tau_v) f_n(\mu) = \sum_{n=0}^N I_n^h(\tau_v) f_n(\mu) + I_j^p(\tau_v) f_j(\mu) \quad , j = p. \quad (1-60)$$

This can be rewritten using (53) and (59) as

$$I_{2v}(\tau_v; \mu) = \sum_{n=0}^N \left[\sum_{k=0}^N A_{vnk}^h e^{-\tau_v/s_{vk}} - \frac{S_p F_v^0}{2\pi P_n} e^{-\tau_v/\mu_n} \delta_{nj} \right] f_n(\mu) \quad , \quad (1-61)$$

where

$$A_{vnk}^h = \frac{Q_{vk}}{1 - \mu_n / s_{vk}} \quad , \quad \delta_{nj} = \begin{cases} 0 & , n \neq j \\ 1 & , n = j \end{cases} \quad , \quad (1-61a)$$

and s_{vk} are the eigenvalues found from (52).

To satisfy the boundary condition (46b), it is necessary that

$$Q_{vk} = 0 \quad , \quad k = 0, 1, \dots, (N-1)/2 \quad , \quad (1-62)$$

because $\Re[s_{vk}]$ is taken to be negative for these value of k whereas $\Re[s_{vk}]$ is positive when $k = (N+1)/2, (N+3)/2, \dots, N$. Thus, (61) becomes

$$I_{2v}(\tau_v; \mu) = \sum_{n=0}^N \left[\sum_{k=\frac{N+1}{2}}^N A_{vnk}^h e^{-\tau_v/s_{vk}} - \frac{S_p F_v^0}{2\pi P_n} e^{-\tau_v/\mu_n} \delta_{nj} \right] f_n(\mu) \quad , \quad (1-63)$$

where $I_n(\tau_v)$ is given by the term in the bracket.

Substituting (61a) and $I_n(\tau_v)$ from (63) into boundary condition (46a) yields the linear system of equations for $(N+1)/2$ unknowns Q_{vk} :

$$\sum_{k=\frac{N+1}{2}}^N \frac{Q_{vk}}{1-\mu_n/s_{vk}} = \frac{S_p F_v^o}{2\pi P_n} \delta_{nj}, \quad n = \frac{N+1}{2}, \frac{N+3}{2}, \dots, N. \quad (1-64)$$

This can be written in matrix form as

$$[a_{v_{nk}}] \cdot [Q_{vk}'] = [c_{vk}] \quad , \quad (1-65)$$

where $[a_{v_{nk}}]$ is an $(N+1)/2 \times (N+1)/2$ square matrix whose elements are

$$a_{v_{nk}} = [1 - \mu_n / s_{vk}]^{-1} \quad , \quad (1-65a)$$

while $[Q_{vk}']$ and $[c_{vk}]$ are $1 \times (N+1)/2$ column matrices whose elements are

$$Q_{vk}' = Q_{vk}/(S_p F_v^o/2\pi), \quad c_{vk} = \frac{1}{P_n} \delta_{kj} \quad , \quad (1-65b)$$

and δ_{kj} is the Kroneker delta function defined in (61b).

The omnidirectional background diffuse intensity is therefore given by

$$I_2(z', t'; \mu) = \Re \left[\sum_{v=0}^{\infty} I_{2v}(z', t'; \mu) e^{jv\omega' t'} \right] \quad (1-66a)$$

$$= \Re \left[\sum_{v=0}^{\infty} \frac{S_p F_v^o}{2\pi} \left[\sum_{n=0}^N \left[\sum_{k=\frac{N+1}{2}}^N \frac{Q_{vk}'}{1-\mu_n/s_{vk}} e^{-\tau_v/s_{vk}} - \frac{1}{P_n} e^{-\tau_v/\mu_n} \delta_{nj} \right] f_n(\mu) e^{jv\omega' t'} \right] \right] \quad (1-66b)$$

in which (11) and (63) have been used; note that in (11) p is replaced by 1 and 2 because of (17).

I.5 Power Received by Highly Directive Antenna

For the normal incidence case ($\mu_p = \mu_j = 1$), the total intensity is determined from (16), (39) and (66) using (41b) and (61a) as

$$\begin{aligned}
 I_{\text{tot}} = I_c + I_1 + I_2 = & \Re \left[\sum_{v=0}^{\infty} e^{jv\omega' t} \frac{S_p F_v^o}{2\pi} \left[e^{-\eta_v z'} \delta(\mu - \mu_j) \right. \right. \\
 & + \frac{1}{2} e^{-\eta_v z'} \sum_{m=1}^M \frac{(W\alpha z')^m}{m!} q_m(\theta) \left\{ 1 + \xi_m(\theta) \left[1 - \frac{\eta_v z'}{m+1} \right] \right\} \\
 & \left. \left. + \left\{ -e^{-\eta_{2v} z'} \frac{f_j(\mu)}{P_j} + \sum_{k=(N+1)/2}^N [Q_{vk}' e^{-\eta_{2v} z'/s_{vk}} \sum_{n=0}^N \frac{f_n(\mu)}{1 - \mu_n/s_{vk}}] \right\} \right] \right] , \quad (1-67)
 \end{aligned}$$

where

$$\eta_v = (1 + jv\omega') , \quad \eta_{2v} = (1 + jv\omega' - W\alpha) , \quad j=p. \quad (1-67a)$$

The above relation is based on the assumption that a plane wave is incident onto the forest from the air half-space; this plane wave can be physically generated by locating a transmitting antenna at a sufficiently large distance from the edge of the forest.

Assume that a highly directive receiving antenna of narrow beamwidth is located inside the forest. The receiving antenna is characterized by an effective aperture $A_o(\gamma_M)$, where γ_M is the angle included between the direction of observation (θ, ϕ) and the pointing direction of the antenna axis, *i.e.*, the main beam direction (θ_M, ϕ_M); see Fig. 5. Evidently,

$$\cos \gamma_M = \cos(\phi - \phi_M) \sin \theta \sin \theta_M + \cos \theta \cos \theta_M \quad (1-68a)$$

$$= \cos(\phi - \phi_M) (1 - \mu^2)^{1/2} (1 - \mu_M^2)^{1/2} + \mu \mu_M \quad (1-68b)$$

with

$$\mu_M = \cos\theta_M . \quad (1-68c)$$

The power received by the antenna is the sum of the intensity contributions coming from all directions multiplied by the effective aperture of the antenna, *i.e.*,

$$P_R(z', t'; \mu_M, \phi_M) = \int_0^{2\pi} \int_{-1}^1 A_e(\gamma_M) I_{\text{tot}}(z', t'; \theta, \phi) d\mu d\phi . \quad (1-69)$$

Since in (69) the receiving antenna is taken to be polarization matched, impedance matched and lossless, the effective aperture is expressed in terms of the directive gain of the antenna by the general relationship

$$A_e(\gamma_M) = \frac{\lambda_0^2}{4\pi} D_R(\gamma_M) , \quad (1-70)$$

where λ_0 is the free-space wavelength. The directive gain is assumed to be gaussian, *i.e.*,

$$D_R(\gamma_M) = \left[\frac{2}{\Delta\gamma_R} \right]^2 e^{-\left(\frac{\gamma_M}{\Delta\gamma_R}\right)^2} , \quad \Delta\gamma_R \ll \pi , \quad (1-71)$$

which is normalized such that

$$\int_0^{2\pi} \int_{-1}^1 D_R(\gamma_M) d\mu d\phi = 4\pi , \quad (1-71a)$$

and $\Delta\gamma_R$ is the beamwidth of the receiving antenna.

Using (67) in (69), the total received power is found to be expressed in terms of three normalized power quantities, namely, the coherent power \mathcal{P}_c , the narrow lobe diffuse power \mathcal{P}_{d1} and the

omnidirectional background diffuse power \mathcal{P}_{d2} (see Appendix E):

$$\mathcal{P}_R \equiv \frac{P_R(z', t'; \mu_M, \phi_M)}{P_{\text{norm}}} = \mathcal{P}_c + \mathcal{P}_{d1} + \mathcal{P}_{d2} , \quad (1-72)$$

where

$$\mathcal{P}_c = \mathcal{R}_e \left[\sum_{v=0}^{\infty} e^{jv\omega' t'} \left[F_v^o e^{-\left(\frac{\gamma_{PM}}{\Delta \gamma_R}\right)^2 - \eta_v z'} \right] \right] , \quad (1-72a)$$

$$\mathcal{P}_{d1} = \mathcal{R}_e \left[\sum_{v=0}^{\infty} e^{jv\omega' t'} \left[\frac{F_v^o}{4} e^{-\eta_v z'} \sum_{m=1}^M \frac{(W_{\alpha z'})^m}{m!} \left[\frac{4}{h m \Delta \gamma^2} (1 - e^{-4h}) - \left(1 - \frac{\eta_v z'}{m+1} \right) \right. \right. \right. \\ \left. \left. \cdot \left[\frac{1}{3} \frac{(m^2 - 1)}{m} \frac{1}{h} (e^{-4h} - 1) + \frac{m+1}{m^2 \Delta \gamma^2} \frac{2m+1}{3} \frac{1}{h^2} (e^{-4h(4h+1)} - 1) \right] \right] \right] \right] \quad (1-72b)$$

$$\mathcal{P}_{d2} = \mathcal{R}_e \left[\sum_{v=0}^{\infty} e^{jv\omega' t'} \left[\frac{\Delta \gamma_R^2 F_v^o}{2} e^{-\eta_{2v} z'} \frac{f_j(\mu_M)}{P_j} + \sum_{k=(N+1)/2}^N \left\{ Q'_{vk} e^{-\eta_{2v} z' / s_{vk}} \sum_{n=0}^N \frac{f_n(\mu_M)}{1 - \mu_n / s_{vk}} \right\} \right] \right] \quad (1-72c)$$

with

$$\mu_p = 1, \gamma_{pM} = \theta_M, h = 1/\Delta \gamma_R^2 + 1/m \Delta \gamma^2 \quad (1-72d)$$

and the normalization used is

$$P_{\text{norm}} = \frac{\lambda_0^2}{4\pi} D_R(0) S_p , \quad (1-73)$$

which is proportional to the time-averaged power received by the antenna placed at $z' = 0$.

I.6 Numerical Results for normal incidence

From (72), the normalized received powers in dB,

$$\mathcal{P}_{i,db} \equiv 10 \log [\mathcal{P}_i] \quad , i = r, c, d1, d2 \quad , \quad (1-74)$$

are obtained numerically and are plotted versus normalized time t' in Figs. 1-6 to 1-30. While the first and second terms of (72), which correspond to the contributions of I_c and I_1 have explicit forms, the third term as seen in (72c) contains eigenvalues $s_{\nu k}$ and amplitudes $Q_{\nu k}'$ of I_2 which have to be determined numerically by solving (52) and (65), respectively. This is accomplished by using the commercially available library of mathematical routines known as "IMSL". Complete computer programs are included in Appendix G.

For numerical evaluation of (74), the incident gaussian signal envelope $F(0,t)$ defined in (1a) is normalized so that it decreases from a maximum value at $t' = 0$ to a value at $t' = \pm T'/4$ of e^{-5} times the maximum value. This corresponds to a decrease of approximately 20 dB and, as a result, α in (1a) and (3b) equals $4\sqrt{5}$. This pulse shape simulates a digital signal which is essentially "on" over half the pulse period and "off" over the remaining portion of the period. The receiving antenna is assumed to be aligned to accept maximum power from the normally incident radiation, *i.e.*, $\gamma_M = 0$. The receiving antenna is also assumed to have a 3 dB beamwidth of 1.2° , *i.e.*, in (71) $\Delta\gamma_R$ is 0.7° , which ensures a high directive gain. Furthermore, $\Delta\gamma$ is taken to be 3.5° so that the scatter profile in (5b) has a strong narrow forward lobe. Table 1 summarizes the range of parameter values used. The parameters

are the normalized pulse repetition rate T' , albedo $W = \sigma_s/(\sigma_s + \sigma_A)$, the ratio of the probability of intensity being scattered in the forward direction to the probability of intensity being scattered in all directions α , and the normalized penetration depth z' .

Table 1. Summary of parameters for Fig. 1-6 through Fig. 1-30

Set A : First order approximation

T'	W	α	z'
2.	0.75 , 0.95	0.2 , 0.8	1., 10., 20., 30.
10.	0.95	0.8	30.

Set B : Zero order approximation

T'	W	α	z'
2.	0.75	0.2	1., 10., 20., 30.
2.	0.95	0.8	1., 10., 20., 30.

In Figs. 1-6 to 1-9, powers are plotted over a time interval of twice the period $T' = 2$ for $W = 0.75$, $\alpha = 0.2$ and $z' = 1, 10, 20$ and 30 , respectively. At small penetration depths, the coherent power \mathcal{P}_c is seen to dominate significantly over the "on" portion of the period ; only over a small time interval does the omnidirectional diffuse power \mathcal{P}_{d2} take over. This interval of time corresponds to the "off" segment of the signal. As the depth of penetration increases, the total signal level decreases as expected; but at sufficiently large z' , the effects of pulse broadening are seen to occur, *i.e.*, \mathcal{P}_{d1} gets distorted as shown in

Fig. 1-9 at $z' = 30$. This result is evident from (72b) due to the appearance of the term $\eta_y e^{j\nu\omega t'} = (1+j\nu\omega')e^{j\nu\omega t'}$, which gives rise to a time derivative of the input signal and therefore indicates pulse signal distortion.

It was just observed that as z' increases and for small α , the coherent power \mathcal{P}_c became the strongest portion of the power received in the "on" time interval. In Figs. 1-10 through 1-13, α is set equal to 0.8, which characterizes the forest with a stronger forward scattering phase function. Comparing Fig. 1-10 to Fig. 1-6, it is evident that for larger α , the narrow-lobe diffuse power \mathcal{P}_{d1} is stronger during the "on" portion of the period, while the omnidirectional power \mathcal{P}_{d2} is weaker. Note that the signal drawn in Fig. 1-10 is easier to detect than that of Fig. 1-6. Thus, a medium with a larger α permits better detection of transmitted data. Also, the signal depicted in Fig. 1-10 has a lower power level in the "off" time segment than that in Fig. 1-6. Hence, the signal of Fig. 1-10 has better noise immunity. In Fig. 1-11 it is seen that at $z' = 10$, the power \mathcal{P}_{d1} remains stronger than \mathcal{P}_c in contrast to that drawn in Fig. 1-7. This is a consequence of α being larger. Distortion is also now seen to occur at smaller penetration depths; compare Figs. 1-11 and 1-12 to Figs. 1-7 and 1-8, respectively, and observe the shift of \mathcal{P}_{d1} . Note in Figs. 1-12 and 1-13 that the total received power \mathcal{P}_R in the "on" time segment is non-symmetric. Observe, furthermore, that there appear to be two minima in each time period in the plot of \mathcal{P}_{d1} . In the time interval between these two minimum values, P_{d1} was found to be negative. The corresponding portion of the curve in Fig. 1-12 is a plot of $10 \log_{10}(-P_{d1})$, which is positive. This non-physical segment of the \mathcal{P}_{d1} curve results because the approximation used in the derivation of I_1 (needed for P_{d1}) breaks down when either

the incident pulse has a fast rising slope or the product ($W\alpha z'$) is very large; hence, the term after the minus sign in (40) then dominates and I_1 is negative. On the other hand, in the time interval where the signal has a fast falling slope, the narrow-lobe diffuse power remains positive and the corresponding portion of the total power curve \mathcal{P}_R displays the development of a "tail". In Fig. 1-13, the signal is lower and the distortion is more pronounced than was found in Fig. 1-12. Note that in the time interval where P_{d1} is negative, the total power \mathcal{P}_R is calculated without the contribution from I_1 . Therefore, the fact that the total power appears to fall below $(-P_{d1})$ in Fig. 1-13 is of no concern. The appearance of negative power, unless extremely small, indicates that the first order solution is no longer valid; curves nonetheless were drawn to gain further insight.

In Figs. 1-14 through 1-21, the albedo is taken to be 0.95, which characterizes a highly scattering medium. In Figs. 1-14 through 1-17, α is small ($\alpha = 0.2$) while in Figs. 1-18 through 1-21, α is large ($\alpha = 0.8$). Observe that the signal is lost at $z' = 20$ in Fig. 1-16 for $\alpha = 0.2$, while it is detectable in Fig. 1-20 when $\alpha = 0.8$. Also, the background power \mathcal{P}_{d2} in Figs. 1-14 to 1-19 are larger than that in Figs. 1-6 to 1-9. This is to be expected because the albedo W is now large. Note that in Fig. 1-16, $\mathcal{P}_R \approx \mathcal{P}_{d2}$ which is not the case in Fig. 1-8. Finally, observe that distortion of \mathcal{P}_R occurs in Fig 1-17, but not in Fig. 1-9. This is due to large values of the product of W , α and z' , as was previously explained. More distortion is seen in Fig. 1-13 as compared to Fig. 1-17 because the product of W , α and z' is larger.

Comparisons of Figs. 1-20 and 1-21 to Figs. 1-16 and 1-17, respectively, demonstrate that a medium which not only is highly scattering (W large) but also is characterized by a stronger forward

lobe in its scattering profile (α large) will permit signal detection at large penetration depths.

Increasing the normalized period from $T' = 2.0$ in Fig. 1-21 to $T' = 10.0$ in Fig. 1-22 shows that a larger T' eliminates pulse distortion in the total power when W and α remain fixed. This is due to the fact that a constant α fixes the input gaussian signal amplitude while a smaller T' produces a sharper pulse shape. Hence, the derivative in (40) is larger when T' is smaller and the pulse is then more distorted.

Figs. 1-23 to 1-30 are included to show that the zero order solution given in Appendix C agrees with the first order solution in (72), which is depicted by Figs. 1-6 to 1-9 and Figs. 1-18 to 1-21 when the product of $F'(t'-z')$ and $W\alpha z'$ is sufficiently small, where the prime means differentiation with respect to normalized time t' (see (40)). Hence, when W and α are large, the agreement is limited to a smaller penetration range.

I.7 Conclusions and Suggestions

A forest is a highly scattering medium (W large) at millimeter wave frequencies. Experimental data [2] verified that cw transmission is indeed possible over lengths of the order of a few hundred meters and that a forest acts to strongly scatter energy in the forward direction (α large). A theory of millimeter wave pulse propagation in vegetation was undertaken using the scalar time-dependent equation of radiative transfer to verify and explain these observations and in particular to show pulse broadening effects. A periodic sequence of gaussian plane wave pulse was taken to impinge upon a forest half-space. The forest was assumed to be statistically homogeneous and to consist of a random distribution of particles which scatter and absorb radiation. Four parameters σ_A , σ_s , $\Delta\gamma$, and α were used to characterize this scatter medium.

The power received by a highly directive antenna placed in the forest was calculated numerically. It was ascertained that pulse broadening occurred significantly at large penetration depths in a forest characterized by a large albedo and a large α for fast rising pulses. Data transmission with these pulses through such a forest with large W and α was shown to be feasible. To obtain meaningful results at even deeper penetration depths, higher order approximate solutions are needed. Preliminary considerations show the analysis to be complicated.

It remains necessary to determine more accurately the values of the above four parameters. Part II discusses a method involving extracting these parameters from experimental data.

II. Determination of Forest Parameters using the Capturing Technique and the Time-Independent Transport Equation

II.1 Introduction

In Part I a model of pulse millimeter wave propagation in a forest using the time-dependent transport equation was presented. For a normally incident gaussian plane wave pulse train, curves were drawn of instantaneous powers received by a highly directive gain antenna placed in the forest for different values of the parameters W , α and z' . Recall that the albedo W equals $\sigma_s/(\sigma_A + \sigma_s)$, where σ_s and σ_A are the scatter and absorption cross-sections per unit volume of the forest, the parameter α is the probability of intensity $I(r,t;s)$ being scattered in the forward direction and z' is the normalized penetration depth. To estimate these parameters, a parametric inversion scheme is performed which uses the zero order solution to the transport equation. Since experimental data of scattered intensity is available for the problem of a uniform plane wave incident from free-space striking a forest, the parametric inversion scheme is applied to the time-independent transport equation.

From experimental results [2], the power received by an antenna in a pecan grove (the forest) is known over a symmetric range of angles measured in a horizontal plane. At particular angles in this range, the transport equation is solved by initially choosing values for W , α and z' . This choice of initial parameters will not normally give values of intensity which agree with the experimentally determined ones. By judiciously varying parameters using an optimization technique similar in concept to "simulated annealing" and by requiring that the difference

between experimental and determined values of received power be minimal, the desired unknown parameters W , α and z' are found.

In Section II.2 expressions are given for the zero order power received by a highly directive gain antenna placed in a forest which is illuminated from free-space by a plane wave with time-invariant intensity. Curves of zero order received power versus scan angle θ_M are drawn ; these show the effect of varying one of the parameters W , α or z' . Section II.3 discusses how experimental data was taken and how a previous theoretical study curve-fit the data [3,8]. The optimization scheme used in the present investigation is discussed in Section II.4 along with a sample case which uses synthetic data to justify the validity of the method. In Section II.5 actual experimental data is used in the optimization scheme to find W and α at various penetration depths z' . To characterize the forest correctly, an ensemble average of these values is obtained. A physical explanation of these values is presented in Section II.6. Therein suggestions are made on how to obtain more complete data so that better estimates of parameters could be obtained from the optimization scheme.

II.2 Power Calculation

The solution to the time-independent transport equation for specific intensity follows directly from the theory of Part I by setting $\nu = 0$. Hence, the total relative power received by a highly directive gain antenna placed in the forest at location z' (see Fig. 1-5) is specified to zero order by (1-72) when ν is set to zero and the narrow lobe relative power portion is given by \mathcal{P}_{d1}^0 which is derived in Appendix C. Hence, to zero order and for normal incidence

$$\mathcal{P}_R^0 = P_R^0(z'; \mu_M) / P_{\text{norm}} = \mathcal{P}_c + \mathcal{P}_{d1}^0 + \mathcal{P}_{d2}^0, \quad (2-1)$$

where

$$\mathcal{P}_c = P_c / P_{\text{norm}} = e^{-\left(\frac{\gamma_{pM}}{\Delta \gamma_R}\right)^2 - z'}, \quad (2-1a)$$

$$\mathcal{P}_{d1}^0 = P_{d1}^0 / P_{\text{norm}} = \frac{\Delta \gamma_R^2}{4} e^{-z'} \sum_{m=1}^M (W \alpha z')^m \frac{1}{m!} q_m(\gamma_{pM}) \quad (2-1b)$$

$$\mathcal{P}_{d2}^0 = P_{d2} / P_{\text{norm}} = \frac{\Delta \gamma_R^2}{2} \left[-e^{-\eta z'} \frac{f_j(\mu_M)}{P_j} + \sum_{k=\frac{(N+1)}{2}}^N \left[Q'_{0k} e^{-\eta z' / s_{0k}} \cdot \sum_{n=0}^N \frac{f_n(\mu_M)}{1 - \mu_n / s_{0k}} \right] \right] \quad (2-1c)$$

with $\mu_j = \mu_p = 1$, $\gamma_{pM} = \theta_M$ and

$$q_m(\gamma_{pM}) = \frac{4}{\Delta\gamma_R^2 + m\Delta\gamma^2} e^{-\gamma_{pM}^2/(\Delta\gamma_R^2 + m\Delta\gamma^2)}, \quad \eta = (1-W\alpha) \quad (2-1e)$$

Quantities μ_n , f_n , P_j , s_{0k} and Q_{0k}' are obtained from (1-43), (1-44a), (1-52) and (1-64), respectively. Parameters which remain constant throughout this study are $\Delta\gamma_R = 0.7^\circ$ and $\Delta\gamma = 3.5^\circ$; the former value insures a highly directive gain antenna while the latter restricts consideration to a forest which can be characterized by a scatter (phase) function that possesses a very narrow gaussian lobe in the forward direction. This restriction is physical because experimental results for the power angular spectrum show a very narrow forward lobe at high millimeter wave frequencies; see Fig. 2-5, particularly at the frequency of 57.6 GHz. The scan angle θ_M is taken to vary from -0.3 to +0.3 radians.

In Figs. 2-1, the total received power $\mathcal{P}_R^0(z';\mu)$ using (2-1) is plotted versus scan angle θ_M for the normal incidence case. Scan angle range is chosen to vary from -0.3 to +0.3 radians and plots are drawn for $W = 0.5$, $\alpha = 0.2$ and $z' = 0.1, 1.0$ and 10.0 . Observe that the received power has a strong narrow lobe centered around the $\theta_M = 0$ direction and decreases quickly to a low uniform power level near $\theta_M = \pm 0.3$. As z' increases from a value of 0.1 to 10., the maximum power decreases in the $\theta_M = 0$ direction, although in the background region the constant low power level first increases and then decreases. It was shown previously in the isotropic scattering case [7] that the diffuse intensity when plotted versus z' first increases rapidly to a maximum level at z' equal to unity and then decreases more gradually as z' is increased further. This is substantiated in Fig. 2-1 in the background region where the level first increases when z' is increased to unity and

then decreases when z' is increased to 10. Note the relatively smaller dB change in power in the background region as compared to the region near $\theta_M = 0$, although the overall shape of the curve remains similar. The strong contribution in the forward direction $\theta_M = 0$ is predominantly determined by the coherent intensity because of the strong decay which occurs at the largest penetration depth. In the region $|\theta_M| < 0.05$ occupied by the forward lobe, the strong forward portion of the diffuse intensity I_1 plays a major role while in the background regime, the I_2 portion of the diffuse intensity controls the power flow. The values of z' , i.e., the point in the forest where the power is measured, will shortly be shown to be the most significant parameter which determines the shape of the angular power spectrum.

In Fig. 2-2, the received power is plotted using three different values for albedo W while z' and α are fixed at 1.0 and 0.2, respectively. Note that for larger values of albedo, the level of the background power is higher than for smaller albedo values, while the peak power at $\theta_M = 0$ remains unchanged. This was to be expected because for large values of W , the diffuse intensity is stronger at a given z' . This enhances the background power level. A larger W means that less power is lost due to absorption and hence more incoherent power reaches

$$P = \frac{4\pi^2 E^2 |G|^2 V_h}{K} \quad (39)$$

Fig. 2 - 3, the received power is plotted using three different values for α (0.2, 0.5 and 0.8) while z' and W are fixed at 1.0 and 0.5, respectively. Observe that as α increases, the background levels in the ranges $\theta_M < -0.2$ and $\theta_M > 0.2$ decrease while the power level of the forward lobe in the range of $-0.2 < \theta_M < 0.2$ increases. In other words, more energy gets channeled in the forward direction at higher values of

α . This means that the narrow lobe diffuse intensity I_{d1} becomes stronger while the omnidirectional diffuse intensity becomes weaker, which results in a reduction of the background level.

Based on Figs. 2-1 to 2-3, the following observations on the effect of varying one of the parameters z' , W or α can be made.

- (1) Changes in z' alter the overall power level of the total received power more significantly than changes in W or α .
- (2) Changes in α strongly affect the values of the received power in the angular range outside of the very narrow portion of the forward lobe.
- (3) Changes in W strongly affect the power level outside the narrow lobe region.

II.3 Experimental Results

Experiments were conducted at the three different frequencies 9.6, 28.8 and 57.6 GHz [2]. All transmitting antennas had a comparatively broad beamwidth of 10° and provided wide angle illumination of the forest. The receiving antennas had narrow beamwidths, i.e., 4° at X-band and 1.2° at the two millimeter wave frequencies. In the numerical evaluation of the theory, the 1.2° beamwidth was assumed.

The antennas were linearly polarized. Experiments showed that at millimeter wave frequencies, the propagation conditions in vegetation are practically the same for both vertical and horizontal polarizations. This means that polarization effects are not important. This supports the use of the scalar theory of radiative transfer. The received power includes contributions from both the co-polarized and cross-polarized field components. In the experiments only the co-polarized component is measured. Cross-polarization experiments, on the other hand, have shown that for the distances involved millimeter waves do not meaningfully become depolarized in vegetation and that the cross-polarized component remains several dB below the co-polarized component. Hence, the cross-polarization contribution to the received power is negligible and theoretical and experimental results can be compared.

To simplify the random environment in a forest, the experiments were performed in a regularly planted, well-groomed orchard of pecan trees which roughly approximates a statistically homogeneous medium. The trees in this orchard were equally spaced, separated about 13 m apart one from another and approximately 10 m tall. Maximum vegetation density occurred in the leaf region between 4 and 6 m above ground.

Measurements were taken both when trees were bare as well as when they were fully in leaf.

The experimental configuration is shown in Fig. 2-4. The transmitting antenna was located in free-space at a distance of ~ 300 m from the first row of trees in order to produce an incident plane wave carrying constant power. The receiving antenna was situated within the orchard and was moved to different locations as indicated in the figure by circles. In each case, the receiving antenna was placed at the same height as the transmitting antenna so that the line-of-sight followed a path of maximum vegetation density through one column of trees. Measurements were taken at different heights above the ground; only data measured at a height of 6 m is used here. The receiving antenna then performed scans in azimuth and in elevation. Measured values of the received power versus azimuthal scan angle are given in Fig. 2-5 for trees without leaves. Lighter trace in the figures show the power received at the forest-air interface, which is the radiation pattern of the receiving antenna in free-space. Note that good qualitative agreement between the measured results in Fig. 2-5 and the theoretical values in Figs. 2-1 to 2-3 is obtained. At the highest frequency of 57.6 GHz, the plots in Fig. 2-5 show the best correlation with the strong forward scattering model. This results because at the highest frequency, wavelength is the smallest compared to scatter objects in the forest as required for strong forward scattering. At vegetation depths of one or three trees, the presence of the coherent component is evident in Fig. 2-5 at 57.6 GHz by the narrow peak in the scan pattern. At larger vegetation depth, corresponding to a propagation path through eight trees, the coherent component has been severely attenuated so that the incoherent component now dominates.

Fluctuations of the received power in the experimental data comes from interference effects (fading). By taking multiple measurements at different antenna positions, these fluctuations may disappear in a plot of averaged values. Since transport theory neglects interference effects, the corresponding theoretical curves of Figs. 2-1 to 2-3 are without fluctuations.

Even though theoretical and experimental results show the same trends and are in good qualitative agreement, one has to use caution to extract the parameters z' , W and α . Schwering *et al* [8] tried to establish limited quantitative agreement between theory and experiments by determining numerical values for σ_t , W and α from measured z' dependent curves (see Fig. 11 in [8]). Specifically, the authors collected maximum values of the received power in the $\theta_M = 0$ direction at various physical distances z in the forest. Using measured data at small and large distances z , values for σ_t , W and α were found by curve fitting the measured values to theoretical determined ones using (2-1). In [8], σ_t was found first by curve fitting the measured values of the received power to the exponential expression $\exp (- \sigma_t z)$ for the normalized coherent power, which approximately equals the received power at short penetration distances. It was found that $\sigma_t \approx 0.25 \text{ m}^{-1}$ for trees without leaves. Consideration of large penetration depths lead to a reduction of the values to $\sigma_t \approx 0.2 \text{ m}^{-1}$. Using this value for σ_t and plotting the \mathcal{P}_R^0 for various values of W and α , it was ascertained that both W and α should have values between 0.9 and 0.95 at large penetration depths. Results of this approach are inconclusive because the curve fitting did not agree with experimental results over the entire range from small to large penetration depths.

To find more accurate parameter values, a different approach is

used. This approach uses the available measured values in Fig. 2-5 and the theoretical calculated ones presented in Figs. 2-1 to 2-3, both of which depict the received power as a function of scan angle at different depths. The procedure involves optimizing the three unknown parameters z' , W and α to get a more accurate curve fit between the theoretically calculated values of received power \mathcal{P}_R^0 from (2-1) and the measured values given in Fig. 2-5. This method is explained in the next section.

II.4 Parametric Inversion (Capturing Technique)

From the experimental values for power in Fig. 2-5, a method is described which permits the determination of the forest parameters σ_t , W and α ; note $z' = \sigma_t z$ where z is known from the experimental setup. Such a process can be referred to as parametric inverse radiative transfer [9,10], since the dependent variable intensity "I" of the transport equation is known while parameters in the equation of radiative transfer remain to be found. The parameters are selected according to an optimization technique which will be called the "Capturing Technique", abbreviated CT. To explain the procedure, it will be applied first to data generated by using (2-1).

Let parameters of a fictitious forest have values z'_0 , W_0 and α_0 . From (2-1), the power received at scan angle θ_j is found to be \mathcal{P}_{0j}^0 , $j=1,2,\dots,N$. These values shall be designated the "synthetic" data. The CT will now be used to estimate the parameter values using the "synthetic" data. The following constraints are imposed on unknown parameters.

$$(1) \quad 0 < z'/z_{\max} < 1.0, \quad (2-2a)$$

where z_{\max} is a reasonable upper bound

$$(2) \quad 0 < W < 1.0 \quad (2-2b)$$

$$(3) \quad 0 < \alpha < 1.0 \quad (2-2c)$$

For each parameter, a uniform distribution of M numbers, M an integer, is obtained by using a random number generator. From these M numbers a gaussian distribution of a new group of M random numbers is generated by choosing both a median and a standard deviation of 0.5. These randomly generated numbers are tagged sequentially and grouped together in sets

of three, *i.e.*, to form parameter sets (z_i, W_i, α_i) , $i=1,2,\dots,M$. For each set of parameters (z_i, W_i, α_i) , $i=1,2,\dots,M$, the received power \mathcal{P}_{ij} is calculated using (2-1) at scan angles θ_j , $j=1,2,\dots,N$. The difference in magnitudes between the CT generated powers \mathcal{P}_{ij} and "synthetic" power \mathcal{P}_{oj} is given by

$$\varepsilon_{ij} \equiv | \mathcal{P}_{ij} - \mathcal{P}_{oj} | > 0, i=1,2,\dots,M \text{ and } j=1,2,\dots,N \quad (2-3)$$

and a total error criterion is defined to be

$$\varepsilon_i \equiv \sum_{j=1}^N \varepsilon_{ij}, i=1,2,\dots,M. \quad (2-4)$$

The parameter set (z_i, W_i, α_i) which gives the smallest value of ε_i is chosen as the optimal solution. Each parameter in this optimal set is taken as a new median value for the corresponding gaussian distribution of the parameter. After picking new standard deviations, a new group of M different randomly distributed numbers for each parameter is generated. Because of the manner in which each parameter was seen to affect the received power versus scan angle as shown in Figs. 2-1 to 2-3, it was ascertain that z' has a stronger effect than either W or α . Hence, the standard deviation for z' is taken to be relatively smaller than that chosen for W and α ; the latter two are assumed to be identical. The above procedure is then repeated K times.

To illustrate the above approach, the following hypothetical data is taken : $z'_0 = 3.45$, $W_0 = 0.456$ and $\alpha_0 = 0.123$. These parameters are used in (2-1) at values of θ_M in the range of -15° to 15° to generate 41 values for the total received power. Assuming that these 41 values of

power are known, *i.e.*, treating them as "synthetic" data, the Capturing Technique is used to determine the unknown parameters z' , W and α .

As can be seen in Figs. 2-6 to 2-8, after 27 iterations the CT scheme is able to generate values for the three parameters which agree excellently with the values initially used ; initially, $z'_0 = 3.45$, $W_0 = 0.456$ and $\alpha_0 = 0.123$ while the CT scheme generated $z' = 3.45$, $W = 0.43$ and $\alpha = 0.13$. These values were obtained for $M = 50$. Increasing the generated numbers for M from 50 to 100 yields better results, namely, $z' = 3.45$, $W = 0.458$ and $\alpha = 0.122$, though *cpu* time increased by about 50 %. This result is for 27 iterations and the pattern of convergence is shown in Fig. 2-9.

Biasing the parameter z' by specifying a smaller relative standard deviation is convenient, but not necessary. If all standard deviation were chosen to be identical, the CT will work, but will take more iteration to converge. Hence, the general procedure is very powerful. Also, it should be noted that the initial values for medians and standard deviations are not significant in reaching the final solution. Again, making the method very useful. To check further on the accuracy of the CT, several sets of synthetic power data were used for this inverse scheme and were shown to yield excellent results. The CT appears to provide a very general systematic approach which yields very accurate results relative to nonsequential factorial searches which uses permissible grid points [11]. The CT is conceptually similar to "simulated annealing", which is a stochastic computational viewpoint derived from statistical mechanics for finding near globally minimum cost solutions to large optimization problems. A discussion of simulated annealing is given in Appendix F and its analogy to CT is explained.

II.5 Optimization Results

To run the CT with the measured data presented in Fig. 2-5 for the 57.6 GHz case, it was first necessary to convert this data to a linear scale in order to properly use the error criterion in the algorithm. Recall that the available measurement data involves three configuration, namely, 1,3 and 8 trees without leaves. The measured data was sampled at intervals of one degree in the range $5^\circ \leq |\theta_M| \leq 15^\circ$ (the background) and at intervals of one-half degree in the remaining portion (extended lobe region)

Case # 1 : 3 tree data

For this case, the three parameters are chosen to exist in the ranges $0 \leq z' \leq 10.0$, $0 \leq W \leq 1.0$ and $0 \leq \alpha \leq 1.0$. The 41 sampled data points taken from the measured values in Fig. 2-5 are plotted in Fig. 2-10. Application of the CT yields optimized values for z' , W and α of 4.36, 0.82 and 0.155, respectively. These are used in (2-1) to calculate the theoretical (optimized) received power \mathcal{P}_R^0 , which is plotted in Fig. 2-10. Observe that good agreement between theoretical and experimental values resulted, particularly in the center lobe region. From the optimized value $z' = 4.364$, the total or extinction cross section per unit volume σ_t is found to be 0.12 m^{-1} since the physical penetration depth is 39 m; recall that each tree is separated by approximately 13 meters. Note that $W = 0.820$ signifies a relatively strong scattering medium whereas $\alpha = 0.155$ indicates weak forward scattering.

Case # 2 ; 8 tree data

Because z' is located at a sizable depth inside the forest, the range of values for z' is chosen to be $0 \leq z' \leq 15$. Range of values for W and α remain fixed between zero and unity. Applying the optimization scheme CT yields the parameter values of $z' = 10.4$, $W = 0.760$ and $\alpha = 0.766$. The value $\alpha = 0.766$ indicates that strong forward scattering is significant; the value $W = 0.76$ states that the medium scatters more energy than it absorbs. In Fig. 2-11 are plotted theoretically optimized and experimentally determined received power. The overall shape of the curves agree, however, it is suspected that the measured data is insufficient for adequate comparison because only one data set was taken. What is needed is an average of several data sets to secure a meaningful comparison between theory and experiment.

Case # 3 ; 1 tree data.

Observe in Fig. 2-12 that the experimental data displays a distortion in the peak region. This might be due to a peculiarity in the forest geometry such as the shape of a particular limb in the one tree consideration. To compensate for this distortion. two situations are used; one with the central region included (set A) and one in which only data in the background region is used (set B), namely, 14 points in the angular range $9^\circ \leq |\theta_M| \leq 12^\circ$. The results of applying the CT to the above two sets of data are:

	z'	W	α
Set A	4.46	0.77	0.427
Set B	3.28	0.92	0.026

Table 2-1 Optimized parameter values for two angular ranges in the one tree case

Observe in set A that z' is larger than was found previously in the 3 tree case. Hence, the parameters of set A are rejected and only parameters of set B are included for discussion. Fig. 2-12 displays the comparison between experimental and theoretical values of received power using set B. In the central lobe region, the experimental and theoretical values agree to some extent. This result together with the rejection of data set A indicate that information was missing in the experimentally measured data which, as previously noted, could have been caused by some non-uniformity in the scatter geometry (the tree). Another explanation might be that the receiving antenna may have been placed in a shadow region behind either a twig or a tree branch.

From the values of set B, the value σ_t was found to be 0.24. Because W is large, the medium is found to be highly scattering and since α is small, the energy scatters most likely isotropically. Since extracted parameter values for the forest are inhomogeneous in contrast to the mathematical model, it is appropriate to calculate ensemble parameter averages to be used in the theory. These average values are summarized in the following table.

trees	z'	W	α	σ_t	σ_s	σ_A
1	3.28	0.92	0.026	0.24	0.221	0.019
3	4.36	0.82	0.155	0.11	0.090	0.02
8	10.4	0.76	0.766	0.1	0.076	0.023
Average	Not Applicable	0.833	0.316	0.15	0.125	0.021

Table 2-2. The optimized parameter values and their averages

Also included in Table 2-2 are associated values for the scatter and absorption cross-section σ_s and σ_A , respectively. Note that σ_A remains approximately constant while σ_s decreases as z' increases

II.6 Conclusions and Suggestions

In this second part, the parametric inversion scheme called the "Capturing technique" was developed which determined the parameters W , α and σ_t of a forest. These parameters appear in the time independent transport equation which is used to describe millimeter wave propagation in vegetation. Before using the available experimental data, the CT was tested by using synthetic data generated from the solution to the time-independent transport equation for arbitrarily chosen parameters. The inversion scheme was more sensitive to values of penetration depth z' than to the parameters W and α . Next, three sets of experimentally measured data were used to find the unknown optimal values for the forest parameters; these parameters produced the minimum error when used in comparison with the experimental values. Using these parameters, curves for power were generated theoretically and plotted with experimental results in the three cases. In addition, average optimal parameter values for the forest were determined (see Table 2-2) and found to be $W = 0.833$, $\alpha = 0.316$ and $\sigma_t = 0.15$.

According to the parametric description of the forest presented in Table 2-2, as penetration depth increases, W decreases, α increases, σ_t decrease and σ_A remains relatively constant. With regard to the decrease of W , it should be noted that the theoretical model assumes an infinite half-space while the real forest is finite. Hence, energy is lost through the forest-air interfaces and the forest-ground interface. As a result, the W obtained by the CT using the experimental data for intensity must be underestimated. In actuality, the forest is expected to exhibit a larger albedo value at each depth than appears in Table

2-2. This can be understood further by noting that if the forest were larger, *i.e.*, approximating a half-space region, more energy would be back scattered into the direction of observation which here is taken as $\theta_M = 0$. Hence, measured intensity would be greater and then the CT would calculate a larger optimal value for W . Since $W = 1/(1 + \sigma_A/\sigma_s)$, this means σ_A/σ_s also would be smaller at larger penetration depths. From our calculated values of σ_A which remains approximately constant at 0.021, it follows that σ_s must also be underestimated in our optimal scheme since we use the half-space model in the theory. The fact that σ_A remains constant is physically reasonable because as energy flows in direction θ_M through the medium which is statistically homogeneous, it simply gets attenuated. The fact that the parameter α gets larger as penetration depth increases indicates that the forest acts to scatter millimeter wave energy more into the forward direction, the further the energy enters into the forest. It is expected that α would increase to a constant value where the forest no longer appears to vary from point to point. Clearly, one trees scattering is significantly different due to scattering from eight tree. Though the data used and the parameter values for α obtained remain inconclusive, α is getting larger which indicates that strong forward scattering is dominant deep inside the forest.

The results found by F. Schwering *et al* [8] are that σ_t is 0.25 for short penetration depths and 0.2 for larger depths and W and α are values close to unity. As seen in Table 2-2, the σ_t values at the shortest distance agrees well; the other values are different; however, in both approaches, σ_t get smaller. These different results from the two approaches can be explained by noting that their curve fitting was performed mostly at values of $z' > 30$, while the optimization for the CT

utilizes data for values of z' which are different and much smaller. Furthermore, since W is underestimated in the CT approach deep inside the forest but near the interface remains more accurate in its determination of W , the expectation that W remains large is feasible. A better comparison with the result in [8] that W lies between 0.9 and 0.95 requires more data so that the CT method could be applied more effectively. A meaningful comparison is not possible using the current measured data.

Even though the CT is able to find optimized parameters when the available data is limited, it is strongly recommended that as complete a data set as possible be obtained over the entire angular spectrum of interest. This can be achieved by taking measurements at several locations along a transverse direction and averaging them. The data collected will then better approximate the mathematical model which is based on a forest being statistically homogeneous. In other words, any power measurement performed in a forest must be repeated several times to ensure that a measured quantity is an averaged one.

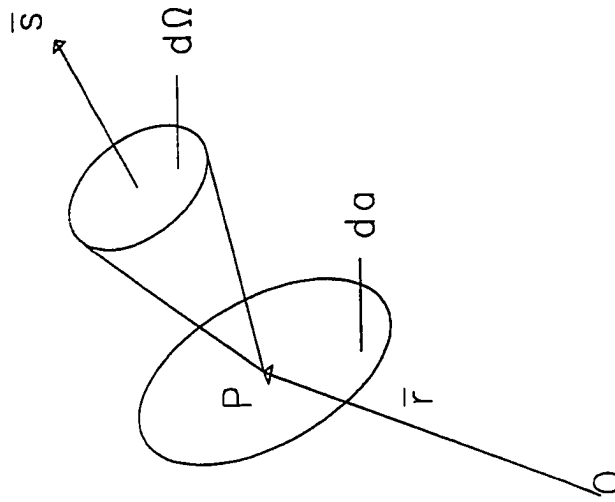


Fig. 1-1 Coordinate geometry used in the definition of the specific intensity $I(\mathbf{r}, \mathbf{s})$ in unit vector direction \mathbf{s} at the point \mathbf{P} a distance r from the origin; da is an element of area normal to \mathbf{s} and $d\Omega$ is an element of solid angle.

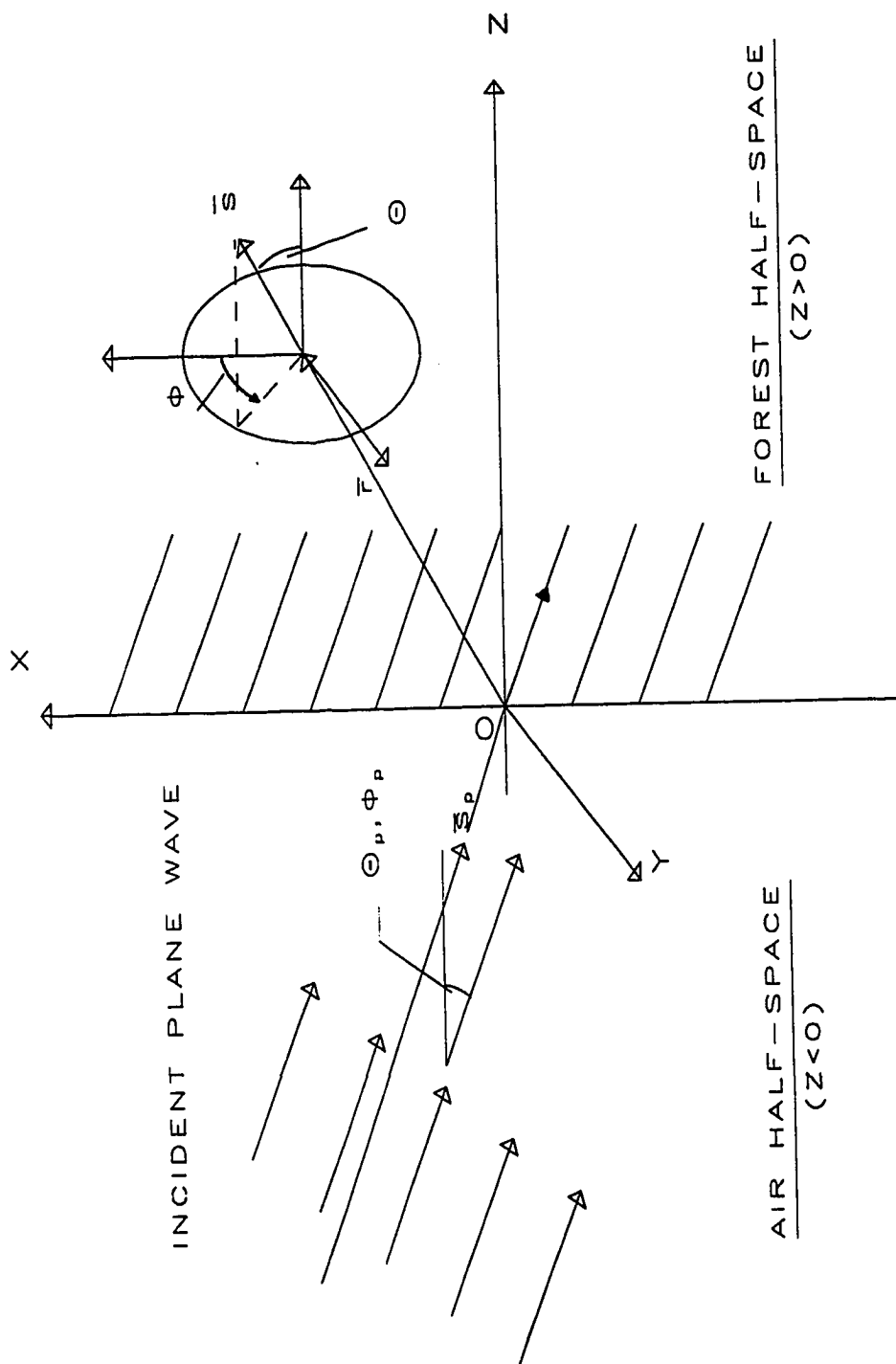


Fig. 1-2 Forest half-space illuminated by an incident plane wave gaussian pulse train.

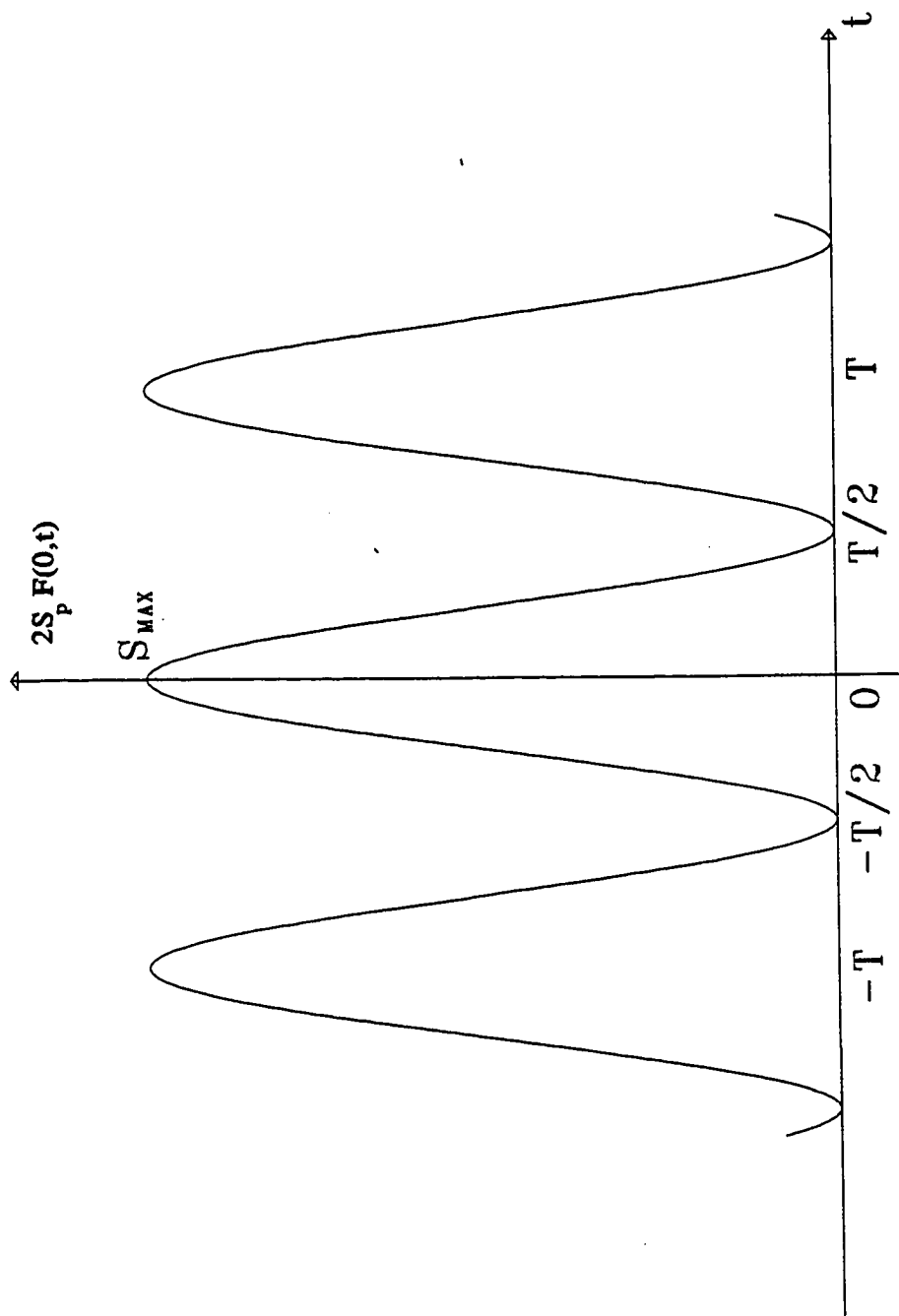


Fig. 1-3 Gaussian envelope of the instantaneous power density of the incident signal versus time t at $s = 0$; $S_{\text{MAX}} = 2a S_p / \sqrt{(\pi)}$.

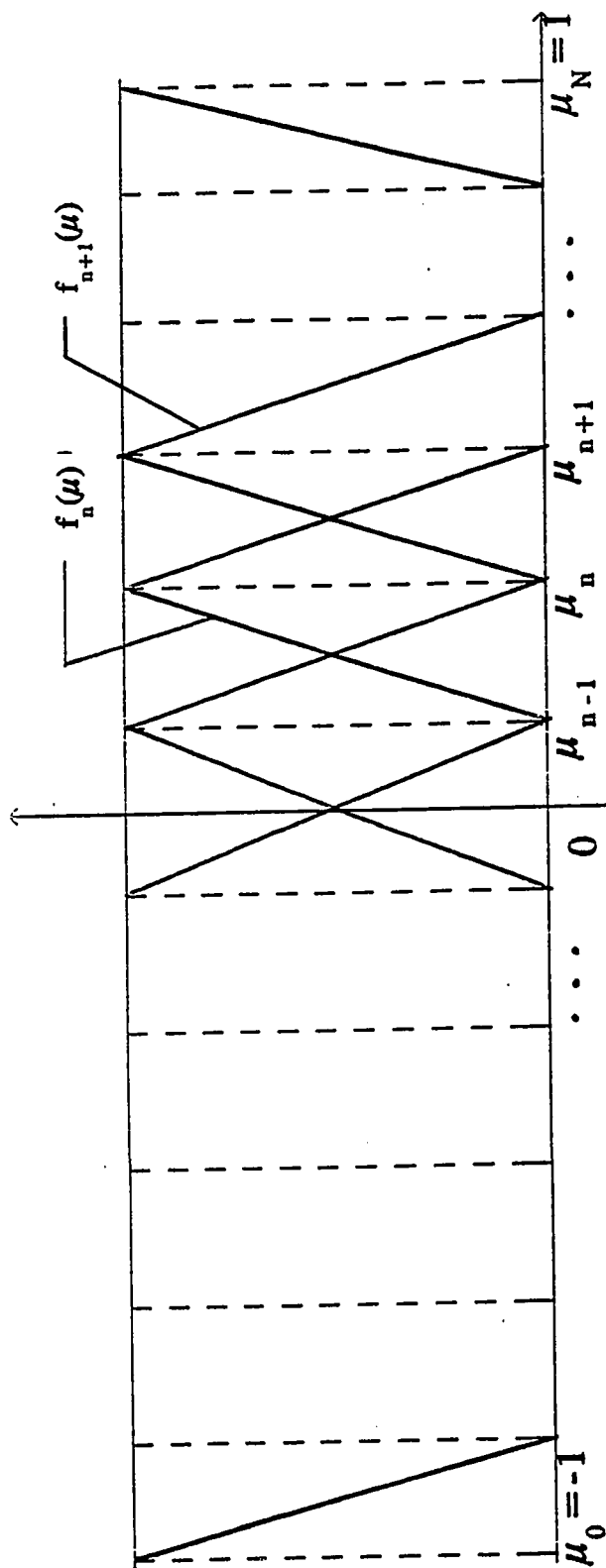


Fig. 1-4 Overlapping triangular basis functions for interval $-1 \leq \mu \leq 1$

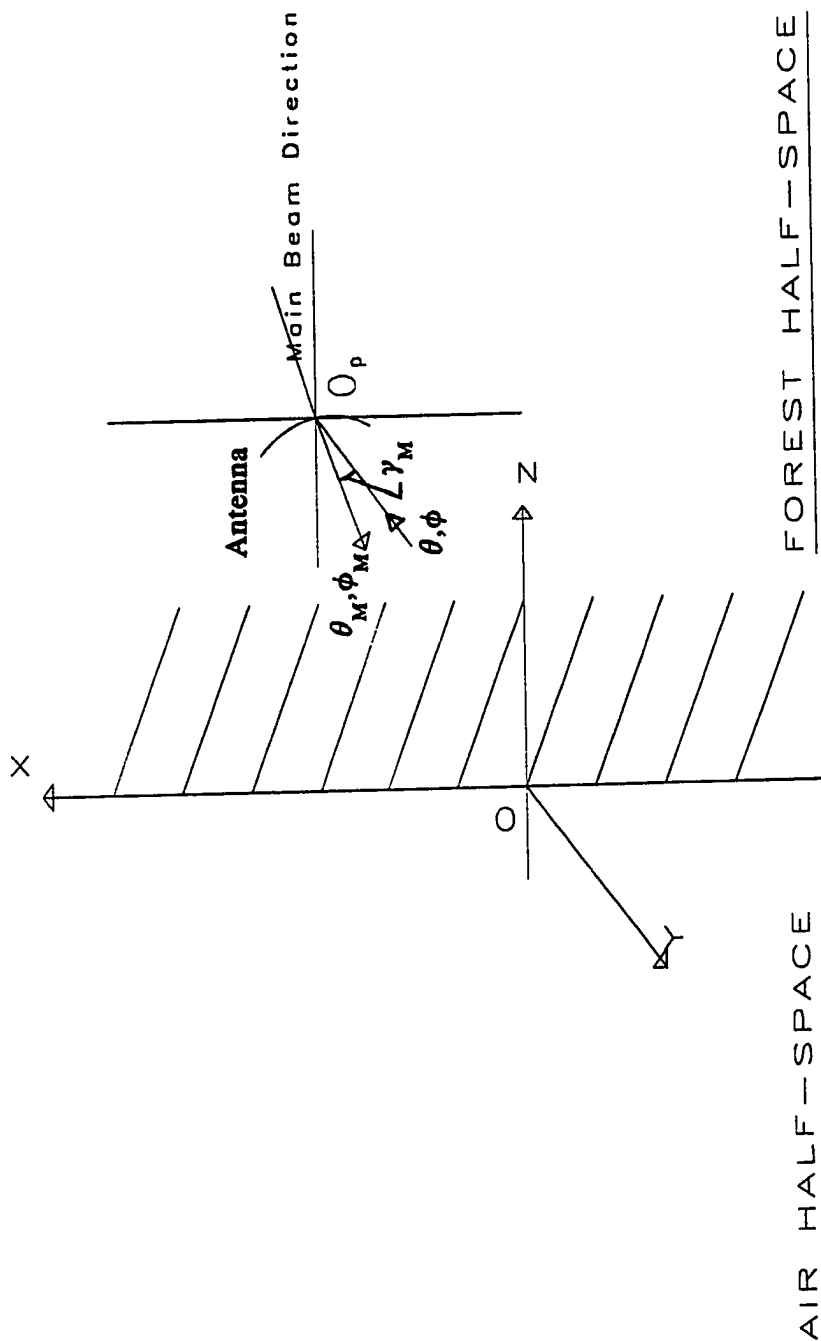


Fig. 1-5 Receiving antenna in a forest half space at point O_p . The angle γ_M is the angle included between the main beam direction of the antenna (θ_M, ϕ_M) and the direction of observation (θ, ϕ)

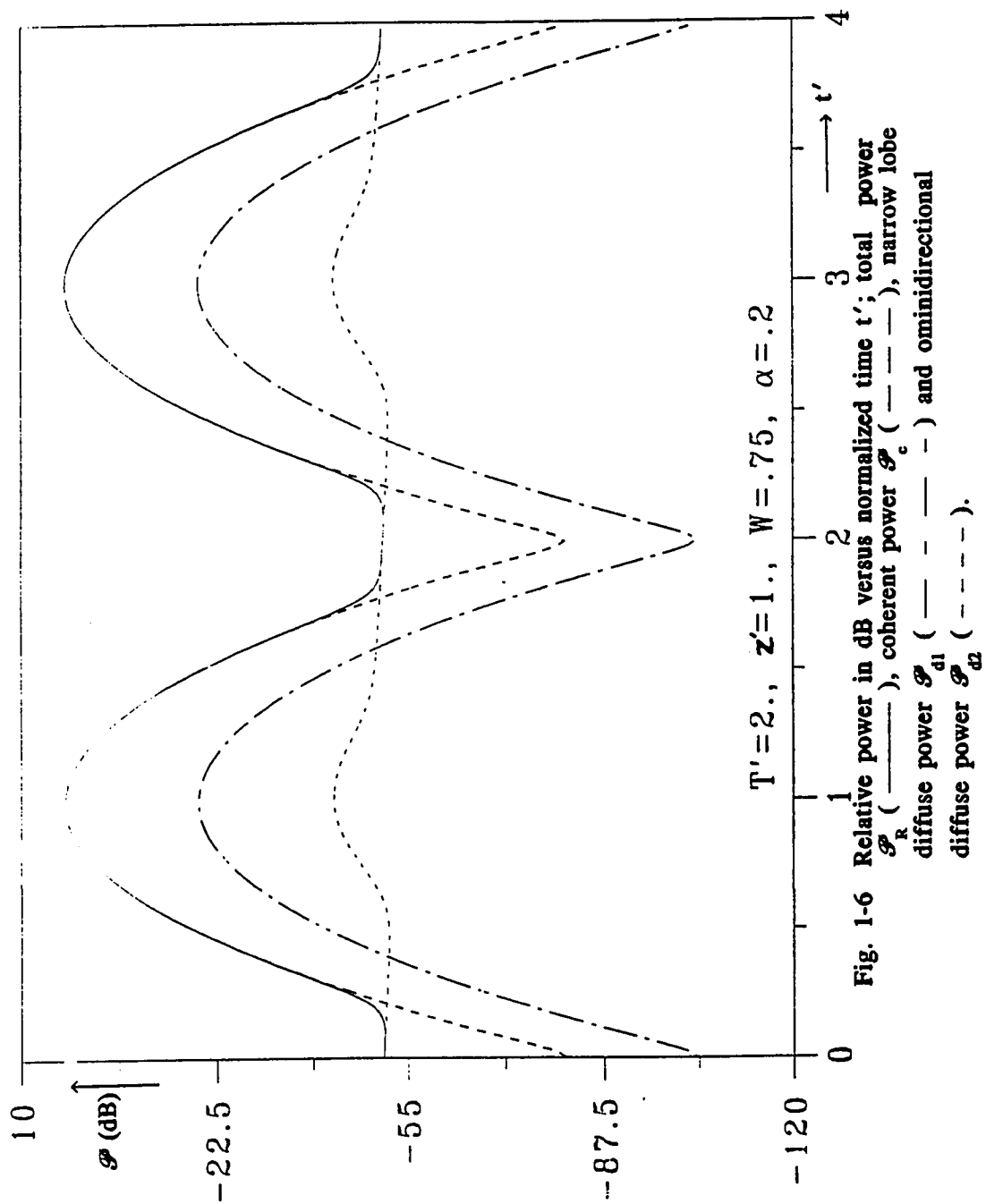


Fig. 1-6 Relative power in dB versus normalized time t' ; total power \mathcal{P}_R (—), coherent power \mathcal{P}_c (---), narrow lobe diffuse power \mathcal{P}_{d1} (---) and omnidirectional diffuse power \mathcal{P}_{d2} (- - - -).

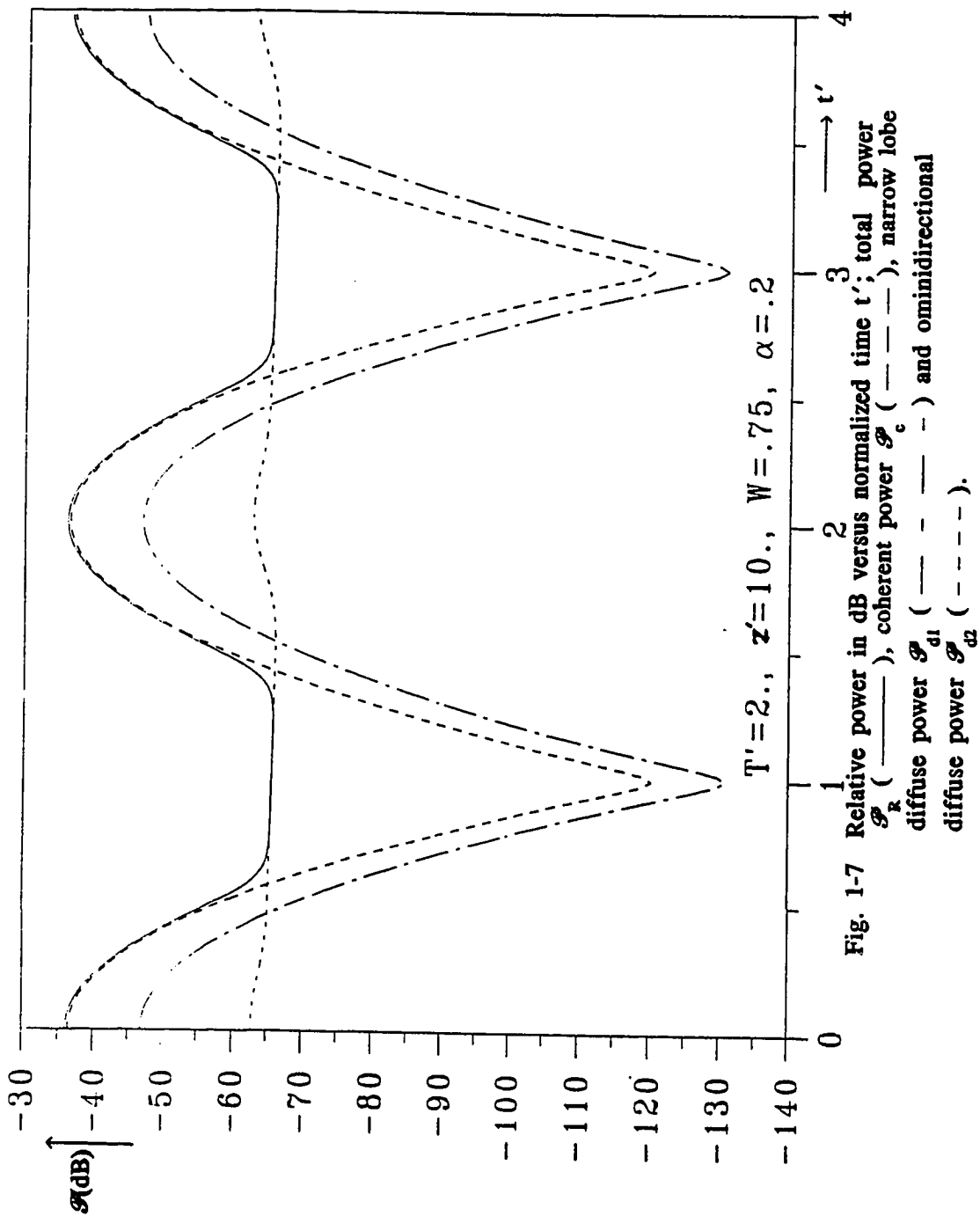


Fig. 1-7 Relative power in dB versus normalized time t' ; total power \mathcal{P}_r (—), coherent power \mathcal{P}_c (---), narrow lobe diffuse power \mathcal{P}_{d1} (- - -) and omnidirectional diffuse power \mathcal{P}_{d2} (- · - ·).

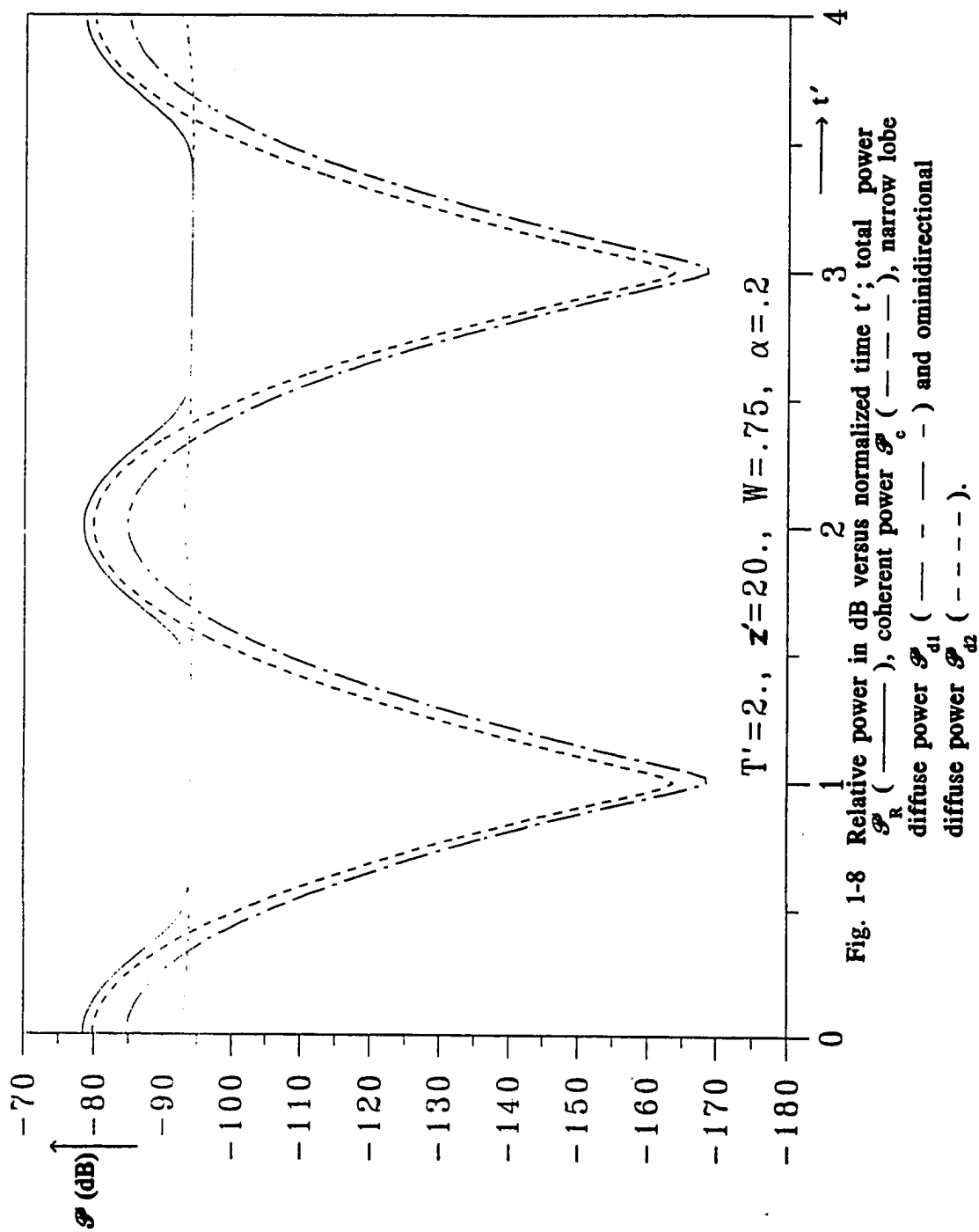


Fig. 1-8 Relative power in dB versus normalized time t' ; total power \mathcal{P}_R (—), coherent power \mathcal{P}_c (---), narrow lobe diffuse power \mathcal{P}_{d1} (---) and omnidirectional diffuse power \mathcal{P}_{d2} (-.-.-).

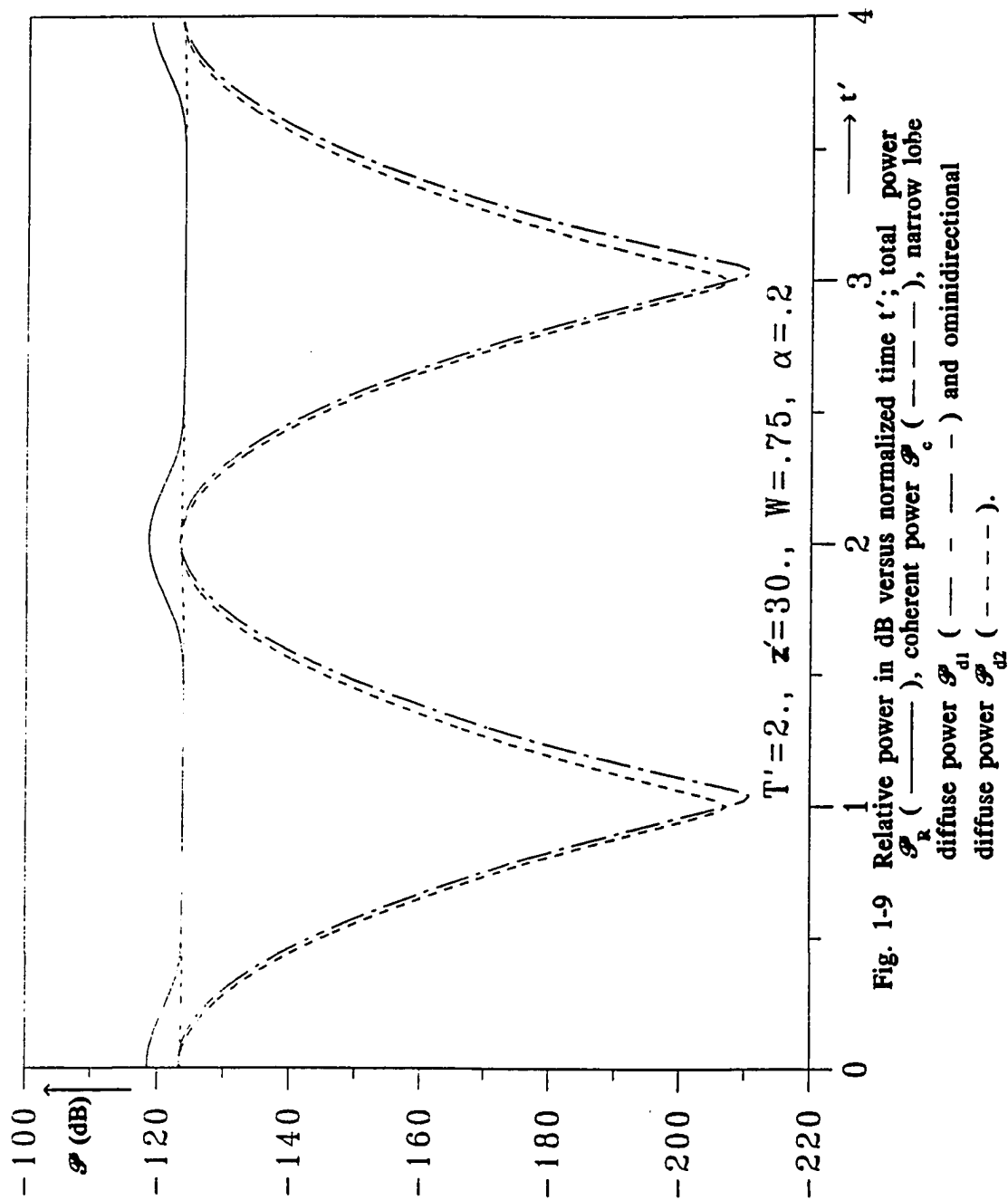


Fig. 1-9 Relative power in dB versus normalized time t' ; total power \mathcal{P}_R (—), coherent power \mathcal{P}_c (---), narrow lobe diffuse power \mathcal{P}_{d1} (---) and omnidirectional diffuse power \mathcal{P}_{d2} (- - - -).

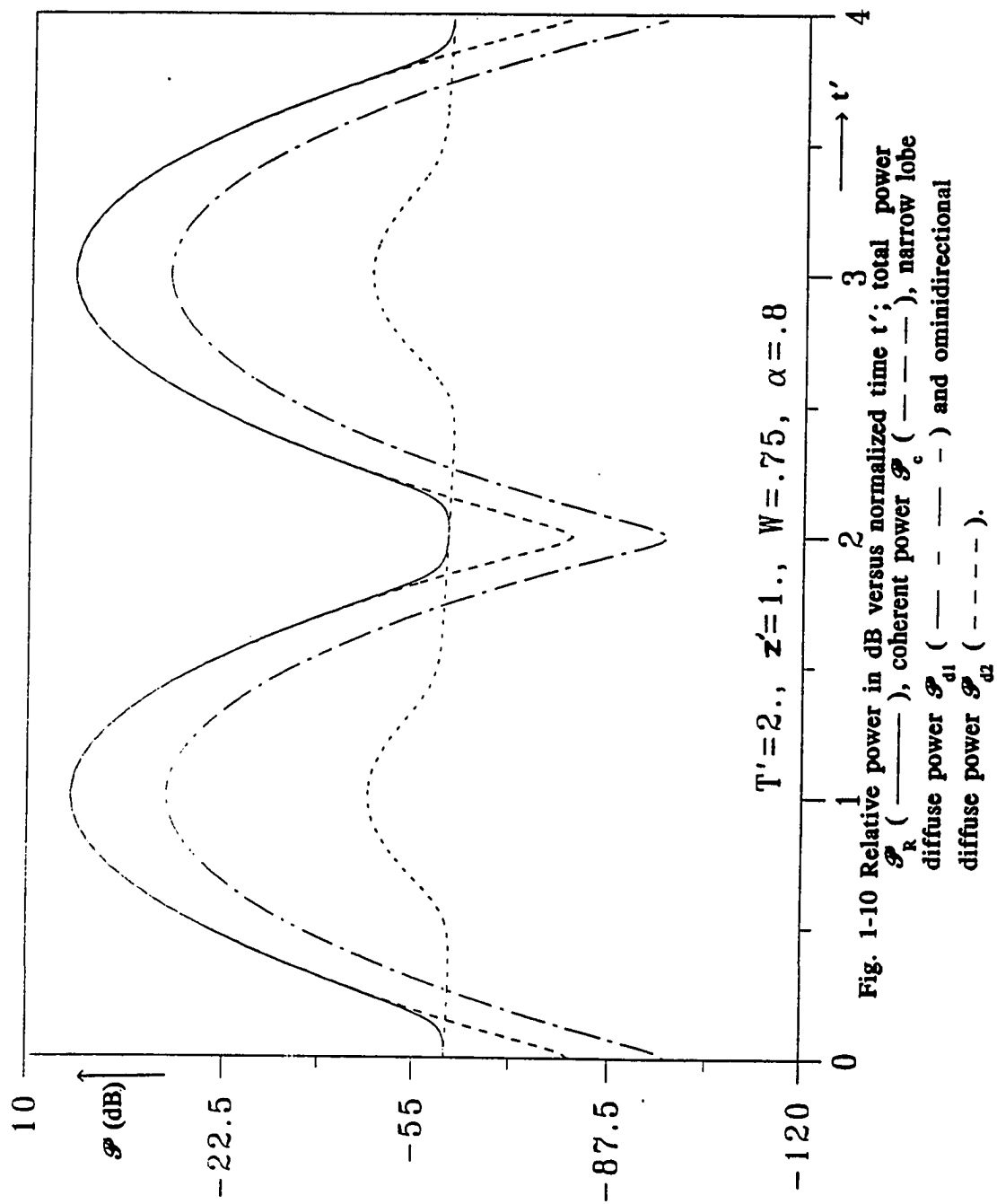


Fig. 1-10 Relative power in dB versus normalized time t' ; total power \mathcal{P}_R (—), coherent power \mathcal{P}_c (---), narrow lobe diffuse power \mathcal{P}_{d1} (- · - ·) and omnidirectional diffuse power \mathcal{P}_{d2} (· · · ·).

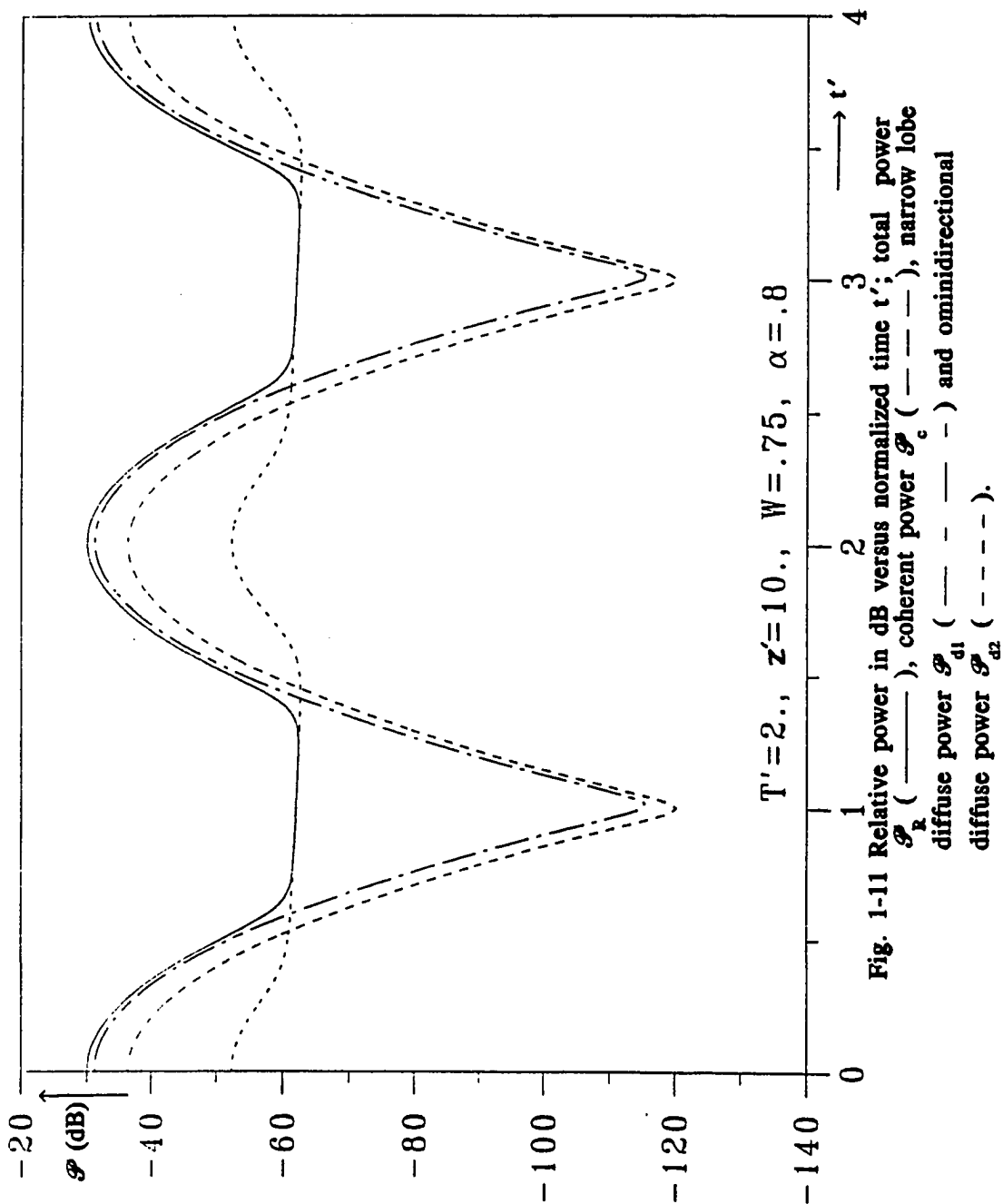


Fig. 1-11 Relative power in dB versus normalized time t' ; total power \mathcal{P}_R (—), coherent power \mathcal{P}_c (---), narrow lobe diffuse power \mathcal{P}_{d1} (- - -) and omnidirectional diffuse power \mathcal{P}_{d2} (- · - ·).

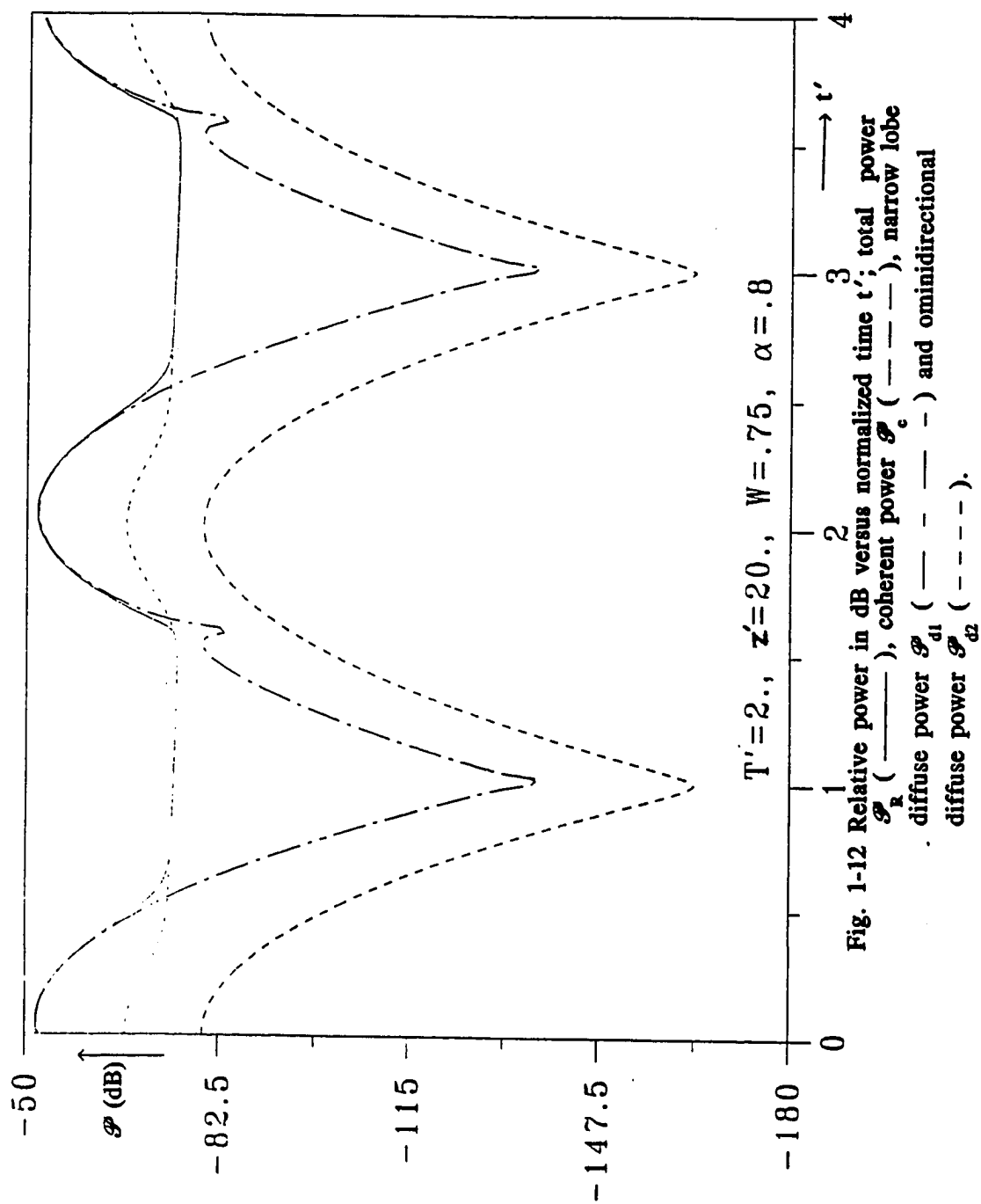


Fig. 1-12 Relative power in dB versus normalized time t' ; total power \mathcal{P}_t (—), coherent power \mathcal{P}_c (---), narrow lobe diffuse power \mathcal{P}_{d1} (- - - -) and omnidirectional diffuse power \mathcal{P}_{d2} (- · - · -).

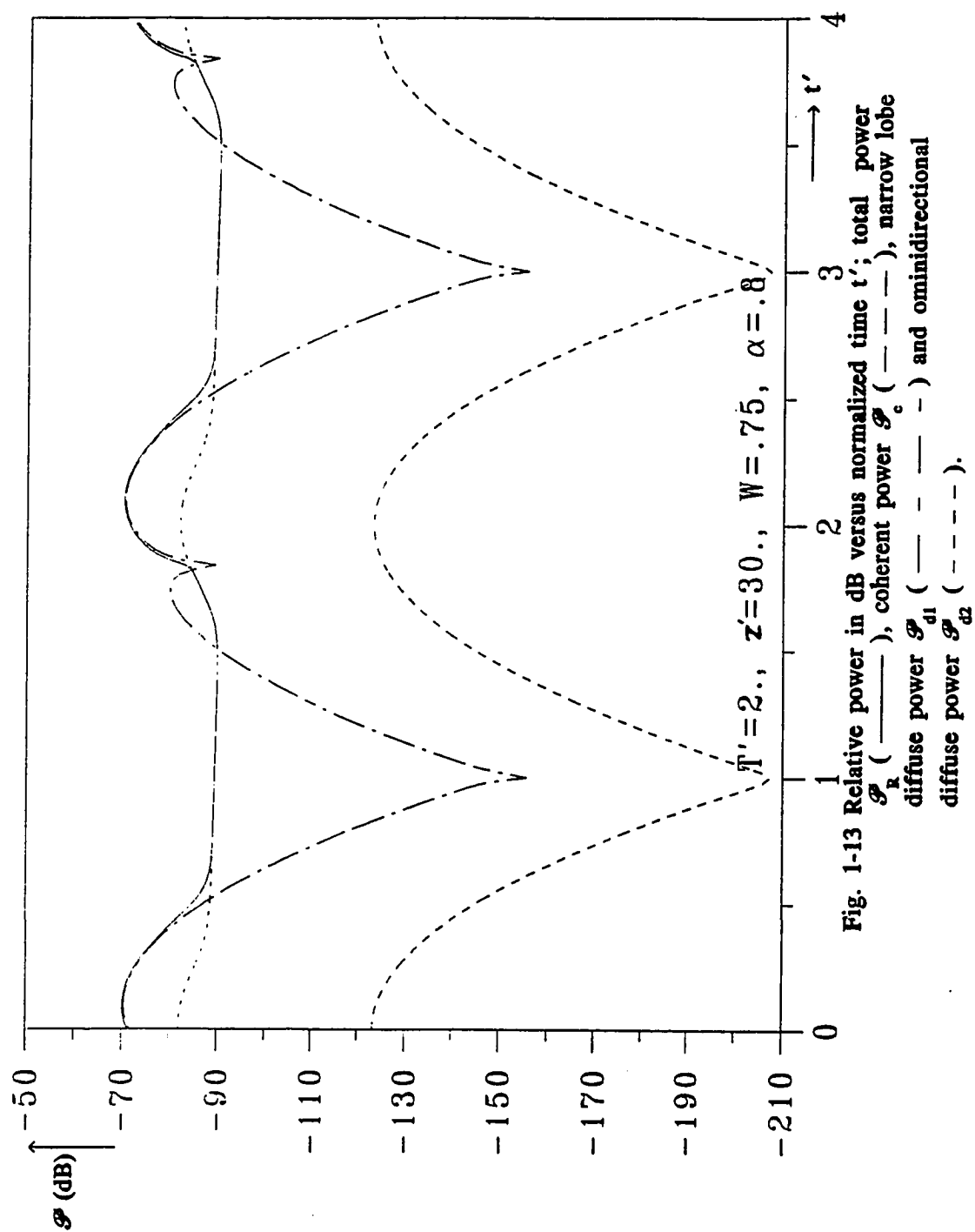


Fig. 1-13 Relative power in dB versus normalized time t' : total power \mathcal{P}_R (—), coherent power \mathcal{P}_c (---), narrow lobe diffuse power \mathcal{P}_{d1} (---) and omnidirectional diffuse power \mathcal{P}_{d2} (-.-.-).

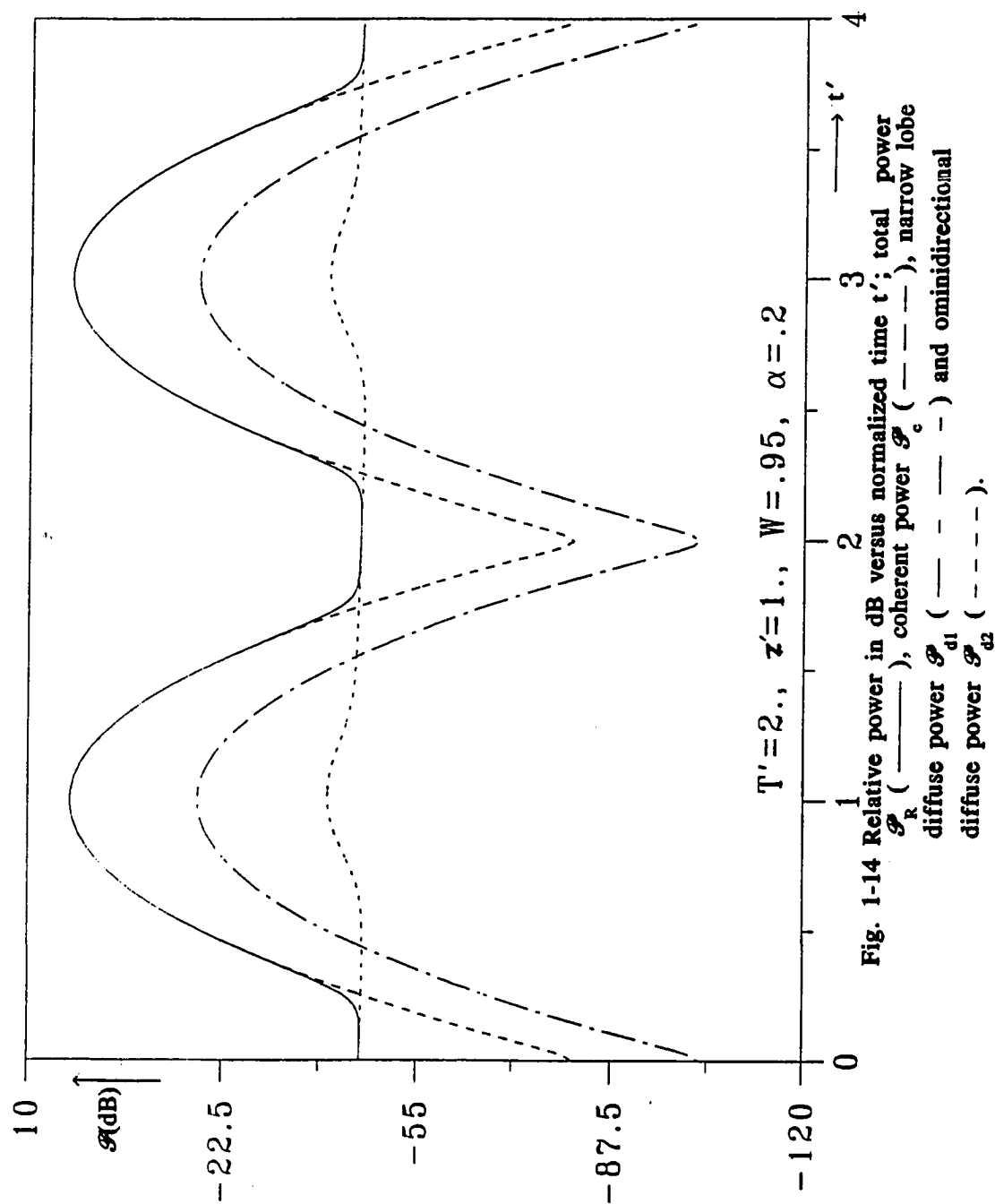


Fig. 1-14 Relative power in dB versus normalized time t' ; total power \mathcal{P}_R (—), coherent power \mathcal{P}_c (---), narrow lobe diffuse power \mathcal{P}_{d1} (---) and omnidirectional diffuse power \mathcal{P}_{d2} (-.-.-).

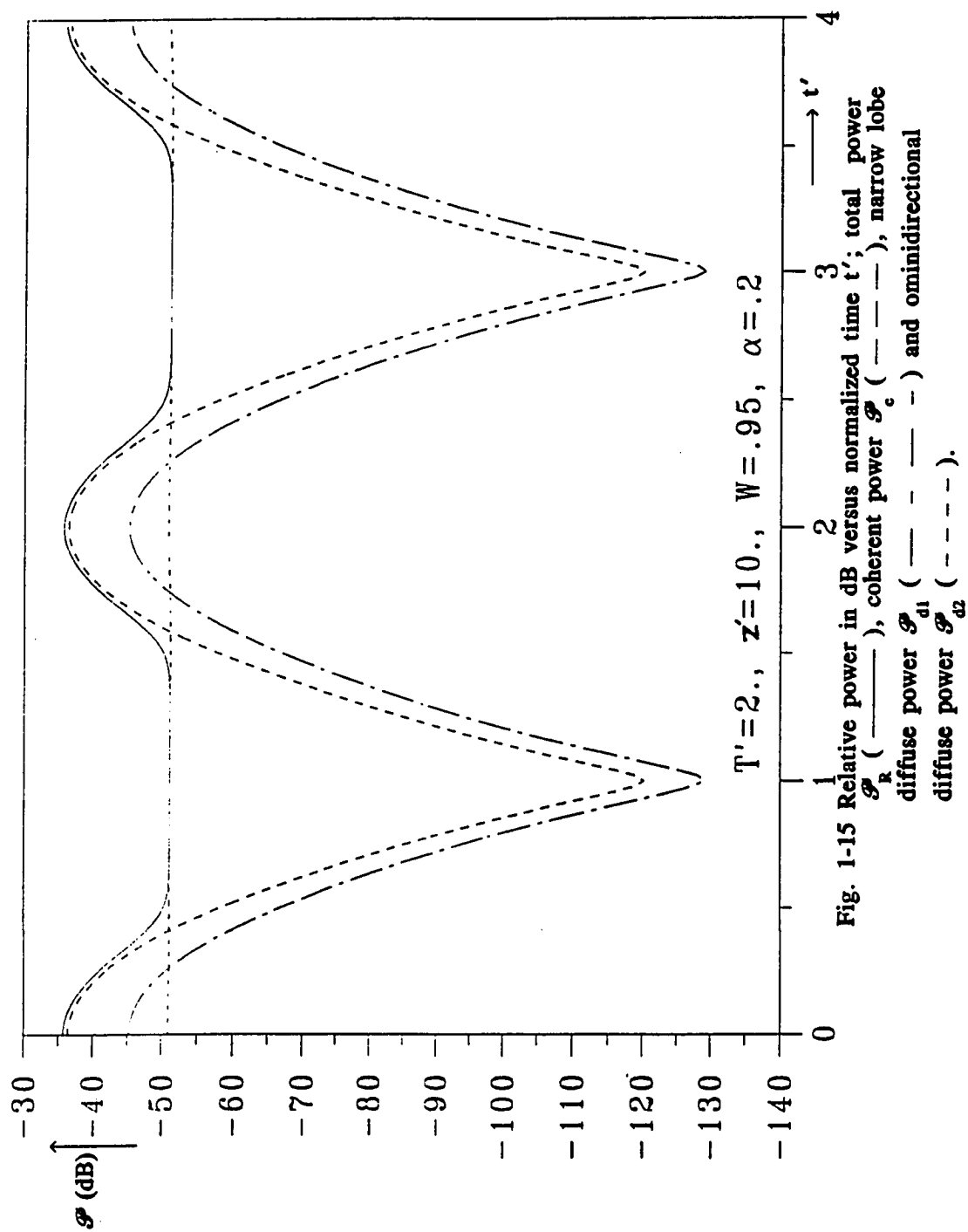


Fig. 1-15 Relative power in dB versus normalized time t' ; total power \mathcal{P}_R (—), coherent power \mathcal{P}_c (---), narrow lobe diffuse power \mathcal{P}_{d1} (---) and omnidirectional diffuse power \mathcal{P}_{d2} (- - - -).

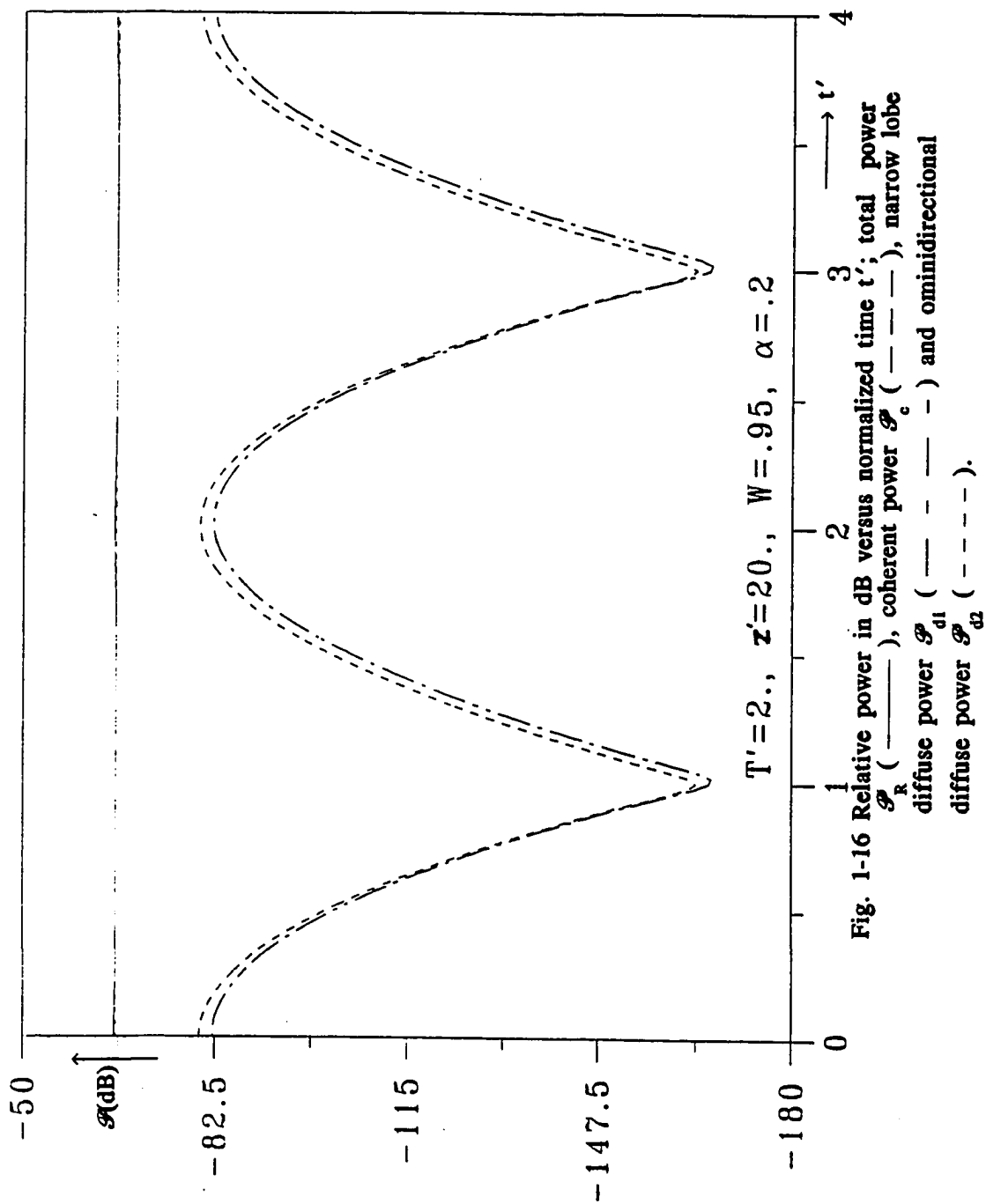


Fig. 1-16 Relative power in dB versus normalized time t' ; total power \mathcal{P}_R (—), coherent power \mathcal{P}_c (---), narrow lobe diffuse power \mathcal{P}_{d1} (---) and omnidirectional diffuse power \mathcal{P}_{d2} (- - - -).

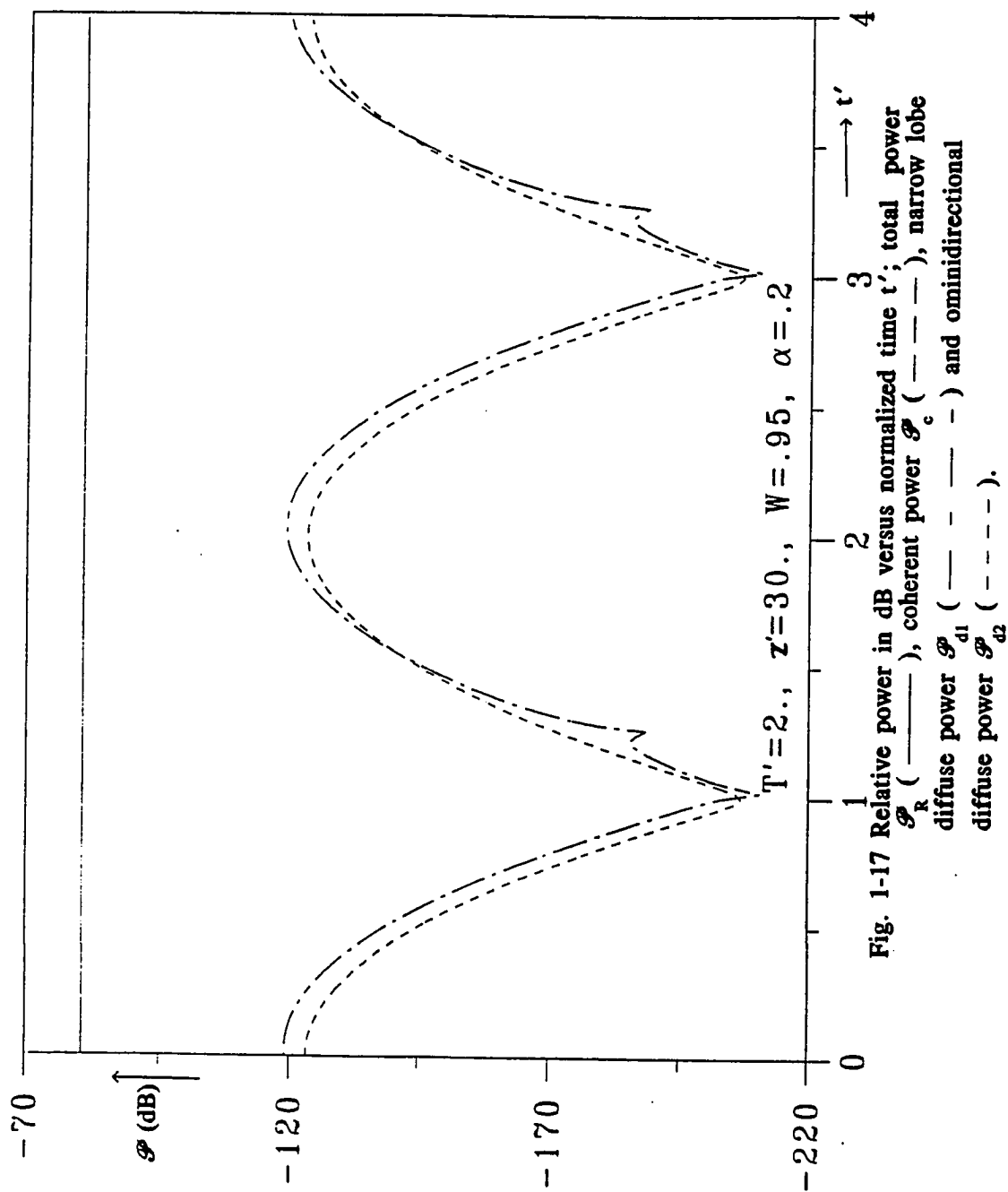


Fig. 1-17 Relative power in dB versus normalized time t' ; total power \mathcal{P}_R (—), coherent power \mathcal{P}_c (---), narrow lobe diffuse power \mathcal{P}_{d1} (- · - · -) and omnidirectional diffuse power \mathcal{P}_{d2} (----).

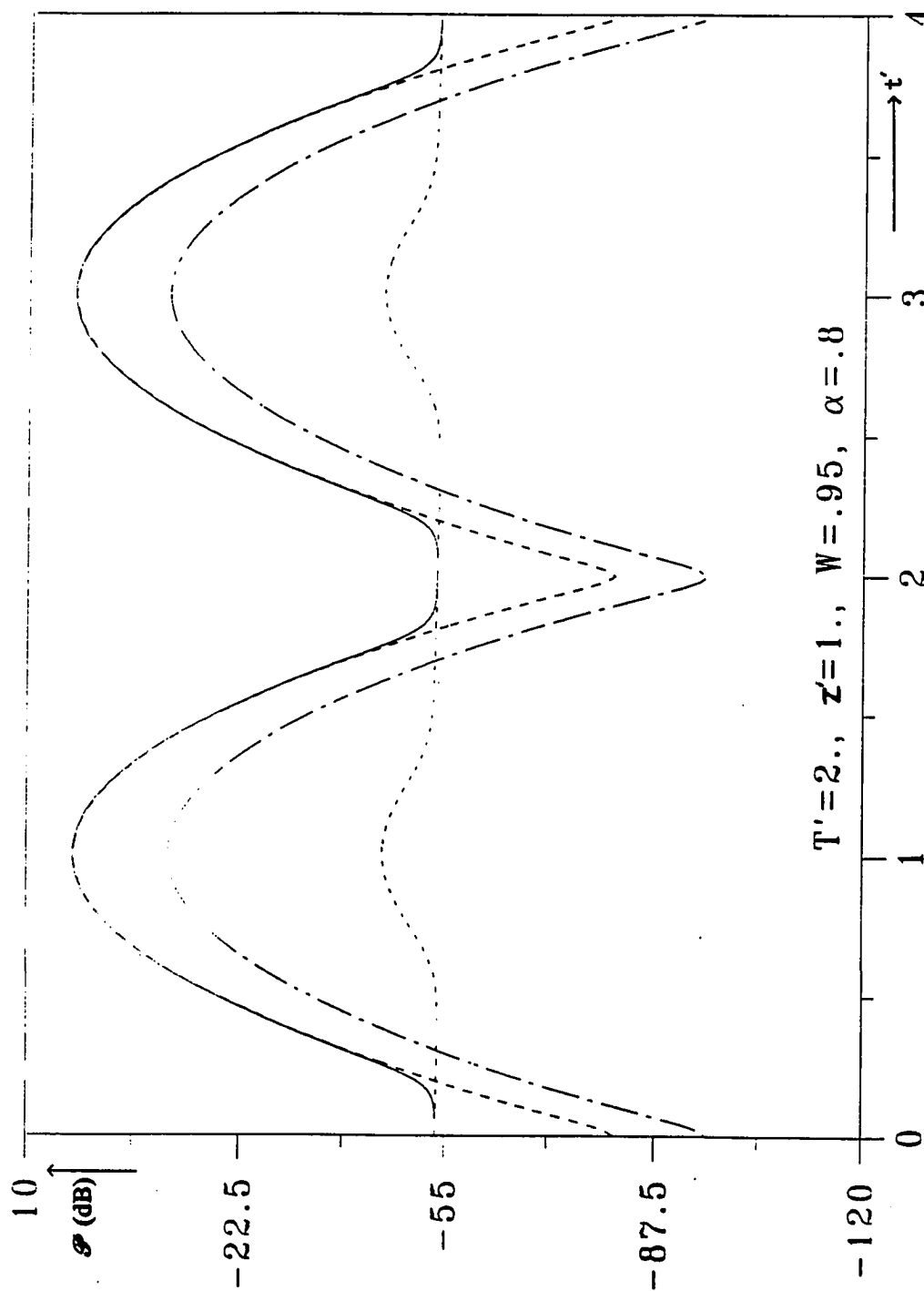


Fig. 1-18 Relative power in dB versus normalized time t' : total power \mathcal{P}_R (—), coherent power \mathcal{P}_c (---), narrow lobe diffuse power \mathcal{P}_{d1} (- - -) and omnidirectional diffuse power \mathcal{P}_{d2} (- · - ·).

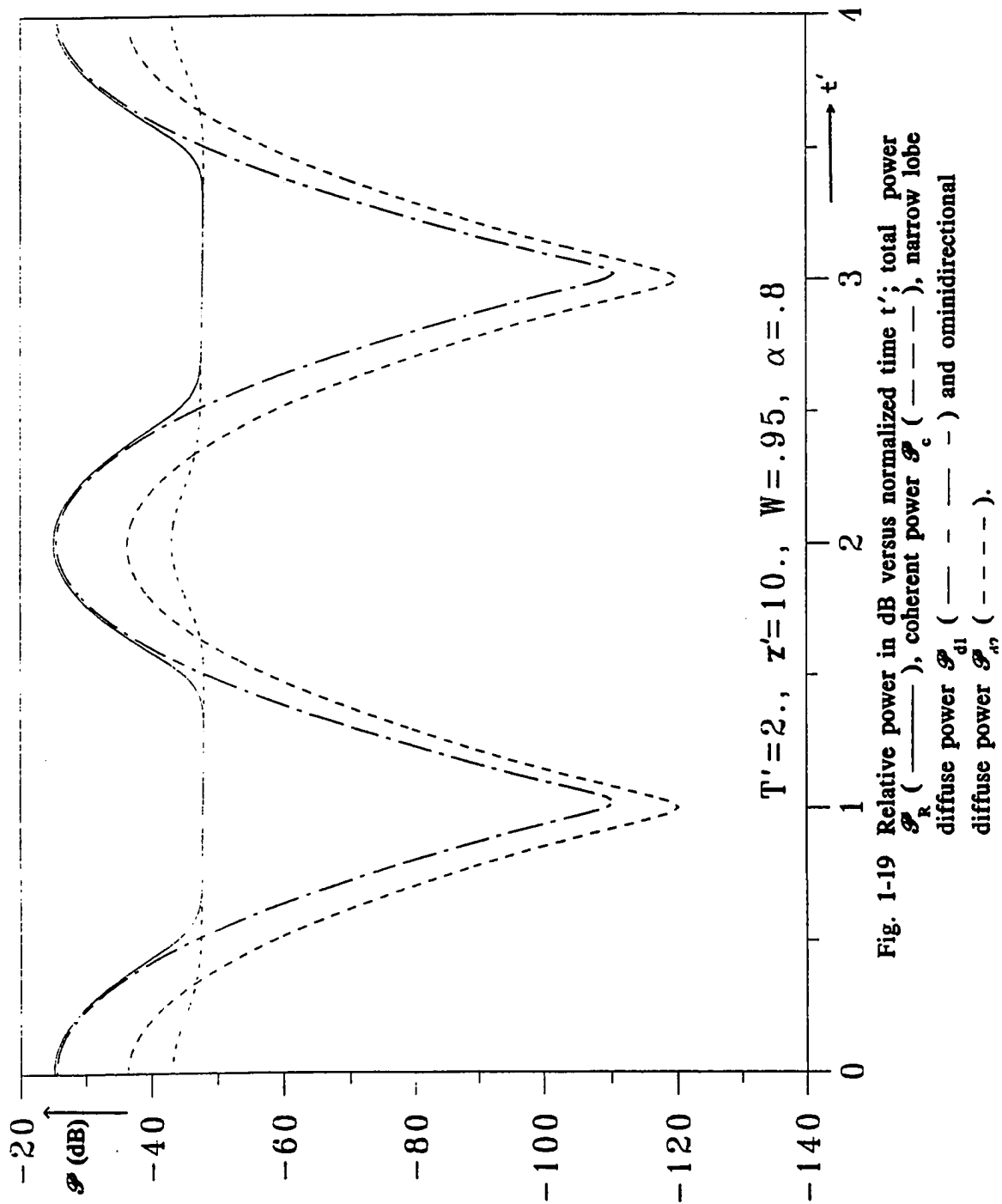


Fig. 1-19 Relative power in dB versus normalized time t' ; total power \mathcal{P}_R (—), coherent power \mathcal{P}_c (---), narrow lobe diffuse power \mathcal{P}_{d1} (---) and omnidirectional diffuse power \mathcal{P}_{d2} (-.-.-).

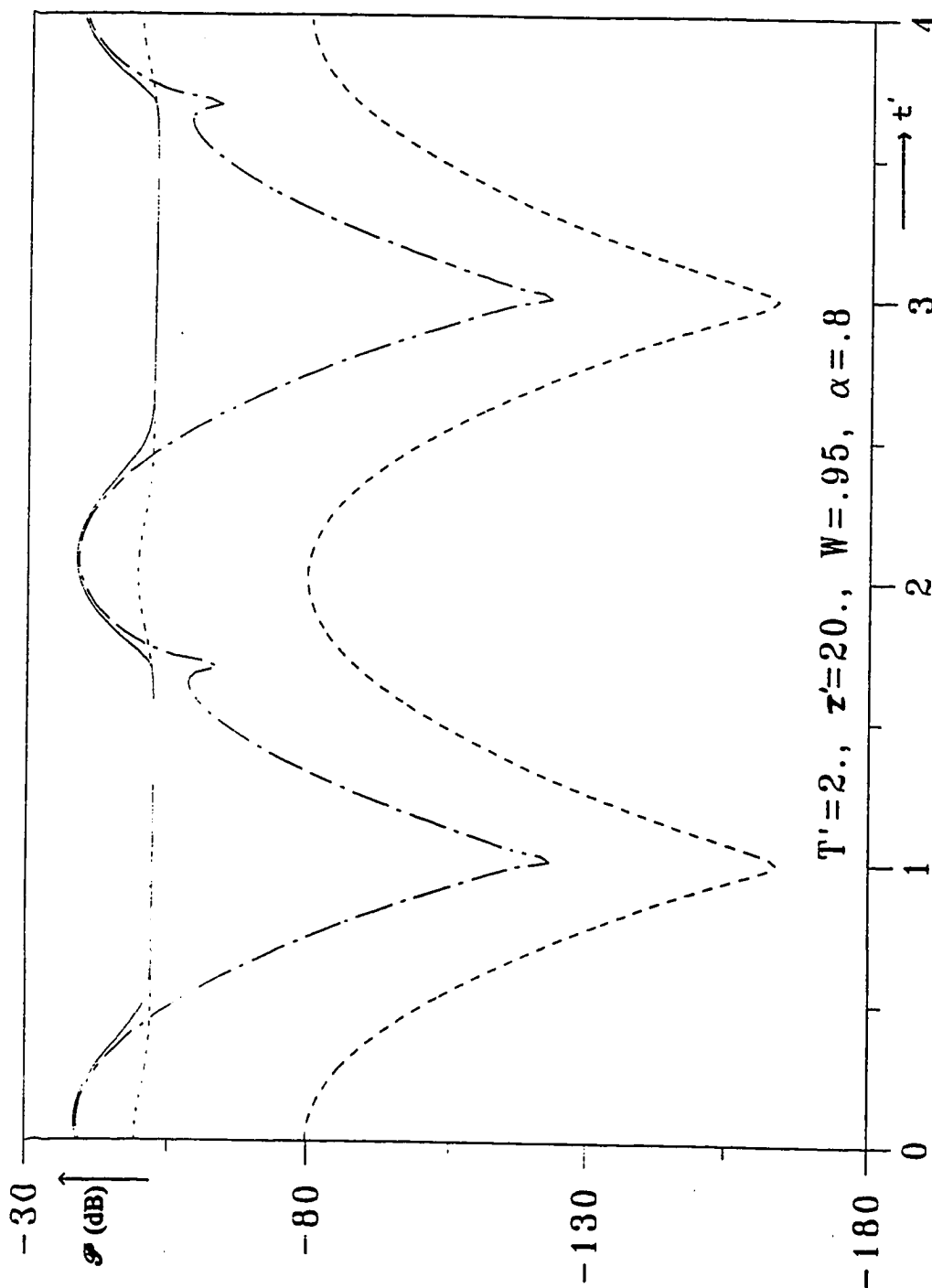


Fig. 1-20 Relative power in dB versus normalized time t' ; total power \mathcal{P}_R (—), coherent power \mathcal{P}_c (---), narrow lobe diffuse power \mathcal{P}_{d1} (- - -) and omnidirectional diffuse power \mathcal{P}_{d2} (- · - ·).

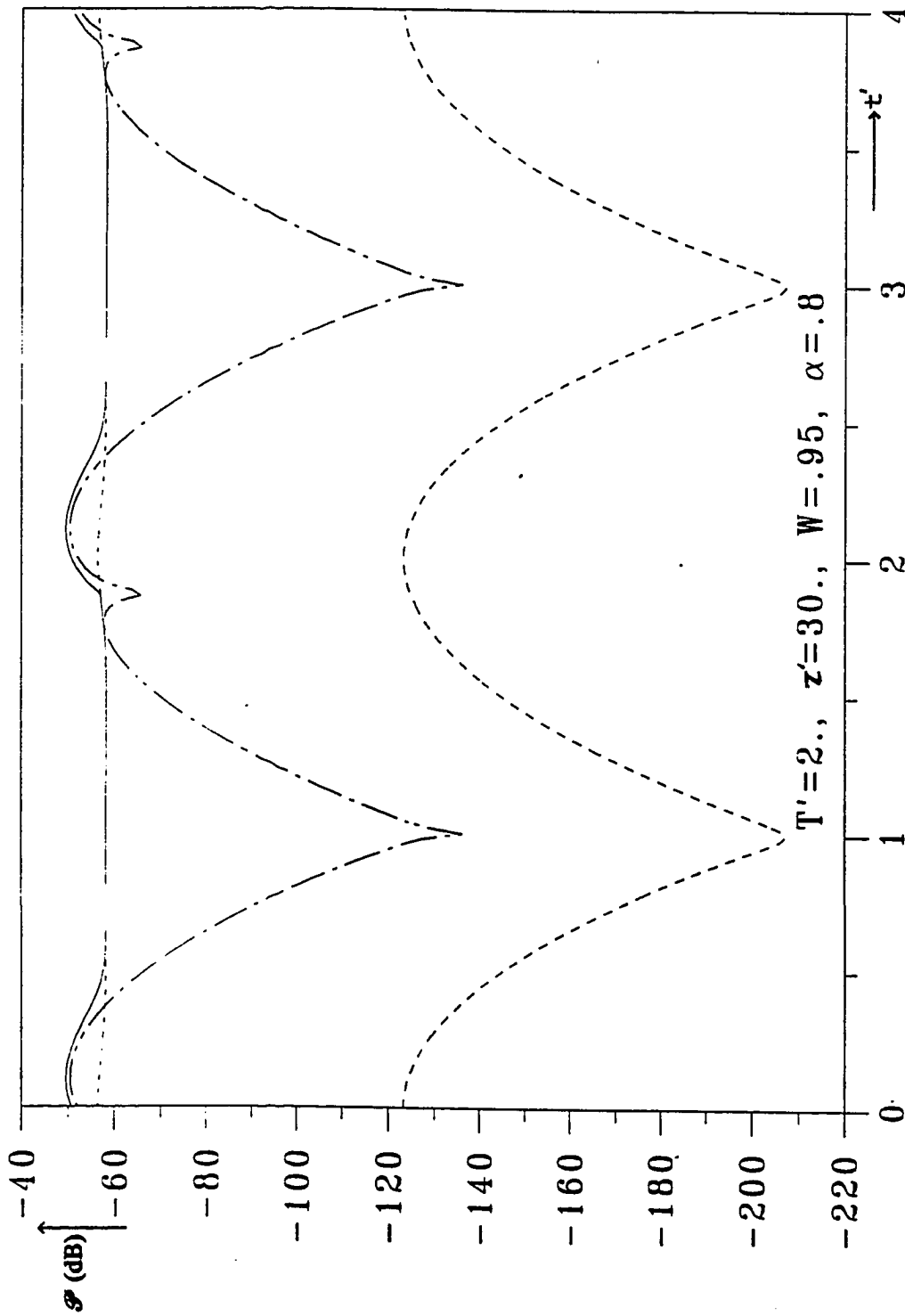


Fig. 1-21 Relative power in dB versus normalized time t' ; total power \mathcal{P}_r (—), coherent power \mathcal{P}_c (---), narrow lobe diffuse power \mathcal{P}_{d1} (- - -) and omnidirectional diffuse power \mathcal{P}_{d2} (- · - ·).

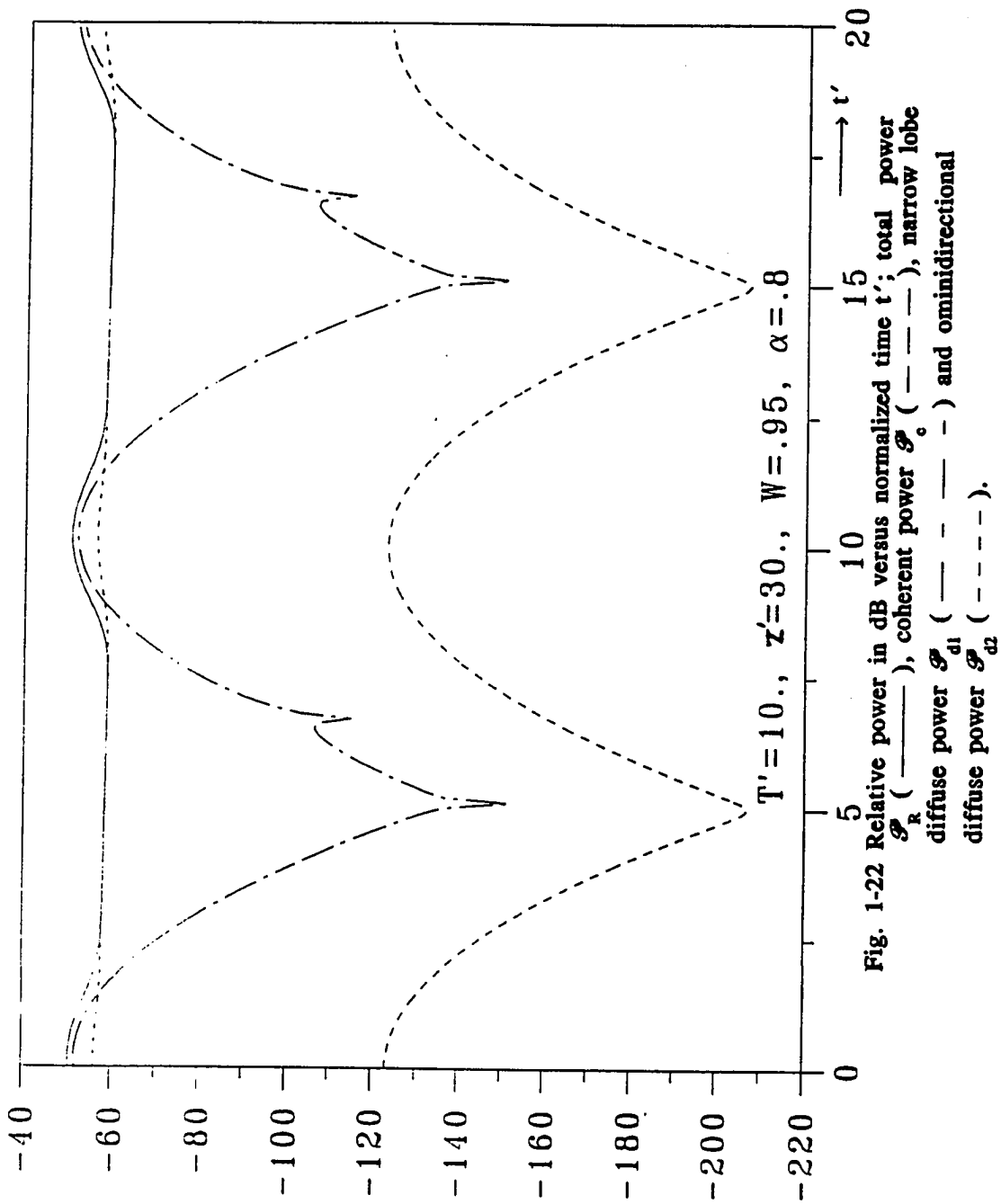


Fig. 1-22 Relative power in dB versus normalized time t' ; total power \mathcal{P}_R (—), coherent power \mathcal{P}_c (---), narrow lobe diffuse power \mathcal{P}_{d1} (---) and omnidirectional diffuse power \mathcal{P}_{d2} (- - - -).

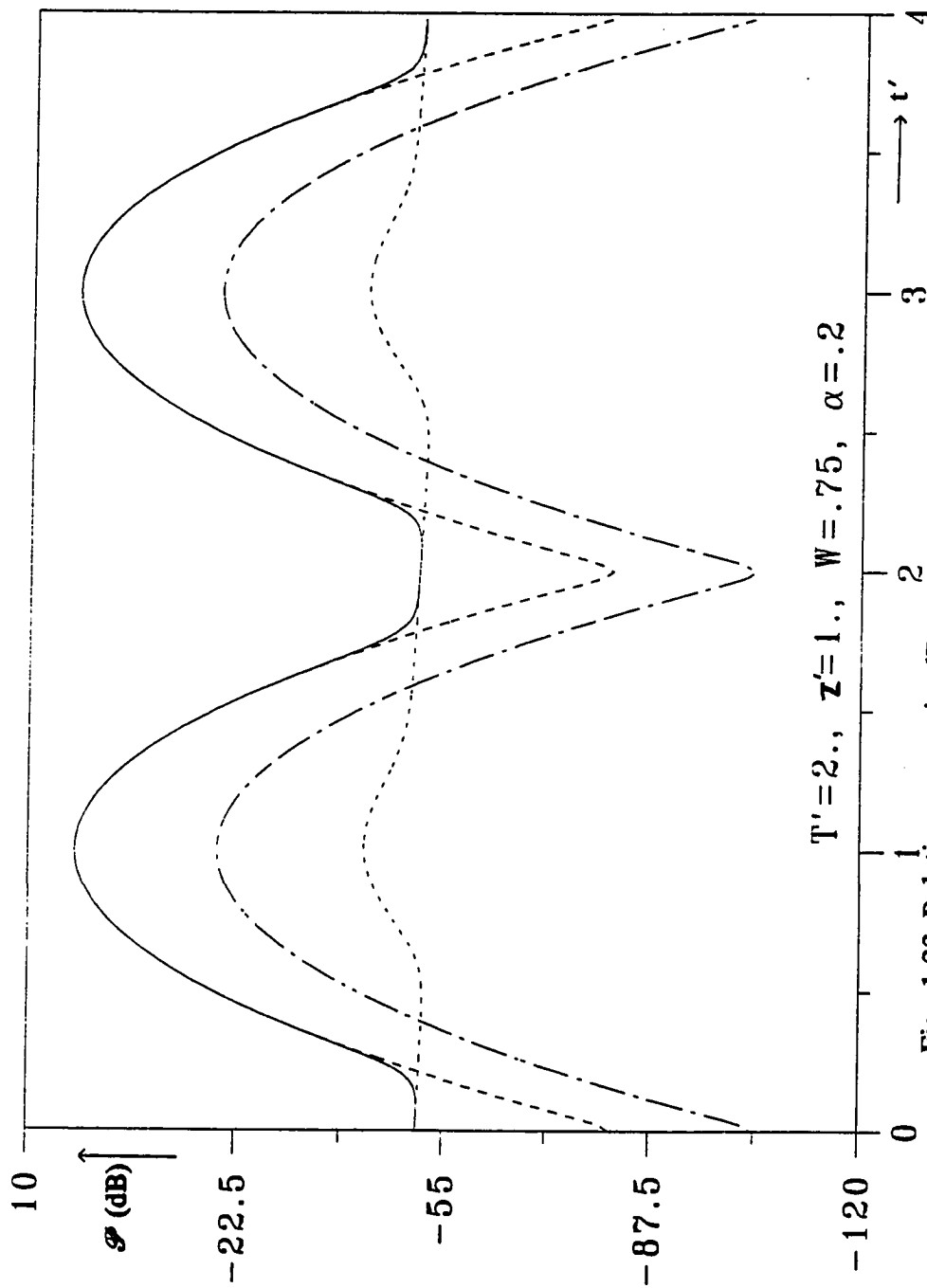


Fig. 1-23 Relative power in dB versus normalized time t' ; total power \mathcal{P}_R (—), coherent power \mathcal{P}_c (---), narrow lobe diffuse power \mathcal{P}_{d1} (- - -) and omnidirectional diffuse power \mathcal{P}_{d2} (· · ·) \therefore zero order approximation case

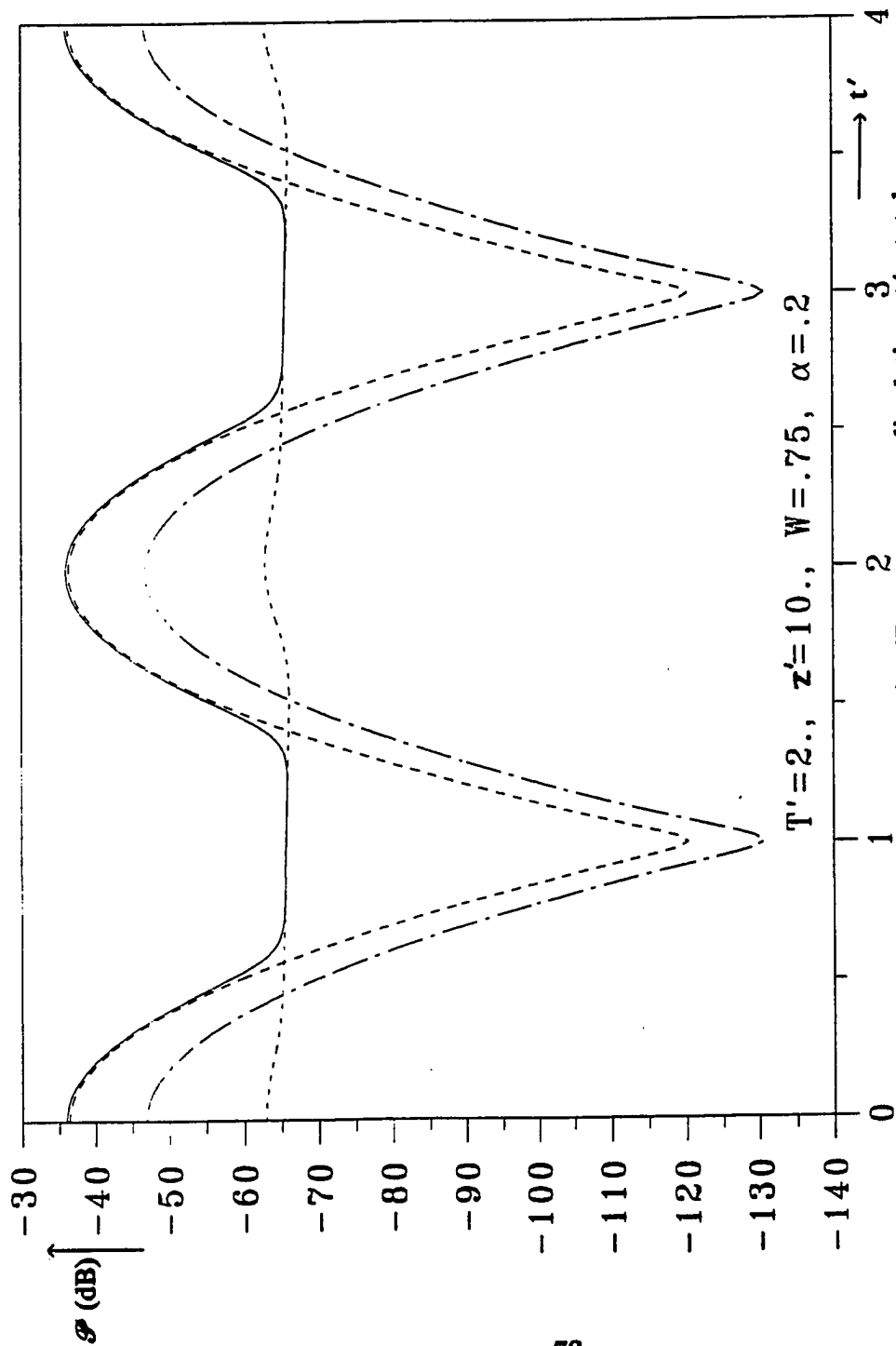


Fig. 1-24 Relative power in dB versus normalized time t' ; total power \mathcal{P}_R (—), coherent power \mathcal{P}_c (---), narrow lobe diffuse power \mathcal{P}_{d1} (- · - · -) and omnidirectional diffuse power \mathcal{P}_{d2} (----): zero order approximation case.

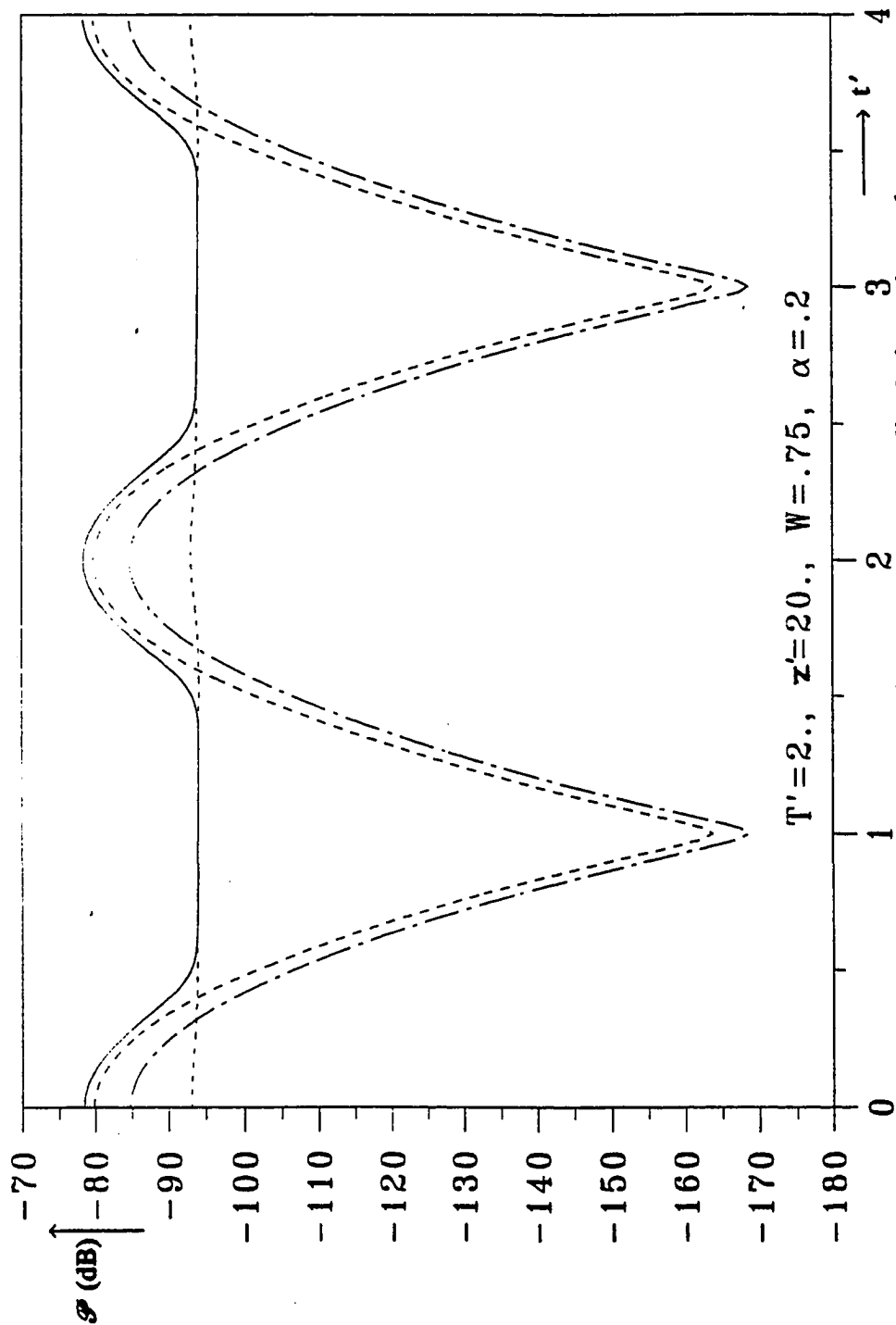


Fig. 1-25 Relative power in dB versus normalized time t' ; total power \mathcal{P}_R (—), coherent power \mathcal{P}_c (---), narrow lobe diffuse power \mathcal{P}_{d1} (---) and ominidirectional diffuse power \mathcal{P}_{a2} (- - - -) : zero order approximation case.

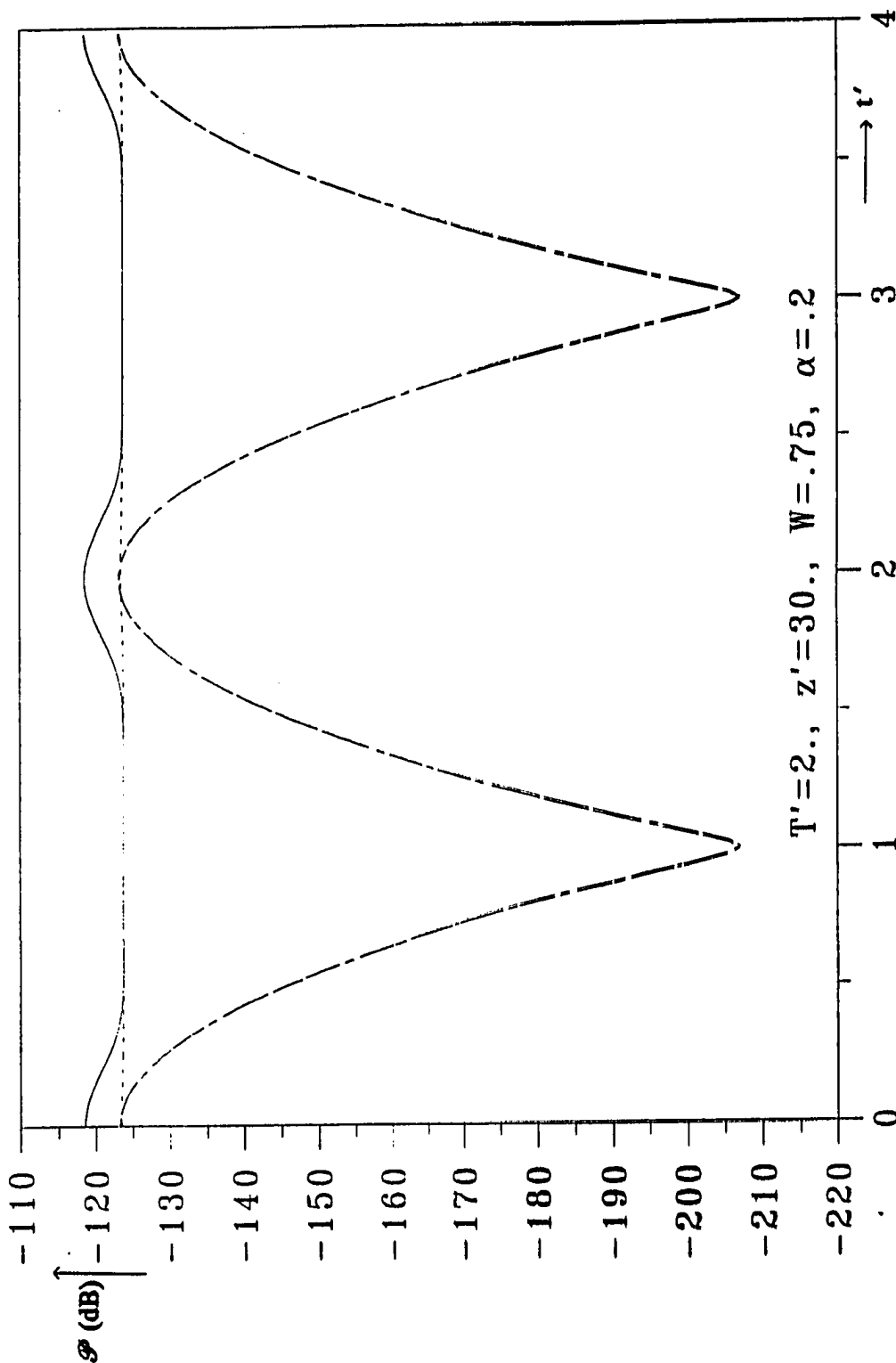


Fig. 1-26 Relative power in dB versus normalized time t' ; total power \mathcal{P}_t (—), coherent power \mathcal{P}_c (---), narrow lobe diffuse power \mathcal{P}_{d1} (---) and omnidirectional diffuse power \mathcal{P}_{d2} (- · - · -); zero order approximation case.

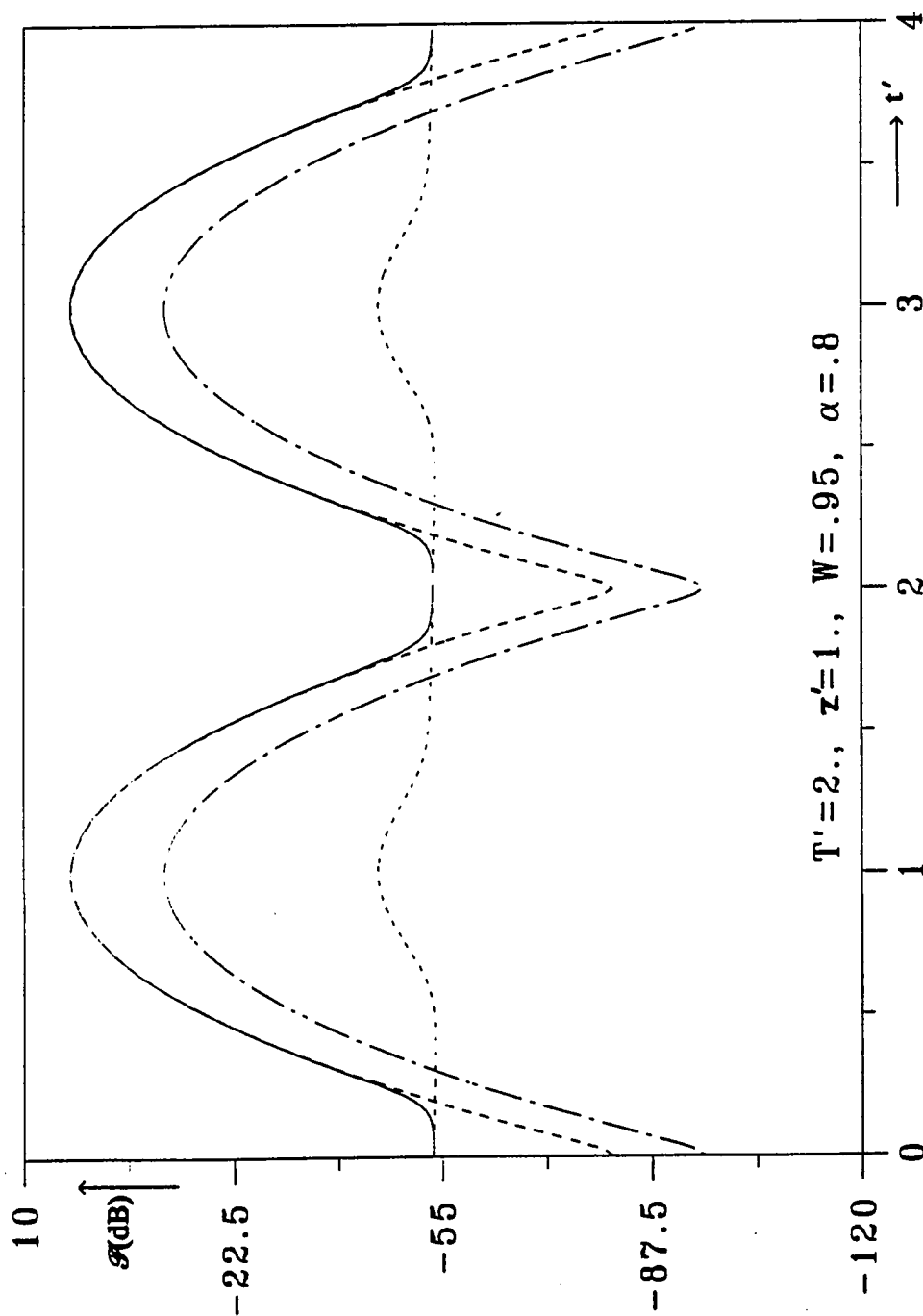


Fig. 1-27 Relative power in dB versus normalized time t' ; total power \mathcal{P}_R (—), coherent power \mathcal{P}_c (---), narrow lobe diffuse power \mathcal{P}_{d1} (---) and omnidirectional diffuse power \mathcal{P}_{d2} (- - - -): zero order approximation case.

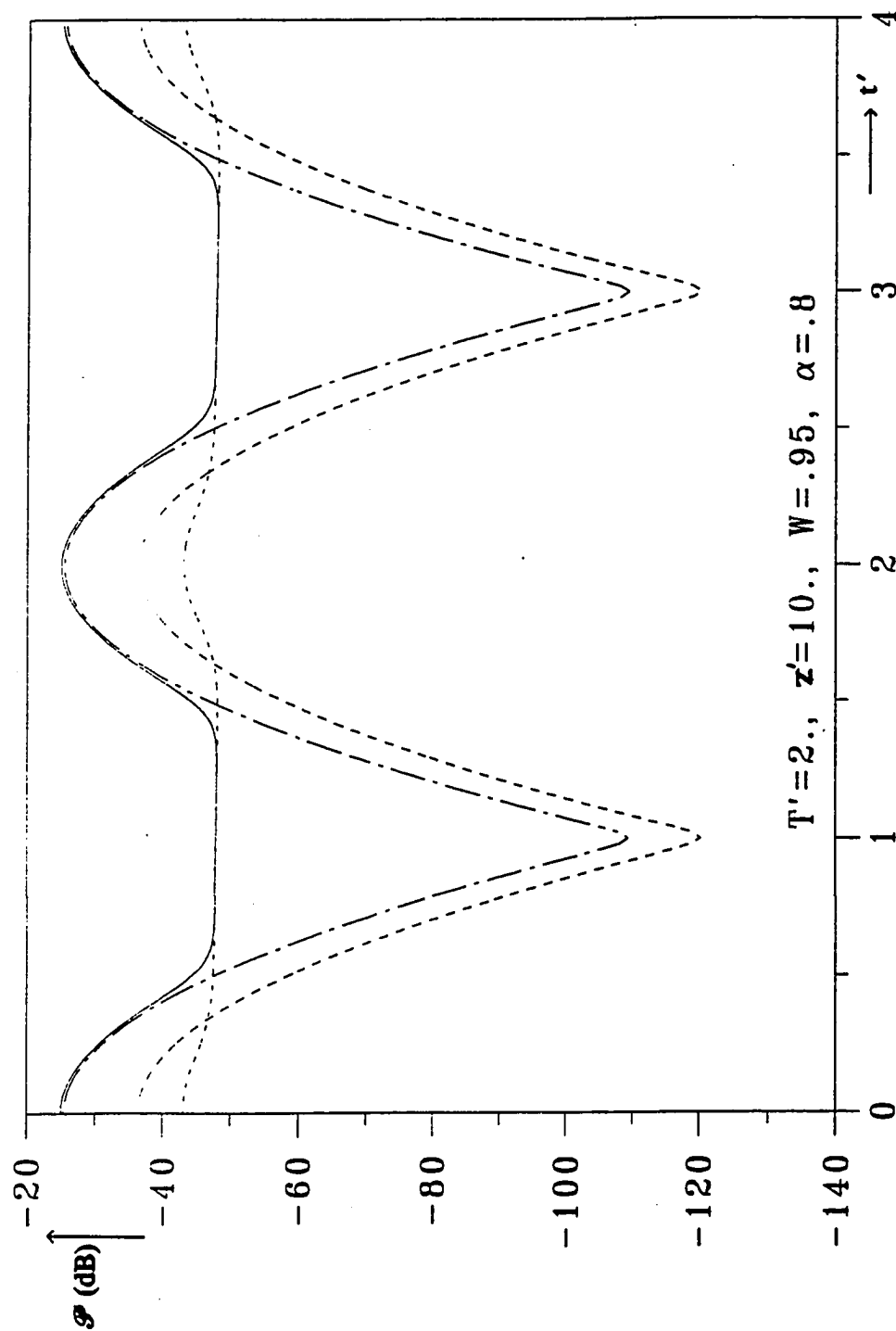


Fig. 1-28 Relative power in dB versus normalized time t' ; total power \mathcal{P}_R (— — —), coherent power \mathcal{P}_c (— — — —), narrow lobe diffuse power \mathcal{P}_{d1} (— — — —) and omnidirectional diffuse power \mathcal{P}_{d2} (— · — · —); zero order approximation case.

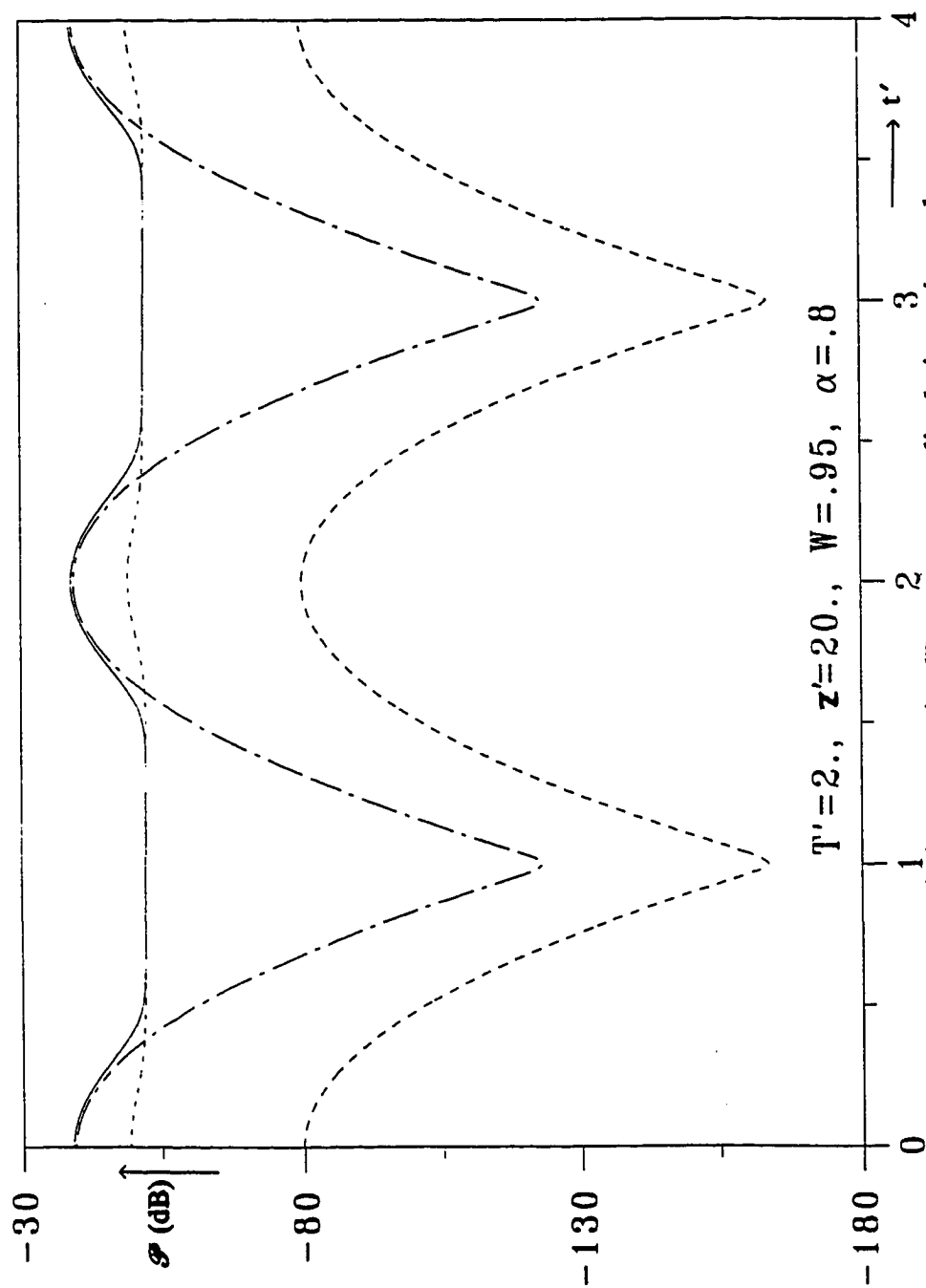


Fig. 1-29 Relative power in dB versus normalized time t' ; total power P_R (—), coherent power P_c (---), narrow lobe diffuse power P_{d1} (- · - · -) and omnidirectional diffuse power P_{d2} (- - - -): zero order approximation case.

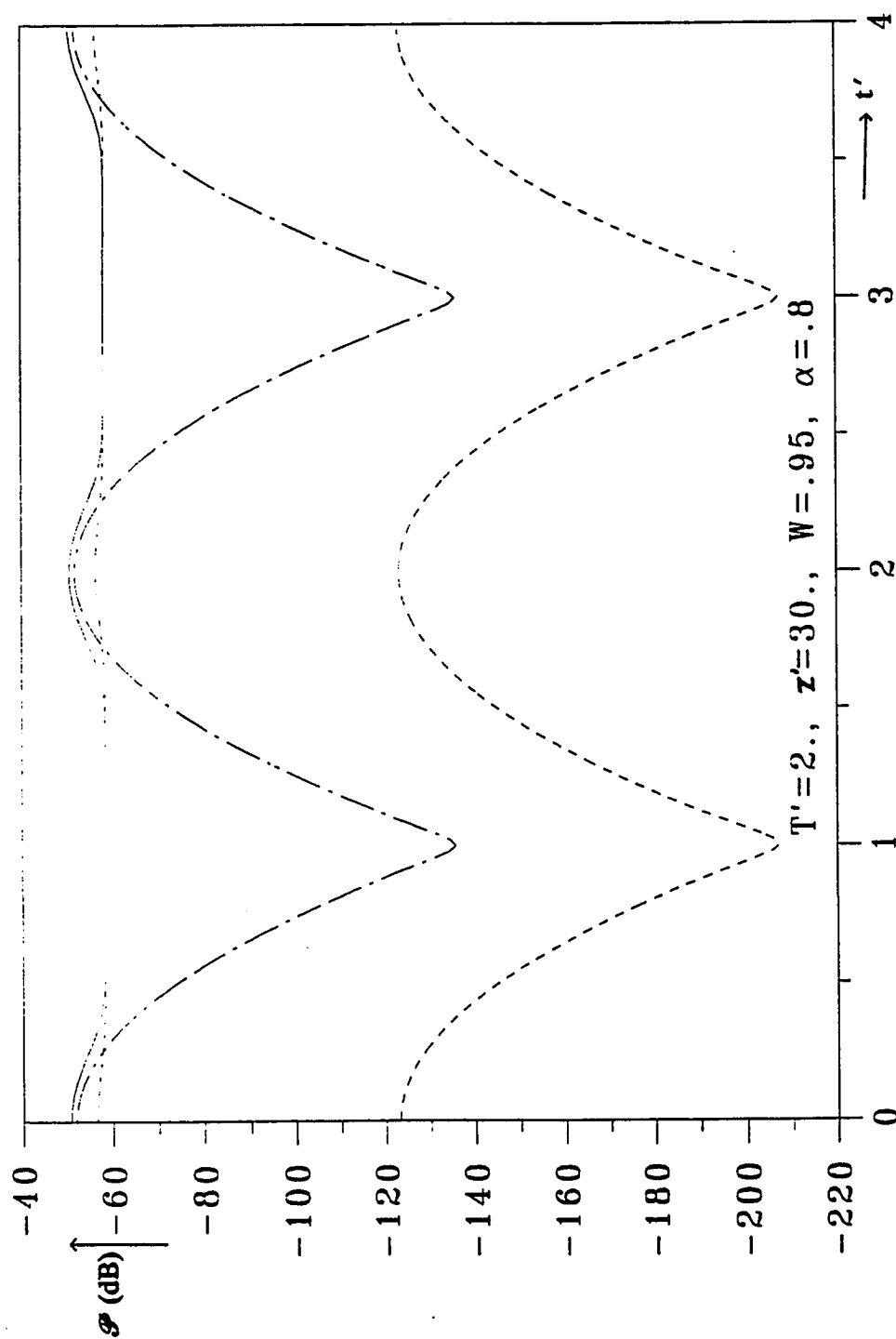


Fig. 1-30 Relative power in dB versus normalized time t' ; total power \mathcal{P}_R (—), coherent power \mathcal{P}_c (---), narrow lobe diffuse power \mathcal{P}_{d1} (---) and omnidirectional diffuse power \mathcal{P}_{d2} (- - - -); zero order approximation case.

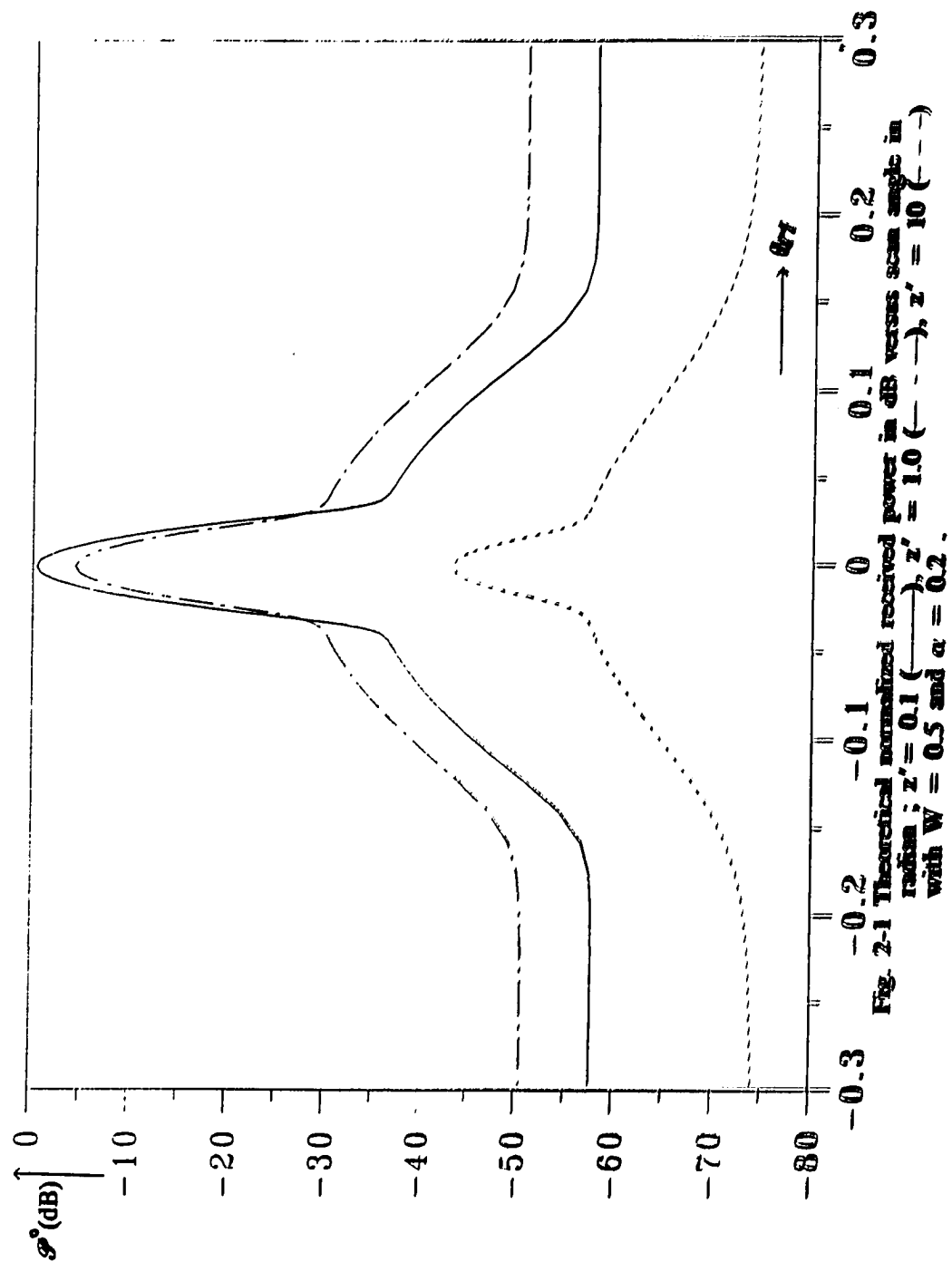


Fig. 2-1 Theoretical normalized received power in dB versus scan angle in radians ; $z' = 0.1$ (—), $z' = 1.0$ (---), $z' = 10$ (· · ·) with $W = 0.5$ and $\alpha = 0.2$.

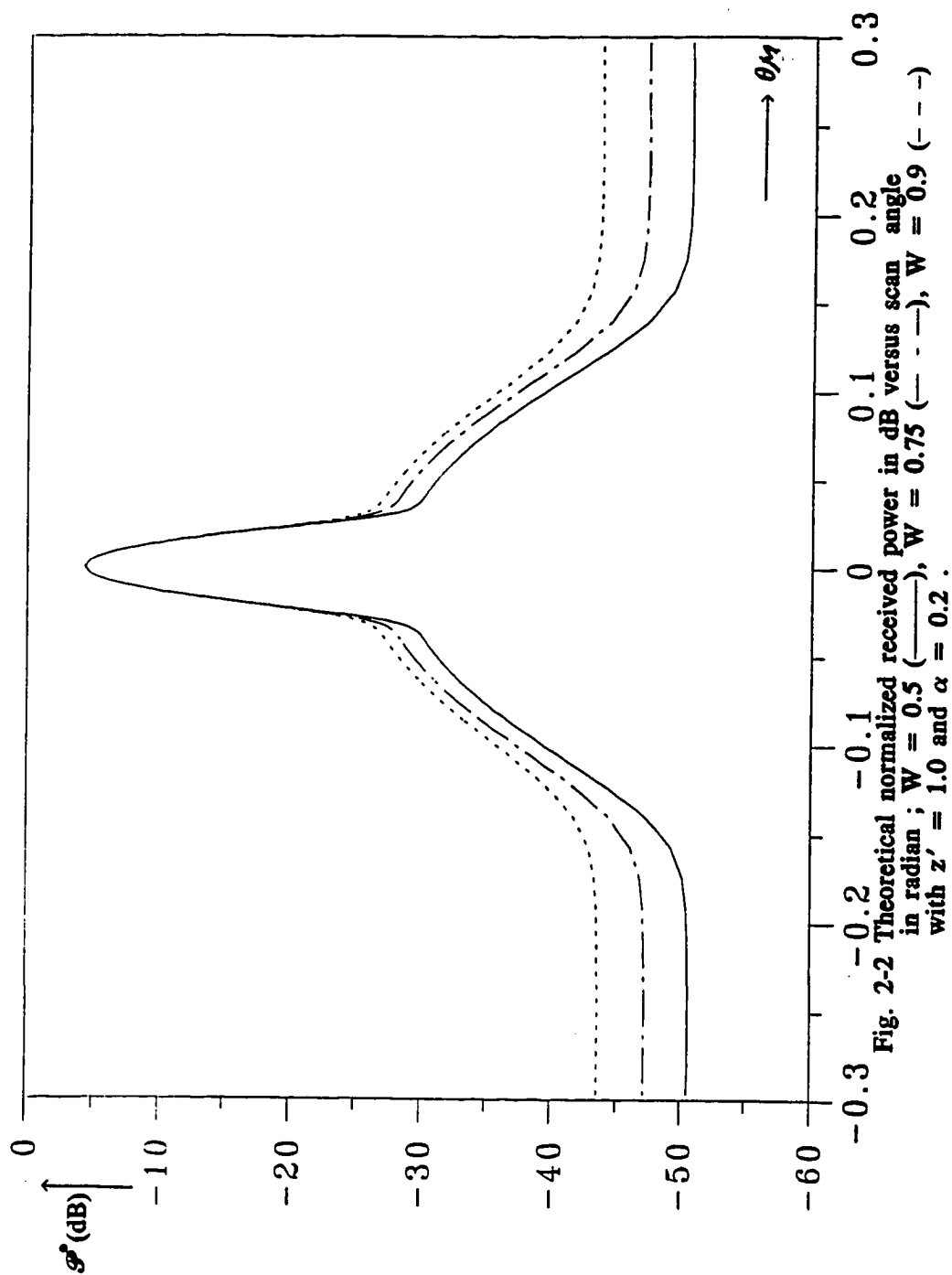


Fig. 2-2 Theoretical normalized received power in dB versus scan angle in radian ; $W = 0.5$ (—), $W = 0.75$ (---), $W = 0.9$ (- - -) with $z' = 1.0$ and $\alpha = 0.2$.

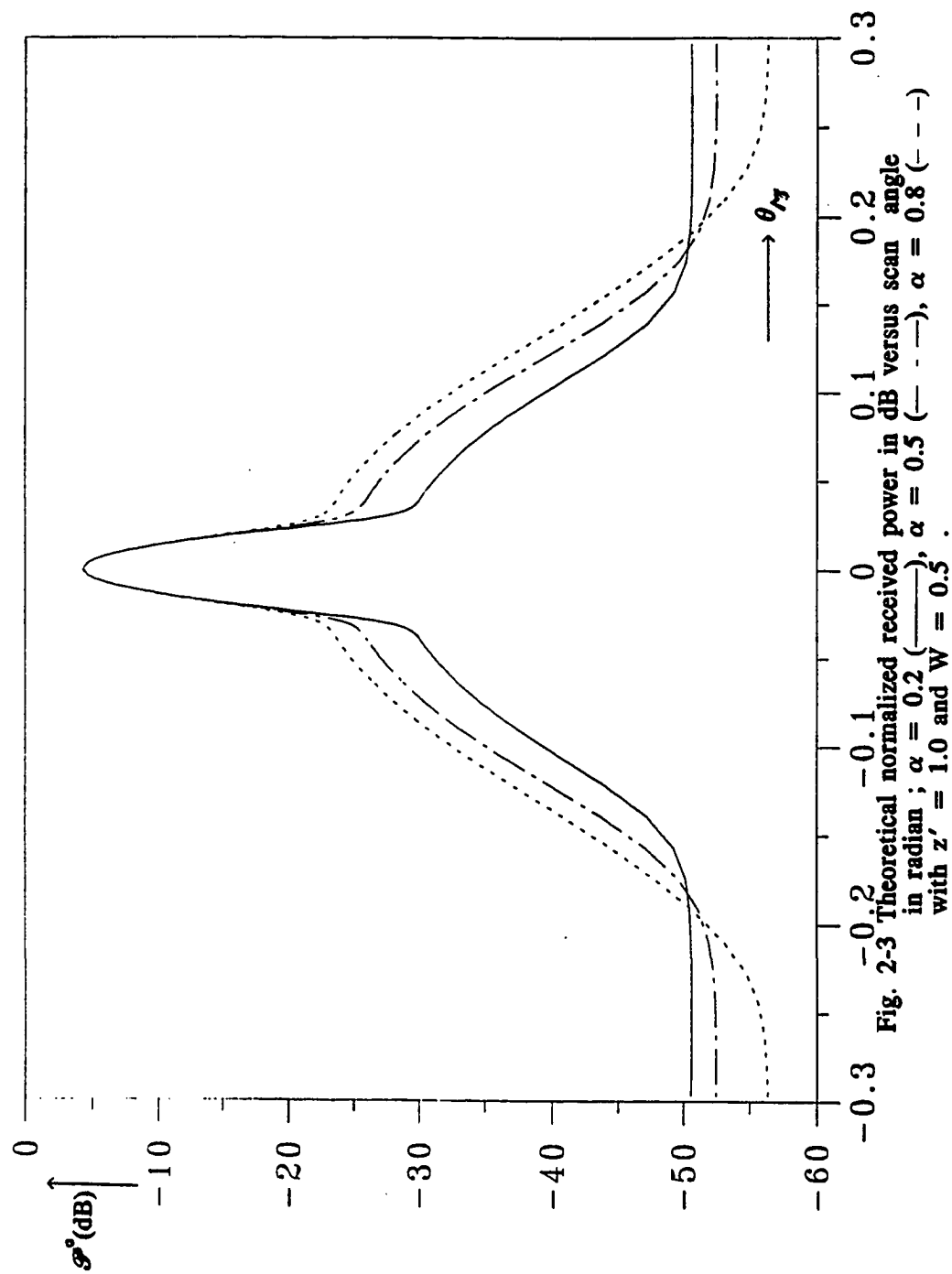


Fig. 2-3 Theoretical normalized received power in dB versus scan angle in radian ; $\alpha = 0.2$ (—), $\alpha = 0.5$ (---), $\alpha = 0.8$ (- - -) with $z' = 1.0$ and $W = 0.5$.

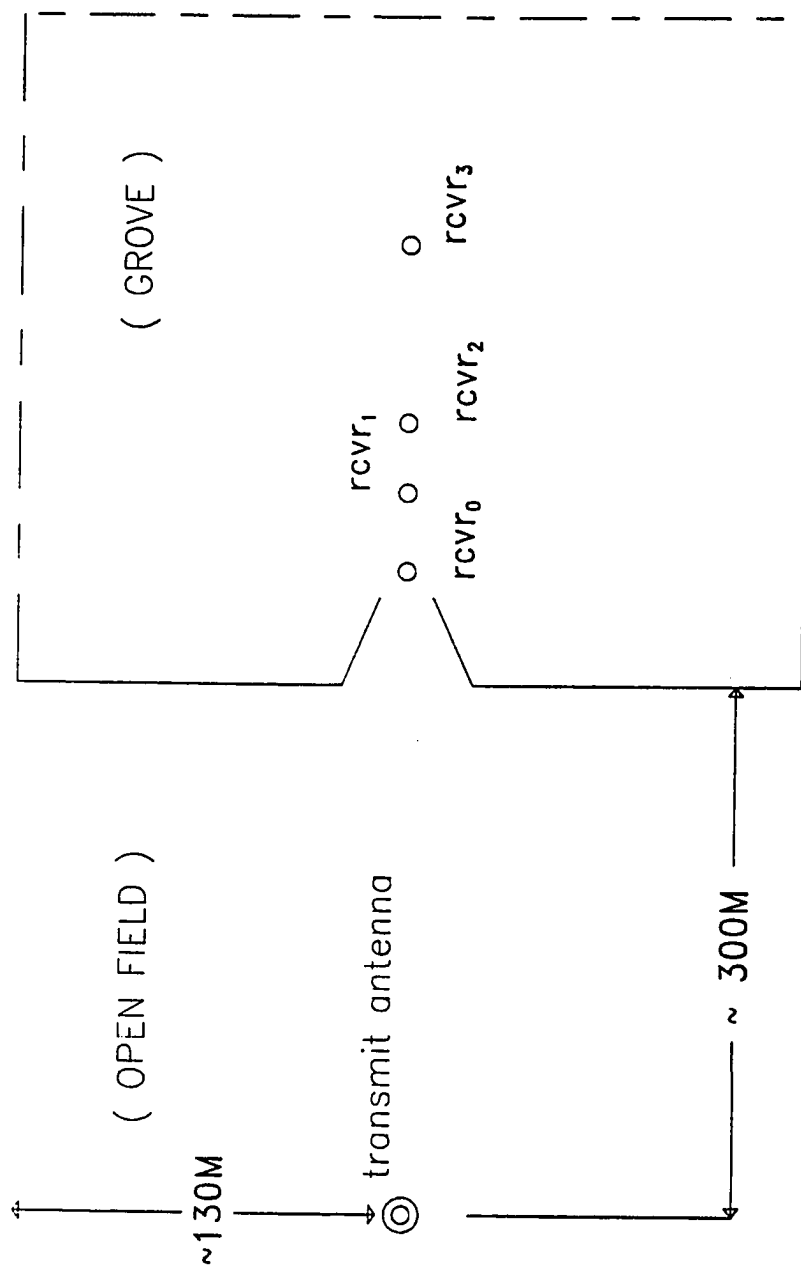


Fig. 2-4 Geometry of the experiment in a forest. The transmitting antenna was placed outside the pecan orchard and the receiving antenna was positioned inside. Small circles represent the locations of the receiving antenna.

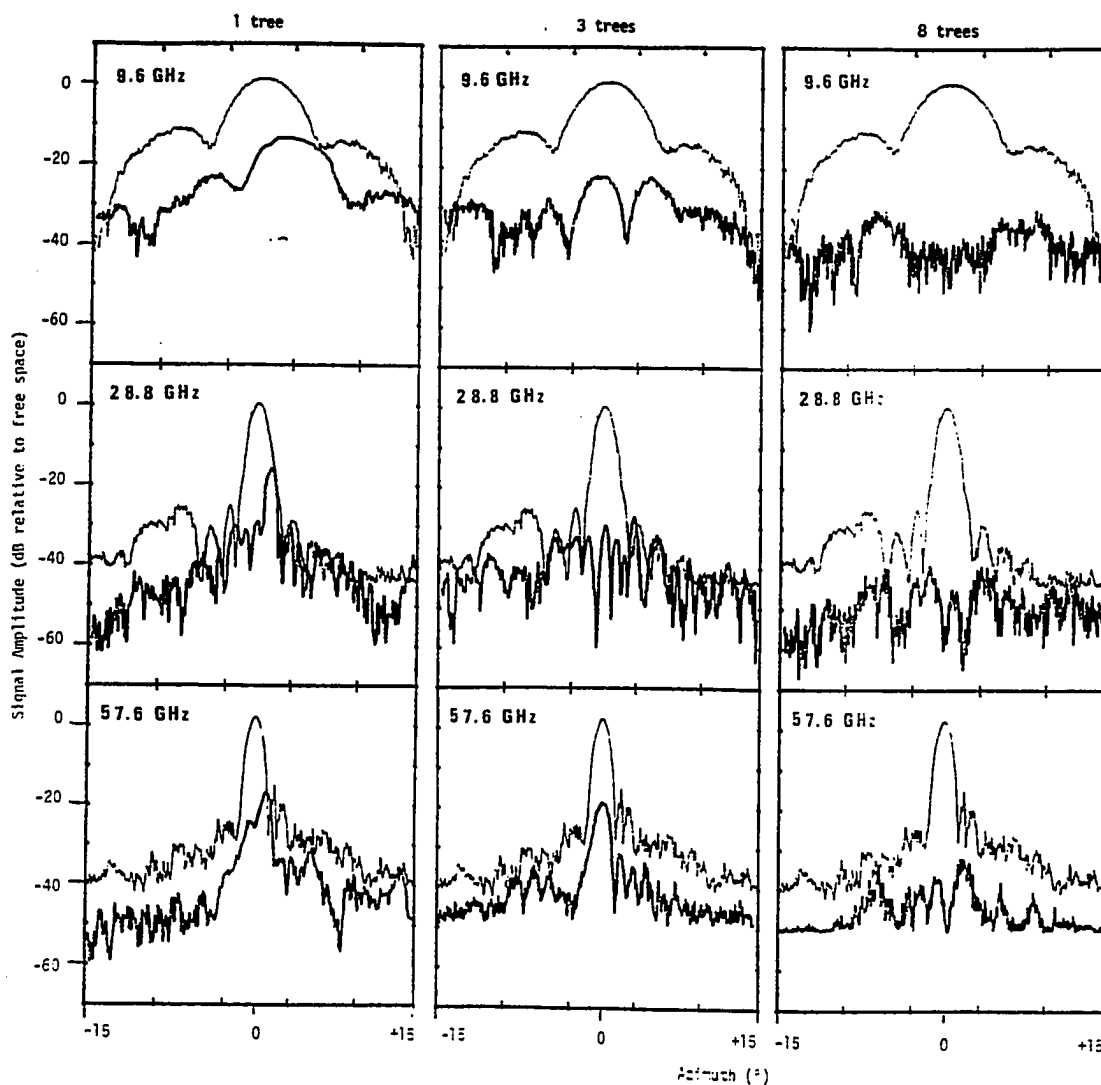


Fig. 2-5 Experimental measured power in dB versus scan angle in degree (the curves of 57.6GHz are used for optimization).

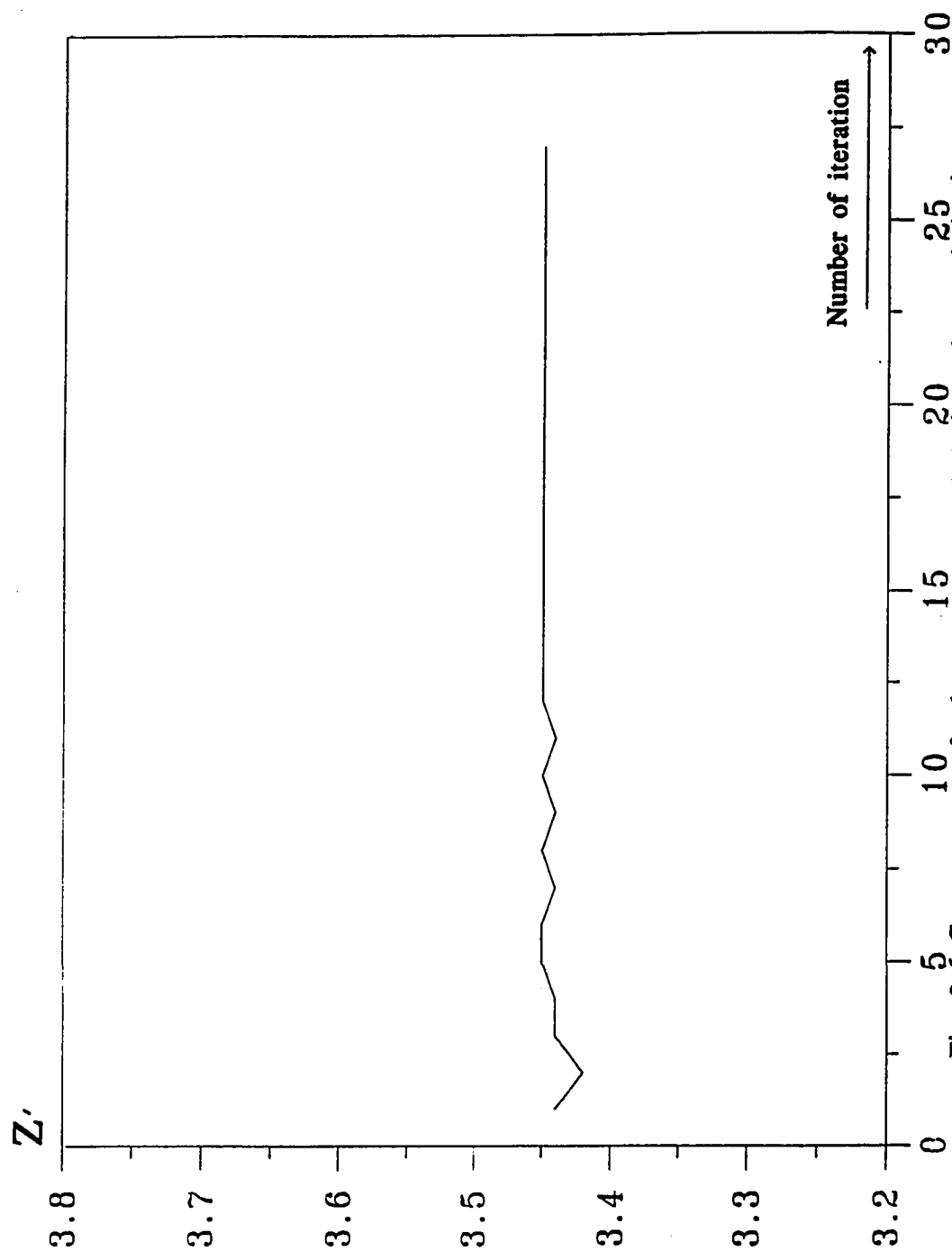


Fig. 2-6 Convergence of the parameter z' during the optimization process using synthetic data (actual z' used was 3.45).

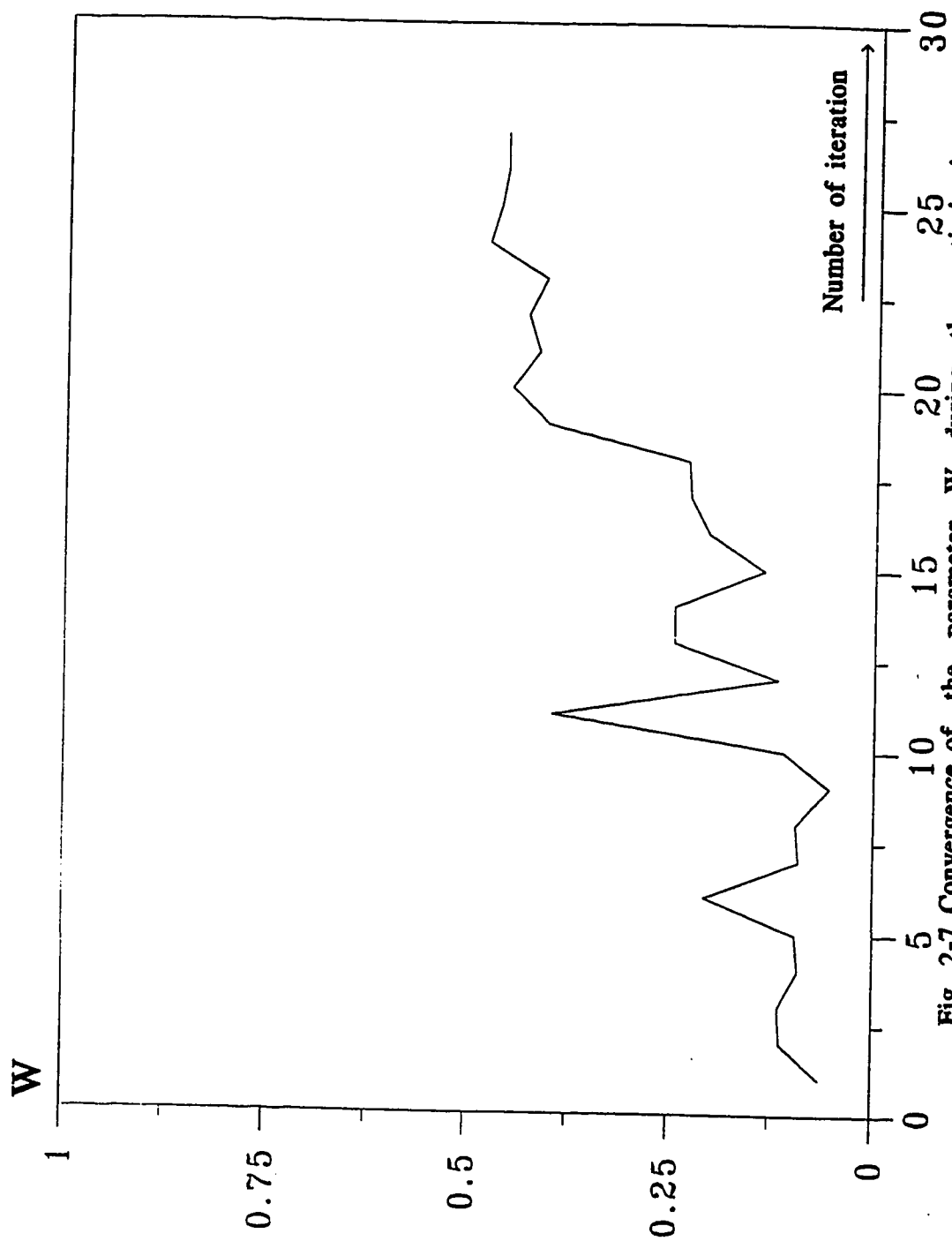


Fig. 2-7 Convergence of the parameter W during the optimization process using synthetic data (actual W used was 0.456).

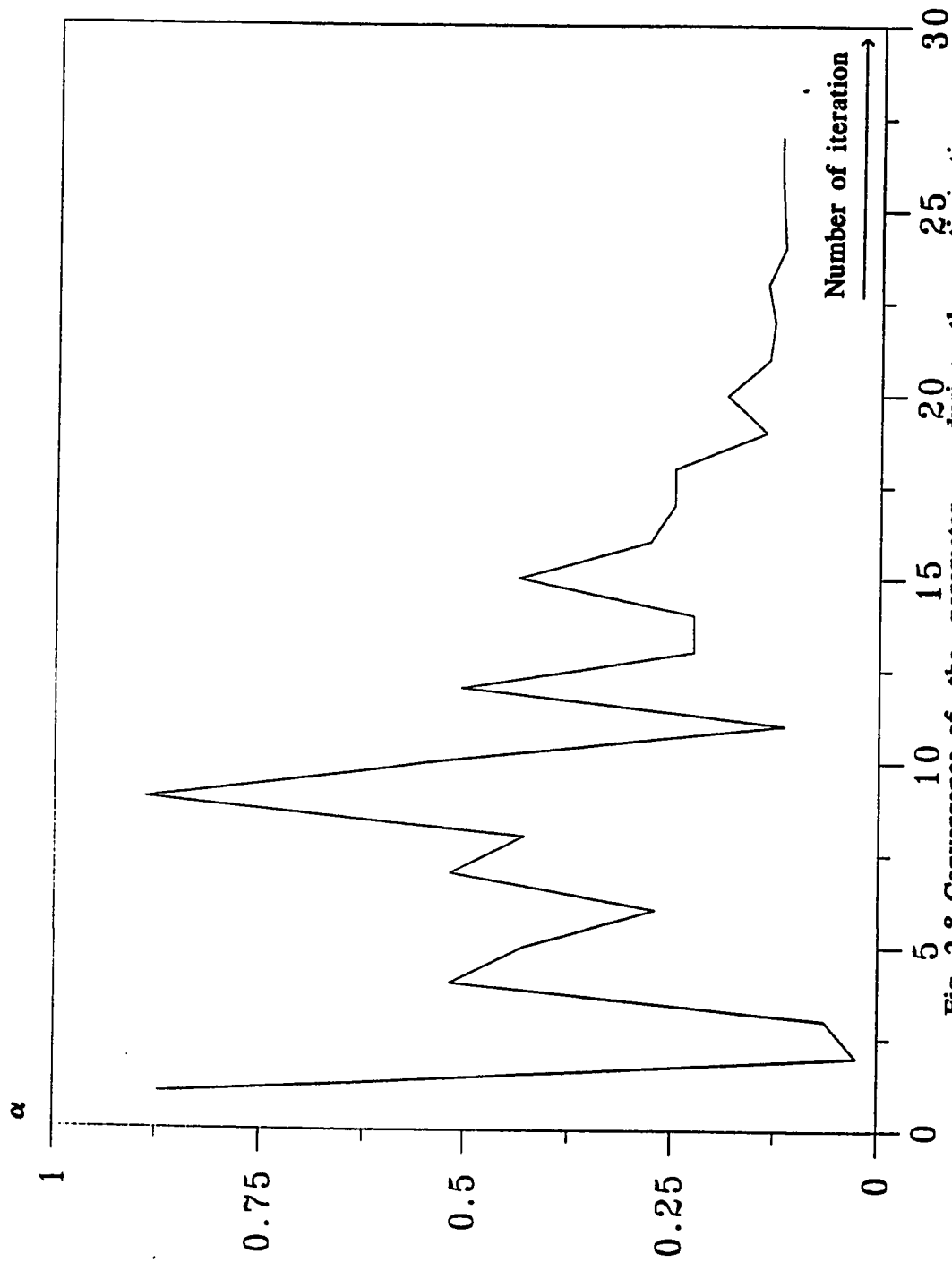


Fig. 2-8 Convergence of the parameter α during the optimization process using synthetic data (actual α used was 0.123).

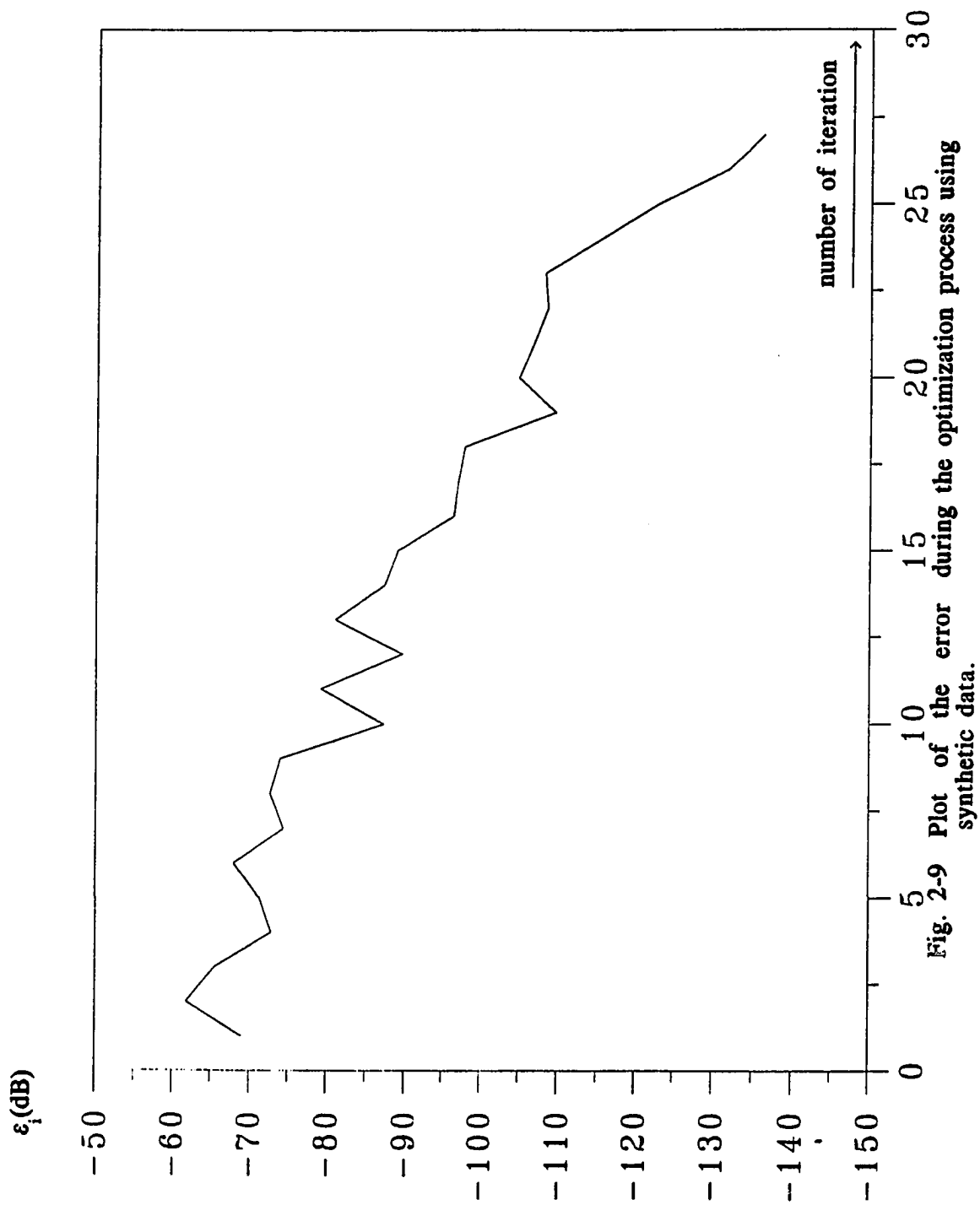


Fig. 2-9 Plot of the error during the optimization process using synthetic data.

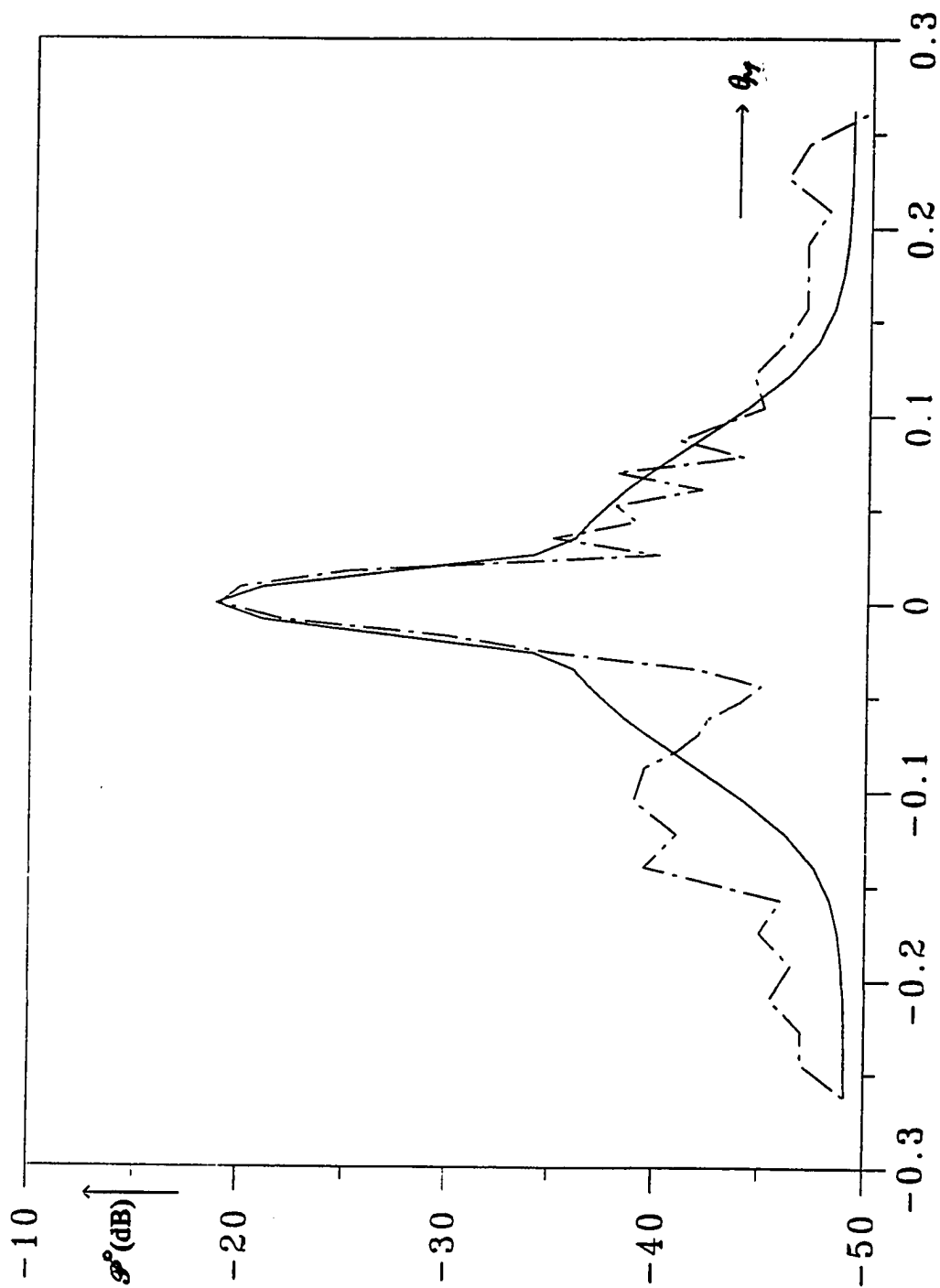


Fig. 2-10 Comparison between theoretical(optimized) and experimental received power ; theoretical (———), experimental (— — — —); three tree case.

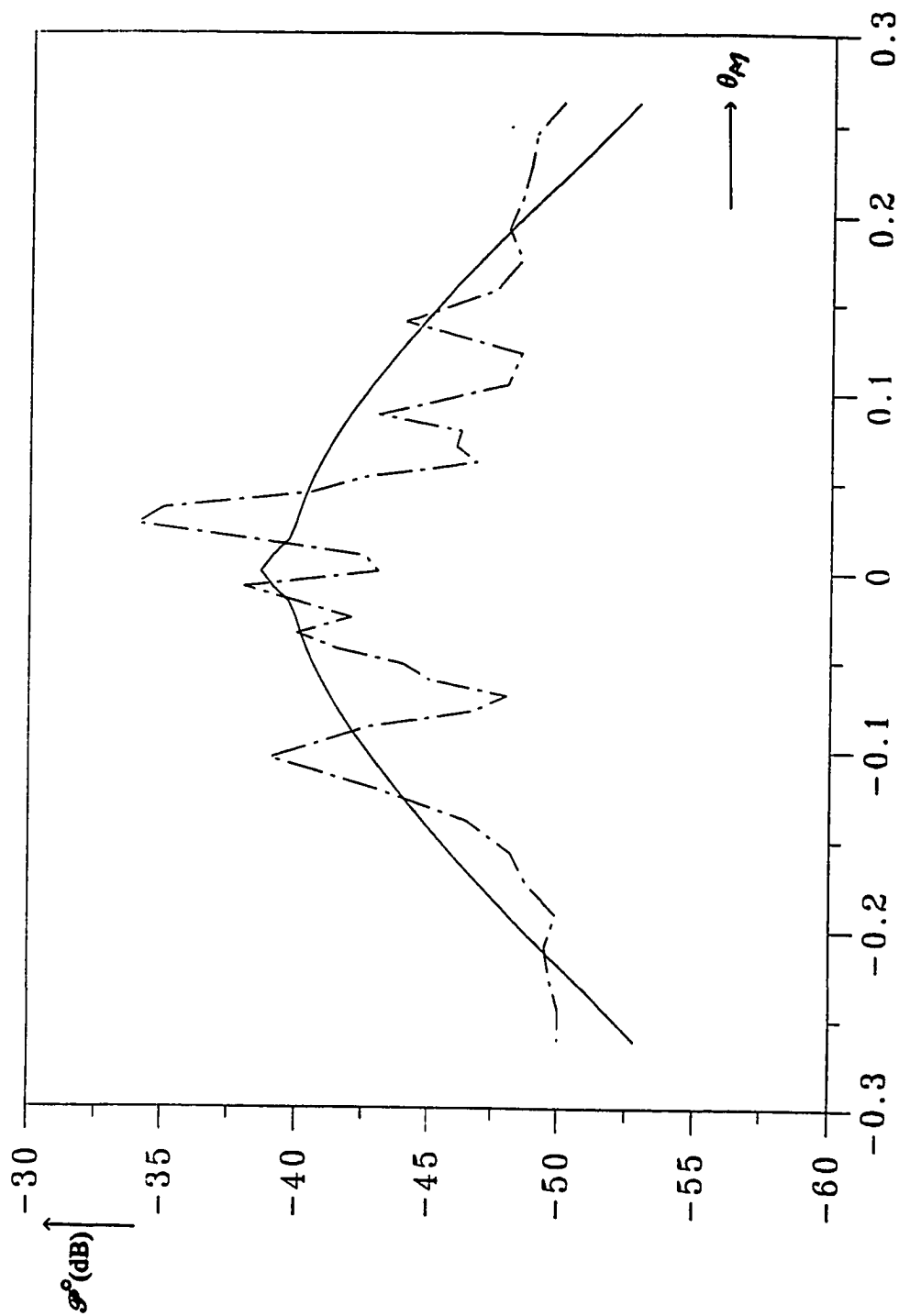


Fig. 2-11 Comparison between theoretical(optimized) and experimental received power ; theoretical (—), experimental (— · —); eight tree case.

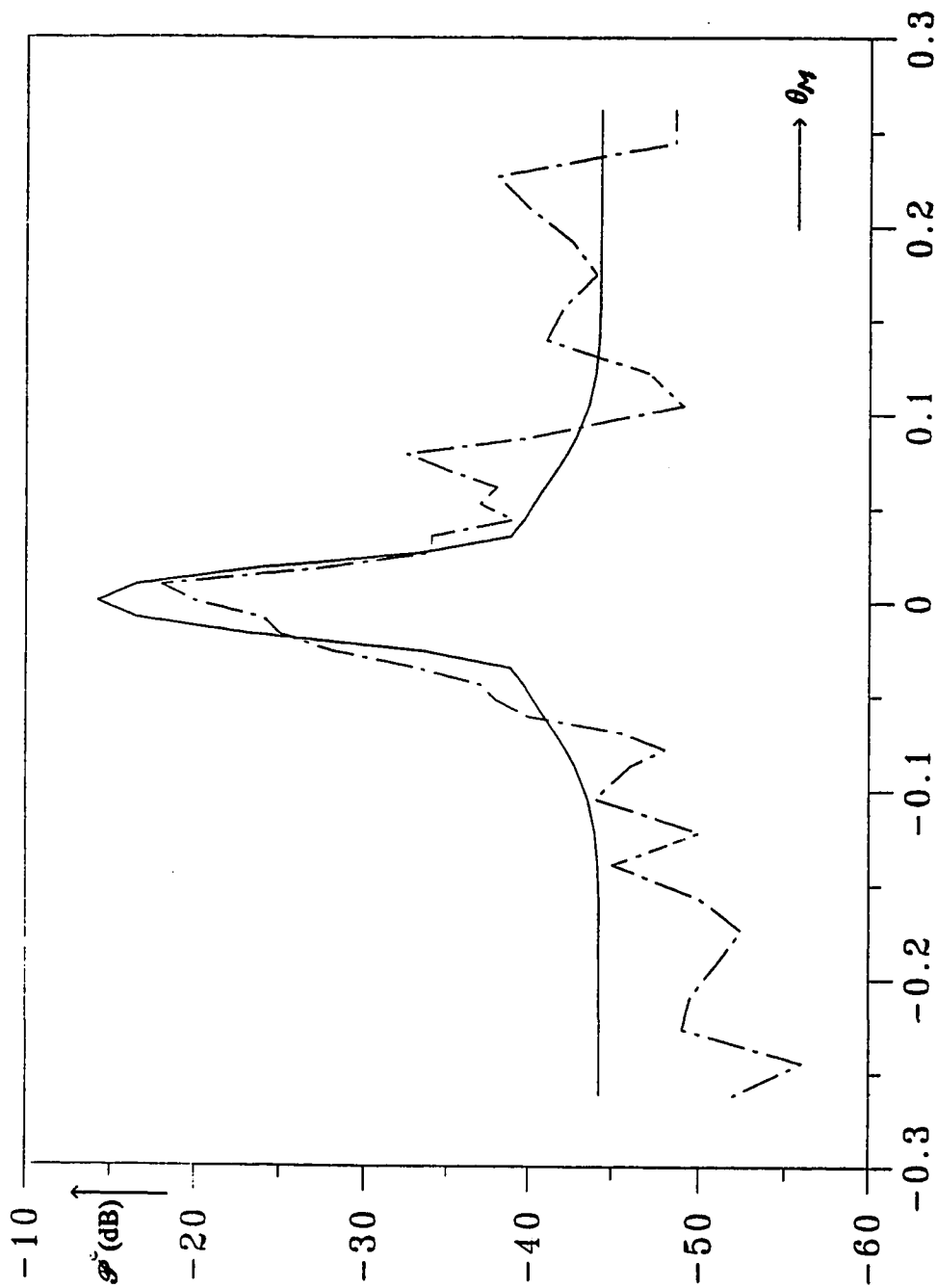


Fig. 2-12 Comparison between theoretical(optimized) and experimental received power ; theoretical (———), experimental (— · — · —); one tree case.

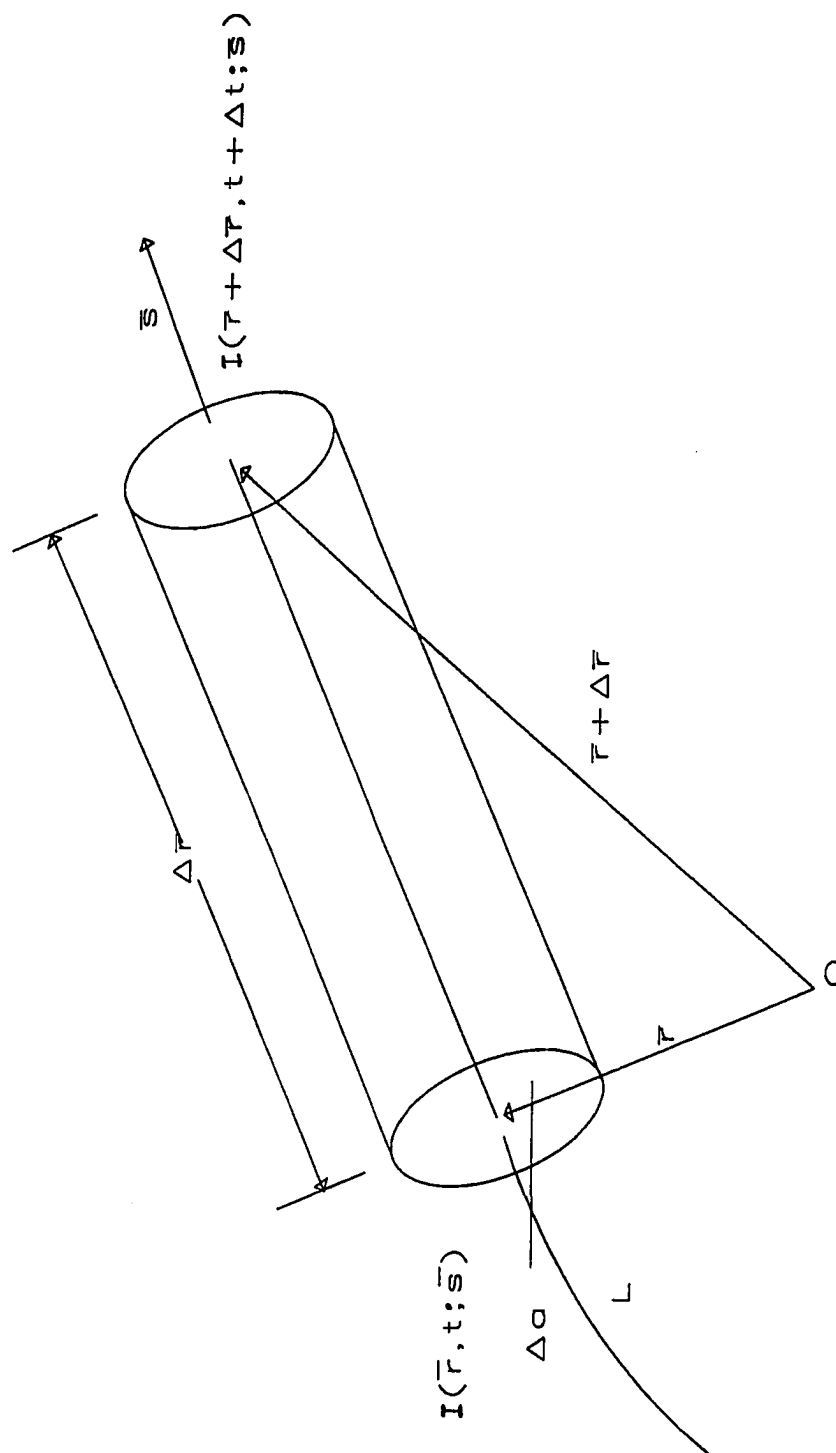


Fig. A1 Differential cylindrical volume element with cross-sectional area Δa and length Δr in direction of \bar{s} .

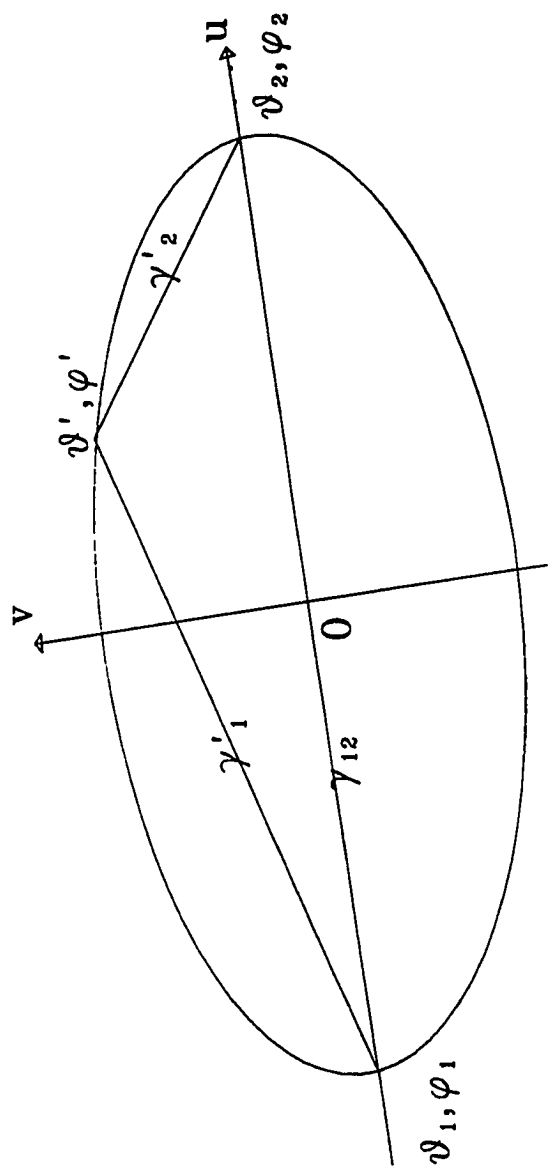


Fig. B1 Local linear two dimensional coordinate system : (θ', ϕ') are angular variables of integration, (θ_1, ϕ_1) and (θ_2, ϕ_2) are constant angles.

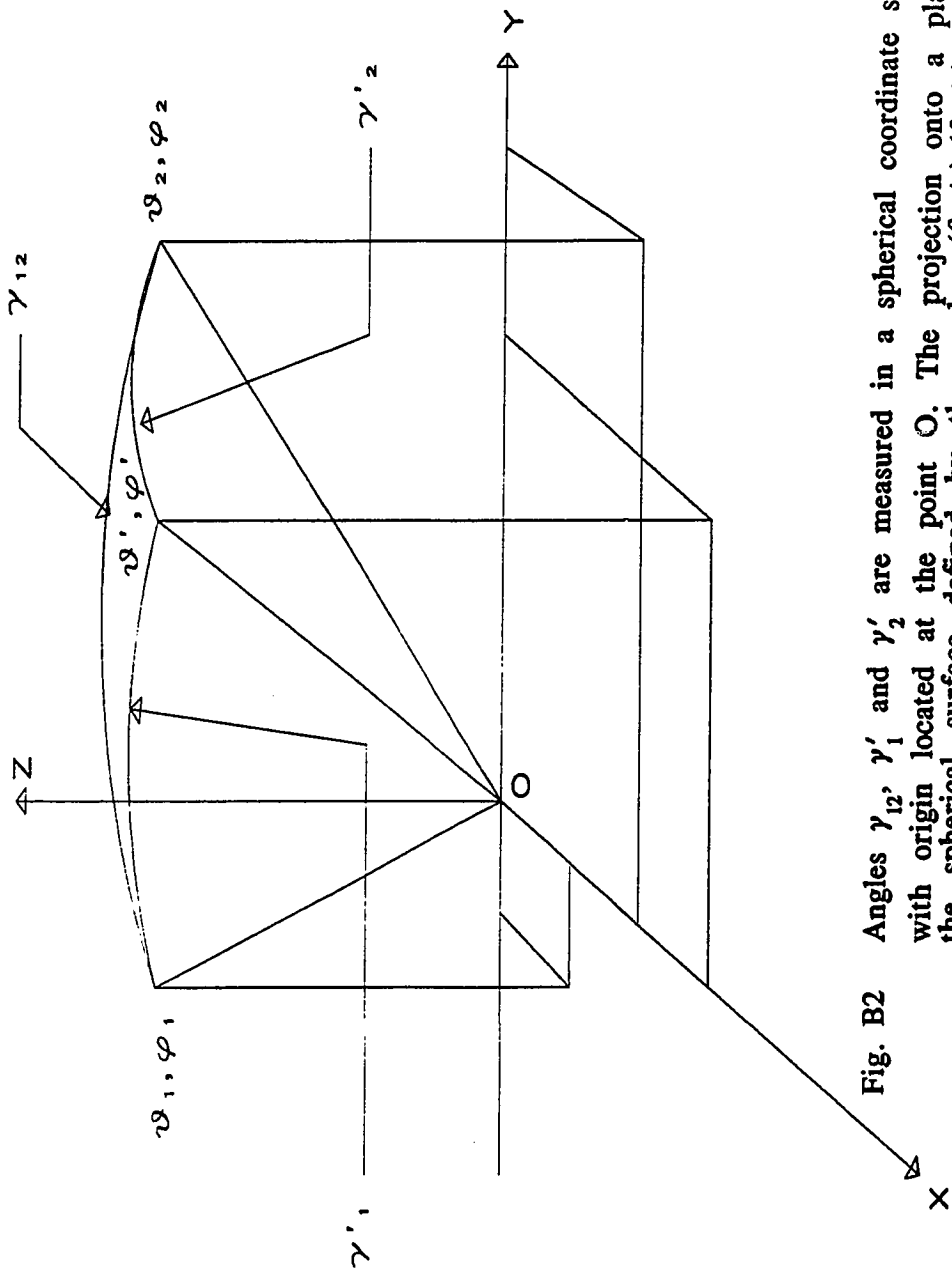


Fig. B2 Angles γ_1, γ_2 and γ'_1, γ'_2 are measured in a spherical coordinate system with origin located at the point O. The projection onto a plane of the spherical surface defined by the angles $(\theta_1, \phi_1), (\theta_2, \phi_2)$ and (θ', ϕ') equidistant from the origin forms an ellipse.

Appendix A. Time-Dependent Transport Equation

The time-dependent transport equation is an integro-differential equation for specific intensity $I(r,t;s)$, which is defined at a position r and time t as the flow of power per unit area and per unit solid angle which crosses a surface normal to the direction of travel s [5,12], *i.e.*,

$$I(r,t;s) = \frac{\Delta P(r, t; s)}{\Delta a \Delta \Omega} , \text{ watts/m}^2(\text{rad}^2) , \quad (\text{A-1})$$

where $\Delta P(r,t;s)$ is an incremental power; see Fig. 1.

To derive the transport equation, consider a medium characterized by absorption and scattering cross-sections σ_A and σ_s , respectively. A beam of radiation is assumed to flow in the direction s along an arbitrary path L as shown in Fig. A1. In this figure, a cylindrical volume element of cross-sectional area Δa and length Δr surrounding a segment of the path is constructed. Let the specific intensity at r and t be $I(r,t;s)$ and at $r+\Delta r$ and $t+\Delta t$ be given by

$$I(r+\Delta r, t+\Delta t; s) = I(r,t;s) + \Delta I , \quad (\text{A-2})$$

where ΔI represents the change in intensity which occurs between position r at time t and $r+\Delta r$ at time $t+\Delta t$.

The difference in radiant energy ΔW between that which entered the volume element at r and that which leaves at $r+\Delta r$ through the cross sectional area Δa in a time interval Δt is given by

$$\Delta W = \Delta I \Delta a \Delta \Omega \Delta t, \text{ joules.} \quad (\text{A-3})$$

The net gain in energy per unit volume, in the differential volume element $\Delta V = \Delta a \Delta r$, per unit time about time t and per unit solid angle about the direction s is therefore

$$W_o = \frac{\Delta W}{\Delta V \Delta \Omega \Delta t} = \frac{\Delta I}{\Delta r}, \text{ watts/m}^3(\text{rad})^2. \quad (\text{A-4})$$

Since the specific intensity in the forest propagates at the speed of light, the distance traveled in time Δt is $\Delta r = c \Delta t$; hence,

$$W_o = \frac{1}{c} \frac{\Delta I}{\Delta t},$$

or, in differential form,

$$W_o = \frac{1}{c} \frac{dI}{dt}. \quad (\text{A-5})$$

From (A-2), the total or substantial derivative of intensity is given by [13,14]

$$\frac{dI}{dt} = \frac{\partial I}{\partial t} + \frac{\partial I}{\partial x} \frac{dx}{dt} + \frac{\partial I}{\partial y} \frac{dy}{dt} + \frac{\partial I}{\partial z} \frac{dz}{dt} = \frac{\partial I}{\partial t} + \frac{dr}{dt} \cdot \nabla I, \quad (\text{A-6})$$

where

$$dr = x_o dx + y_o dy + z_o dz \quad (\text{A-6a})$$

$$\nabla I = x_o \frac{\partial I}{\partial x} + y_o \frac{\partial I}{\partial y} + z_o \frac{\partial I}{\partial z} \quad (\text{A-6b})$$

and x_o, y_o, z_o are unit vectors. Since $dr = dr s = c dt s$, (A-5) and (A-6) yield

$$W_{\circ} = \frac{1}{c} \frac{dI}{dt} = \frac{1}{c} \frac{\partial I}{\partial t} + \mathbf{s} \cdot \nabla I \quad . \quad (\text{A-7})$$

The net gain in radiative energy W_{\circ} is given by

$$W_{\circ} = -W_{\text{abs}} - W_{\text{scat}} + W_{\text{in-scat}} \quad , \quad (\text{A-8})$$

where the loss of energy due to absorption is given by

$$W_{\text{abs}} = \sigma_A I(\mathbf{r}, t; \mathbf{s}) \quad , \quad (\text{A-8a})$$

the loss due to scattering by

$$W_{\text{scat}} = \sigma_s I(\mathbf{r}, t; \mathbf{s}) \quad (\text{A-8b})$$

and the gain due to in-scattering from all directions is

$$W_{\text{in-scat}} = \frac{\sigma_s}{4\pi} \iint_{4\pi} p(\mathbf{s}, \mathbf{s}') I(\mathbf{r}, t; \mathbf{s}') d\Omega' \quad , \quad (\text{A-8c})$$

with normalized scatter (phase) function $p(\mathbf{s}, \mathbf{s}')$; see (1-5c) for normalization. Implicit in writing (A-8a), (A-8b) and (A-8c) is the assumption that the medium is free of dispersion. Hence, all parameter which characterize the medium are independent of frequency. Combining (A-7) and (A-8) yields the time-dependent transport equation

$$\frac{1}{c} \frac{\partial I}{\partial t} + \mathbf{s} \cdot \nabla I = -(\sigma_A + \sigma_s) I + \frac{\sigma_s}{4\pi} \iint_{4\pi} p(\mathbf{s}, \mathbf{s}') I(\mathbf{r}, t; \mathbf{s}') d\Omega' \quad . \quad (\text{A-9})$$

Introducing a total or extinction cross-section per unit volume,

$\sigma_t = \sigma_A + \sigma_s$, and restricting consideration to planar geometry and plane wave incidence cases ($\partial/\partial x = 0, \partial/\partial y = 0$) reduce (A-9) to

$$\frac{1}{c} \frac{\partial I}{\partial t} + \cos \theta \frac{\partial I}{\partial z} + \sigma_t I = \frac{\sigma_s}{4\pi} \int_0^\pi \int_0^{2\pi} p(s, s') I(z, t; \theta', \phi') \sin \theta' d\theta' d\phi'. \quad (A-10)$$

Appendix B. Recursion Relations.

The recursion relation (1-27a) which is used to derive the first order approximation is given by

$$\frac{1}{4\pi} \int_0^{2\pi} \int_0^\pi q(\gamma_2') q_m(\gamma_1') \sin\theta' d\theta' d\phi' = q_{m+1}(\gamma_{12}) , \quad (\text{B-1})$$

where $q(\gamma)$ and $q_m(\gamma)$ are specified in (1-29) and the three angles γ_{12} , γ_1' and γ_2' are defined by

$$\cos \gamma_{12} = \cos(\phi_1 - \phi_2) \sin\theta_1 \sin\theta_2 + \cos\theta_1 \cos\theta_2 \quad (\text{B-1a})$$

$$\cos \gamma_1' = \cos(\phi_1 - \phi') \sin\theta_1 \sin\theta' + \cos\theta_1 \cos\theta' \quad (\text{B-1b})$$

$$\cos \gamma_2' = \cos(\phi_2 - \phi') \sin\theta_2 \sin\theta' + \cos\theta_2 \cos\theta' \quad (\text{B-1c})$$

To evaluate the above integral, a local coordinate system (u,v) is introduced as was done in [8] and is depicted in Figs. B1 and B2. These coordinates are related to the three angles defined in (B-1) by the expressions

$$\gamma_1'^2 = \left[\frac{\gamma_{12}}{2} + u \right]^2 + v^2 \quad (\text{B-2a})$$

$$\gamma_2'^2 = \left[\frac{\gamma_{12}}{2} - u \right]^2 + v^2. \quad (\text{B-2b})$$

By letting $\sin\theta' d\theta' d\phi' = du dv$, expressing $q(\gamma_1')$ and $q(\gamma_2')$ in terms of u and v via (B-2a,b) and extending the limits of the integration to $\pm\infty$, it can be shown that the left-hand side of (B-1) becomes

$$\frac{4}{m\pi\Delta\gamma^4} e^{-(\gamma_{12}^2/\Delta\gamma^2)(m+1)/4m} \int_{-\infty}^{\infty} e^{f(u)} du \int_{-\infty}^{\infty} e^{g(v)} dv, \quad (B-3)$$

where $f(u)$ and $g(v)$ are defined below in (B-5a) and (B-5b), respectively. Using integral evaluations in (B-6a) and (B-6b), (B-1) is obtained.

The second recursion relation in (1-27b) is given by

$$\frac{1}{4\pi} \int_{\mathcal{H}} q(\gamma_2') q_m(\gamma_1') \gamma_i'^2 \sin\theta' d\theta' d\phi' = q_{m+1}(\gamma_{12}) \left[\left(\frac{m}{m+1} \right)^2 \gamma_{12}^2 + \frac{m}{m+1} \Delta\gamma^2 \right]. \quad (B-4)$$

Using (B-1a,b and c) and (B-2a,b), the left-hand side of (B-4) reduces to

$$\frac{4}{m\pi\Delta\gamma^4} e^{-[(\frac{\gamma_{12}}{2})^2 \frac{1}{\Delta\gamma^2} + \frac{1}{m\Delta\gamma^2}]} \int_{-\infty}^{\infty} \int_{-\infty}^{\infty} du dv e^{f(u)} e^{g(v)} \left[u^2 + \gamma_{12} u + (\frac{\gamma_{12}}{2})^2 + v^2 \right], \quad (B-5)$$

where

$$f(u) = -u^2(m+1)/(m\Delta\gamma^2) + u(m-1)\gamma_{12}/(m\Delta\gamma^2) = -au^2 + bu \quad (B-5a)$$

and

$$g(v) = -v^2(m+1)/(m\Delta\gamma^2) = -av^2. \quad (B-5b)$$

An evaluation of (B-5) yields

$$\frac{4}{m\pi\Delta\gamma^4} e^{-[(\frac{\gamma_{12}}{2})^2 \frac{1}{\Delta\gamma^2} + \frac{1}{m\Delta\gamma^2}]} \left[\frac{\gamma_{12}^2}{4} (I_1 I_2) + I_1 I_4 + \gamma_{12} I_1 I_3 + I_2 I_5 \right] \quad (B-6)$$

where

$$I_1 = \int_{-\infty}^{\infty} e^{g(v)} dv = (\pi/a)^{1/2} \quad (\text{B-6a})$$

$$I_2 = \int_{-\infty}^{\infty} e^{f(u)} du = (\pi/a)^{1/2} e^{b^2/4a} \quad (\text{B-6b})$$

$$I_3 = \int_{-\infty}^{\infty} u e^{f(u)} du = (\pi/a)^{1/2} (b/2a) e^{b^2/4a} \quad (\text{B-6c})$$

$$I_4 = \int_{-\infty}^{\infty} u^2 e^{f(u)} du = (\pi/a)^{1/2} [(1+b^2/2a)/2a] e^{b^2/4a} \quad (\text{B-6d})$$

$$I_5 = \int_{-\infty}^{\infty} v^2 e^{g(v)} dv = (\pi/a)^{1/2} / 2a \quad (\text{B-6e})$$

Hence, (B-6) becomes

$$q_{m+1}(\gamma_{12}) \left[\left(\frac{m}{m+1} \right)^2 \gamma_{12}^2 + \frac{m}{m+1} \Delta \gamma^2 \right] \quad (\text{B-7})$$

and the recursion relation (B-4) is proven.

Appendix C. Narrow Lobe Diffuse Intensity and Power in the Zero Order Approximation

In the zero order approximation, it is assumed that the narrow lobe diffuse intensity scatters into very small angular regions in the neighborhood of the incident direction. Hence, (1-18) with $\mu \approx \mu_p$ can be written as

$$\mu_p \frac{dI_{10}}{d\tau_1} + I_{10} = -\frac{W_1 \alpha}{4\pi} \iint_{4\pi} q(\gamma) I_{10} d\mu' d\phi' + \frac{S_p W_1 \alpha}{4\pi} F_0^o e^{-\tau_1/\mu_p} q(\gamma_p), \quad (C-1)$$

where

$$\tau_1 = (1 + j\nu\omega') z', \quad W_1 = W / (1 + j\nu\omega'). \quad (C-1a)$$

The boundary conditions in (1-20) are then reformulated by replacing z' with the new complex variable τ_1 .

The equation (C-1) can be solved by using the method of undetermined coefficients. Let I_{10} take the form

$$I_{10}(\tau_1; \mu, \phi) = (b_1 \tau_1 + b_2 \tau_1^2 + b_3 \tau_1^3 + \dots) e^{-\tau_1/\mu_p}, \quad (C-2)$$

where the b_i , $i=1,2,\dots$, are unknown coefficients which are functions of μ and ϕ . Note that the representation in (C-2) already satisfies the boundary conditions (1-20) in that I_{10} vanishes at $\tau_1 = 0$ and as $\tau_1 \rightarrow \infty$.

To find a recursion relation for the coefficients b_i , $i = 1,2,\dots$, the expression (C-2) is used in (C-1) to yield

$$b_1(\mu, \phi) = \frac{S_p W_1 \alpha}{4\pi \mu_p} F_v^0 \left(\frac{2}{\Delta\gamma}\right)^2 e^{-\left(\frac{\gamma_p}{\Delta\gamma}\right)^2} \quad (C-3)$$

$$\begin{aligned} b_2(\mu, \phi) &= \frac{W_1 \alpha}{8\pi \mu_p} \iint_{4\pi} q(\gamma) b_1(\mu', \phi') d\mu' d\phi' \\ &\cdot \\ &\cdot \\ &\cdot \\ b_m(\mu, \phi) &= \frac{W_1 \alpha}{m 4\pi \mu_p} \iint_{4\pi} q(\gamma) b_{m-1}(\mu', \phi') d\mu' d\phi' \\ &\cdot \\ &\cdot \\ &\cdot \end{aligned}$$

Since each coefficient b_m appears in subsequent integrals, it is assumed to take the general form

$$b_m(\mu, \phi) = B_m \left(\frac{2}{\Delta\gamma_m}\right)^2 e^{-\left(\frac{\gamma_p}{\Delta\gamma_m}\right)^2}, \quad (C-4)$$

with $\Delta\gamma_m \ll \pi$, $m = 1, 2, \dots$.

Substituting (C-4) into the last expression in (C-3) gives

$$B_m \left(\frac{2}{\Delta\gamma_m}\right)^2 e^{-\left(\frac{\gamma_p}{\Delta\gamma_m}\right)^2} = \frac{B_{m-1}}{4\pi} \frac{W_1 \alpha}{\mu_p} \frac{1}{m} \left(\frac{4}{\Delta\gamma \Delta\gamma_{m-1}}\right)^2 \iint_{4\pi} e^{-\left(\frac{\gamma}{\Delta\gamma}\right)^2 - \left(\frac{\gamma_p}{\Delta\gamma_{m-1}}\right)^2} d\mu' d\phi', \quad (C-5)$$

where

$$\cos \gamma_p' = \cos(\phi_p - \phi') \sin \theta_p \sin \theta' + \cos \theta_p \cos \theta' \quad (C-5a)$$

$$\cos \gamma = \cos(\phi - \phi') \sin \theta \sin \theta' + \cos \theta \cos \theta' \quad (C-5b)$$

Using the recursion relation (B-1), it can be shown that the double integral in (C-5) reduces to

$$\frac{\pi}{1/\Delta\gamma^2 + 1/\Delta\gamma_{m-1}^2} \exp(-\gamma_p^2/\{\Delta\gamma^2 + \Delta\gamma_{m-1}^2\}) \quad . \quad (C-6)$$

From (C-5) and (C-6),

$$\frac{1}{\Delta\gamma_m^2} = \frac{1}{\Delta\gamma^2 + \Delta\gamma_{m-1}^2} \quad , \quad B_m = B_{m-1} \frac{W_1 \alpha}{m \mu_p} \quad . \quad (C-7)$$

Using the first equation in (C-3) and (C-4), it follows that

$$\Delta\gamma_1 = \Delta\gamma \quad , \quad B_1 = \frac{S_p F_v^0 W_1 \alpha}{4\pi \mu_p} \quad . \quad (C-8)$$

Hence, it can be inferred from (C-7) and (C-8) that in general

$$\Delta\gamma_m = (m)^{1/2} \Delta\gamma \quad , \quad B_m = \frac{S_p F_v^0}{4\pi} \frac{1}{m!} \left(\frac{W_1 \alpha}{\mu_p}\right)^m \quad . \quad (C-9)$$

From (C-9), (C-4) then becomes

$$\begin{aligned} b_m(\mu, \phi) &= \frac{S_p F_v^0}{4\pi} \left(\frac{W_1 \alpha}{\mu_p}\right)^m \frac{1}{m!} \frac{4}{m \Delta\gamma^2} e^{-\gamma_p^2/m \Delta\gamma^2} \\ &= \frac{S_p F_v^0}{4\pi} \left(\frac{W_1 \alpha}{\mu_p}\right)^m \frac{1}{m!} q_m(\gamma_p) \quad . \end{aligned} \quad (C-10)$$

The functions q_m are gaussian as is the forward lobe q of the phase function, but the beamwidth $\Delta\gamma_m$ is broadened to $(m)^{1/2} \Delta\gamma$.

Combining (C-2) and (C-10) gives the solution for the zero order approximation as

$$I_{10}(\tau_1; \mu, \phi) = \sum_{m=1}^{\infty} \frac{S_p F_v^0}{4\pi} \left(\frac{W_1 \alpha}{\mu_p} \right)^m \frac{1}{m!} \frac{4}{m\Delta \gamma^2} e^{-\gamma_p^2 m \Delta \gamma^2} \tau_1^m e^{-\tau_1 / \mu_p}$$

$$\approx \frac{S_p F_v^0}{4\pi} e^{-\tau_1 / \mu_p} \sum_{m=1}^M \left(\frac{W_1 \alpha}{\mu_p} \right)^m \frac{1}{m!} q_m(\gamma_p) , \quad (C-11)$$

where M is chosen as an upper bound. Substituting (C-11) into (1-39a) yields I_1^0 with the superscript denoting the zero order approximation.

Using the expression for the narrow lobe zero order normalized diffuse power

$$\mathcal{P}_{d1}^0 = \frac{P_{d1}^0(z', t'; \mu_M, \phi_M)}{P_{\text{norm}}} , \quad (C-12)$$

where

$$P_{d1}^0(z', t'; \mu_M, \phi_M) = \iint_{4\pi} A_e(\gamma_M) I_1^0(z', t'; \mu, \phi) d\mu d\phi \quad (C-12a)$$

with P_{norm} defined in (1-73) and $A_e(\gamma_M)$ in (1-70) and (1-71), it can be shown that

$$\mathcal{P}_{d1}^0(z', t'; \mu_M, \phi_M) = \mathcal{R}_e \left[\sum_{v=0}^{\infty} e^{jv\omega' t'} \frac{S_p F_v^0}{4\pi} e^{-\eta_v z' / \mu_p} \sum_{m=1}^M \left(\frac{W_1 \alpha}{\mu_p} \right)^m \frac{1}{m!} \frac{4}{m\Delta \gamma^2} \right.$$

$$\left. \cdot \iint_{4\pi} e^{-\frac{\gamma_p^2}{m\Delta \gamma^2}} e^{-\left(\frac{\gamma_M}{\gamma_R}\right)^2} d\mu d\phi \right] \quad (C-13)$$

where γ_M is given in (1-68a) and η_v in (1-67a).

The integral in (C-13) is evaluated by introducing local coordinates (u, v) as was done in Appendix B. Hence,

$$\mathcal{P}_{d1}^0 = \mathcal{R}_e \left[\sum_{v=0}^{\infty} e^{jv\omega't} \frac{\Delta \gamma_R^2 F^0}{4} v e^{-\eta v z' / \mu_p} \sum_{m=1}^M \left(\frac{W \alpha z'}{\mu_p} \right)^m \frac{1}{m!} q_m(\gamma_{pM}) \right], \quad (C-14)$$

where

$$q_m(\gamma_{pM}) = \frac{4}{\Delta \gamma_R^2 + m \Delta \gamma^2} e^{-\frac{\gamma_{pM}^2}{\Delta \gamma_R^2 + m \Delta \gamma^2}} \quad (C-14a)$$

and

$$\cos \gamma_{pM} = \cos(\phi_p - \phi_M) [(1 - \mu_p^2)(1 - \mu_M^2)]^{1/2} + \mu_p \mu_M. \quad (C-14b)$$

Appendix D. Isotropic Background Diffuse Intensity

To obtain (1-41), it is necessary to evaluate the integral in (1-19) which involves I_{1v} . This is done by integrating (1-18). For convenience, (1-18) is repeated below

$$\mu \frac{dI_{1v}}{dz'} + (1+jv\omega')I_{1v} = \frac{W\alpha}{4\pi} \int_0^\pi \int_0^{2\pi} q(\gamma) I_{1v} d\mu' d\phi' + \frac{S}{4\pi} \frac{W\alpha}{\mu_p} F_v(z'/\mu_p) e^{-z'/\mu_p} q(\gamma_p). \quad (D-1)$$

Let

$$U_{1v}(z') \equiv \frac{1}{4\pi} \int_0^\pi \int_0^{2\pi} I_{1v}(z'; \mu, \phi) d\mu d\phi \quad (D-2)$$

which by definition is the average power density. Integrating (D-1) gives

$$\begin{aligned} \frac{1}{4\pi} \int_0^\pi \int_0^{2\pi} \left[\mu \frac{dI_{1v}}{dz'} + (1+jv\omega') I_{1v} \right] d\mu d\phi &= \frac{W\alpha}{4\pi} \int_0^\pi \int_0^{2\pi} q(\gamma) I_{1v} d\mu' d\phi' \\ &+ \frac{S}{4\pi} \frac{W\alpha}{\mu_p} F_v(z'/\mu_p) e^{-z'/\mu_p} q(\gamma_p) \int_0^\pi \int_0^{2\pi} d\mu d\phi. \end{aligned} \quad (D-3)$$

The integrals on the right-hand side are evaluated by approximating $q(\gamma)$ and $q(\gamma_p)$ as delta functions. Evaluating the remaining integrals in (D-3) yields the new differential equation

$$\mu_p \frac{dU_{1v}}{dz'} + (1+jv\omega' - W\alpha) U_{1v} = S F_v^0 W\alpha e^{-\left(\frac{1+jv\omega'}{\mu_p}\right)z'}. \quad (D-4)$$

Solving for U_{1v} gives

$$U_{1v}(z') = S_p F_v^o \left[e^{-(1+jv\omega'-W\alpha)z'/\mu_p} - e^{-(1+jv\omega')z'/\mu_p} \right] . \quad (D-5)$$

Substituting (D-5) into (1-19) yields

$$\begin{aligned} \mu \frac{dI_{2v}}{dz'} + (1+jv\omega')I_{2v} &= \frac{W\alpha}{4\pi} \int_0^\pi q(\gamma) I_{2v} d\mu' d\phi' + \frac{W(1-\alpha)}{4\pi} \int_0^\pi I_{2v} d\mu' d\phi' \\ &+ \frac{W(1-\alpha)}{4\pi} S_p F_v^o \left[e^{-(1+jv\omega'-W\alpha)z'/\mu_p} - e^{-(1+jv\omega')z'/\mu_p} \right] \\ &+ \frac{W(1-\alpha)}{4\pi} S_p F_v^o e^{-(1+jv\omega')z'/\mu_p} , \end{aligned} \quad (D-6)$$

where

$$\cos \gamma = \cos(\phi - \phi') [(1-\mu^2)(1-\mu'^2)]^{1/2} + \mu\mu' \quad (D-6a)$$

$$\cos \gamma_p = \cos(\phi - \phi_p) [(1-\mu^2)(1-\mu_p^2)]^{1/2} + \mu\mu_p . \quad (D-6b)$$

The boundary conditions obeyed are

$$I_{2v} = 0 \quad \text{for } z' = 0, 0 \leq \mu \leq 1 , \quad (D-6c)$$

$$I_{2v} \rightarrow 0 \quad \text{as } z' \rightarrow \infty . \quad (D-6d)$$

The first term on the right-hand side of (D-6) can be further approximated by replacing $q(\gamma)$ by a delta function. It then follows that (D-6) becomes

$$\mu \frac{dI_{2v}}{d\tau_v} + I_{2v} = \frac{W_v}{2} \int_{-1}^1 I_{2v} d\mu' + \frac{S_p F_v^o W_v}{4\pi} e^{-\tau_v/\mu_p} , \quad (D-7)$$

where

$$\tau_v = (1 + jv\omega' - W\alpha)z', \quad W_v = W(1 - \alpha)/(1 + jv\omega' - W\alpha) \quad .(D-7a)$$

Recognize that (D-7) is identical to the time-independent equation of radiative transfer for the case of isotropic scattering except that τ_v and W_v are complex.

Appendix E. Total Received Power in The First Order Approximation

From (1-67), (1-69), (1-70), (1-71) and (1-72) the coherent power, narrow lobe diffuse power and omnidirectional diffuse power received by a highly directive antenna are obtained for the normal incidence case ($\mu_p = \mu_j = 1$) as follows

$$\mathcal{P}_c = \iint_{4\pi} \mathcal{R}_e \left[\sum_{v=0}^{\infty} e^{jv\omega't} \frac{F_v^0}{2\pi} e^{-\eta_v z'} \delta(\mu - \mu_j) \right] e^{-\left(\frac{\gamma_M}{\Delta \gamma_R}\right)^2} d\mu d\phi \quad (\text{E-1a})$$

$$\mathcal{P}_{d1} = \iint_{4\pi} \mathcal{R}_e \left[\sum_{v=0}^{\infty} e^{jv\omega't} \frac{F_v^0}{4\pi} e^{-\eta_v z'} \sum_{m=1}^M \frac{(W\alpha z')^m}{m!} q_m(\gamma) \left\{ 1 + \xi_m(\theta) \left[1 - \frac{\eta_v z'}{m+1} \right] \right\} \right. \\ \left. \cdot e^{-\left(\frac{\gamma_M}{\Delta \gamma_R}\right)^2} \right] d\mu d\phi, \quad (\text{E-1b})$$

$$\mathcal{P}_{d2} = \iint_{4\pi} \mathcal{R}_e \left[e^{jv\omega't} \frac{F_v^0}{2\pi} \left\{ -e^{-\eta_{2v} z'} \frac{f_j(\mu)}{P_j} + \sum_{k=(N+1)/2}^N [Q'_{vk} e^{-\eta_{2v} z'/s_{vk}} \sum_{n=0}^N \frac{f_n(\mu)}{1 - \mu_n/s_{vk}}] \right\} \right. \\ \left. \cdot e^{-\left(\frac{\gamma_M}{\Delta \gamma_R}\right)^2} \right] d\mu d\phi, \quad (\text{E-1c})$$

where

$$\eta_v = (1 + jv\omega') \quad , \quad \eta_{2v} = (1 + jv\omega' - W\alpha), \quad j = p \quad (\text{E-1d})$$

and

$$\gamma_M = \theta, \quad \theta_M = 0. \quad (\text{E-1e})$$

Because of the delta functions, (E-1a) readily simplifies to

$$\mathcal{P}_c(z', t'; \mu_M, \phi_M) = \mathcal{R}_0 \left[\sum_{v=0}^{\infty} e^{jv\omega' t'} F_v^0 e^{-\left(\frac{\gamma}{\Delta\gamma_R}\right)^2 \eta_v z'} \right], \quad (\text{E-2})$$

where

$$\gamma_{pM} = \theta_j = \theta_p. \quad (\text{E-2a})$$

Following the procedure in [3], the omnidirectional diffuse power becomes

$$\begin{aligned} \mathcal{P}_{d2}(z', t'; \mu_M, \phi_M) = \mathcal{R}_0 \left[\sum_{v=0}^{\infty} e^{jv\omega' t'} \left[\frac{\Delta\gamma_R^2 F_v^0}{2} \{ e^{-\eta_{2v} z'} \frac{f_j(\mu_M)}{P_j} \right. \right. \\ \left. \left. + \sum_{k=(N+1)/2}^N [Q_{vk}' e^{-\eta_{2v} z' / s_{vk}} \sum_{n=0}^N \frac{f_n(\mu_M)}{1 - \mu_n / s_{vk}}] \} \right] \right] \end{aligned} \quad (\text{E-3})$$

after approximating the term $\exp(-(\gamma_M / \Delta\gamma_R)^2)$ in (E-1c), properly normalized, by a delta function.

To determine the narrow lobe diffuse power, (E-1b) is separated into two terms,

$$\mathcal{P}_{d1}(z', t'; \mu_M, \phi_M) = \mathcal{P}_{d1}^0 + \mathcal{P}_{d1}^a, \quad (\text{E-4})$$

where

$$\mathcal{P}_{d1}^0 = \iint_{4\pi} \mathcal{R}_0 \left[\sum_{v=0}^{\infty} e^{jv\omega' t'} \frac{F_v^0}{4\pi} e^{-\eta_v z'} \sum_{m=1}^M \frac{(W_{\alpha} z')^m}{m!} q_m(\gamma) e^{-\left(\frac{\gamma}{\Delta\gamma_R}\right)^2} \right] d\mu d\phi \quad (\text{E-4a})$$

and

$$\mathcal{P}_{d1}^a = \int_0^{2\pi} \int_0^\pi \mathcal{R}_e \left[\sum_{v=0}^{\infty} e^{jv\omega't'} \frac{F_v^0}{4\pi} e^{-\eta_v z'} \sum_{m=1}^M \frac{(W\alpha z')^m}{m!} q_m(\gamma) \xi_m(\theta) \left[1 - \frac{\eta_v z'}{m+1} \right] e^{-\left(\frac{\gamma_M}{\Delta\gamma_R}\right)^2} \right] d\mu d\phi, \quad (\text{E-4b})$$

where $\xi_m(\theta)$ is defined in (1-38a). Recall that for the normal incidence case, the variable γ_M equals θ ; hence (E-4a) reduces to

$$\begin{aligned} \mathcal{P}_{d1}^0 &= \mathcal{R}_e \left[\sum_{v=0}^{\infty} e^{jv\omega't'} \frac{2F_v^0}{\Delta\gamma^2} e^{-\eta_v z'} \sum_{m=1}^M \frac{(W\alpha z')^m}{m!m} \int_0^\pi e^{-\theta^2(1/\Delta\gamma_R^2 + 1/\Delta\gamma^2)} \sin\theta d\theta \right] \\ &= \mathcal{R}_e \left[\sum_{v=0}^{\infty} e^{jv\omega't'} \frac{F_v^0}{\Delta\gamma^2} e^{-\eta_v z'} \sum_{m=1}^M \frac{(W\alpha z')^m}{m!m} \frac{1}{h} (1-e^{-4h}) \right], \quad (\text{E-5}) \end{aligned}$$

where

$$h = \frac{1}{\Delta\gamma_R^2} + \frac{1}{m\Delta\gamma^2} \quad (\text{E-5a})$$

and use is made of (1-29). Similarly, (E-4b) can be shown to reduce to

$$\begin{aligned} \mathcal{P}_{d1}^a &= \mathcal{R}_e \left[\sum_{v=0}^{\infty} e^{jv\omega't'} \frac{1}{2F_v^0} e^{-\eta_v z'} \sum_{m=1}^M \frac{(W\alpha z')^m}{m!} \left(1 - \frac{\eta_v z'}{m+1} \right) \frac{4}{m\Delta\gamma^2} \int_{-1}^1 e^{-\theta^2 h} [a + b(1-\mu)] d\mu \right] \\ &= \mathcal{R}_e \left[\sum_{v=0}^{\infty} e^{jv\omega't'} \frac{2F_v^0}{\Delta\gamma^2} e^{-\eta_v z'} \sum_{m=1}^M \frac{(W\alpha z')^m}{m!} \frac{1}{m} \left(1 - \frac{\eta_v z'}{m+1} \right) \left[\frac{a}{2h} (1-e^{-4h}) \right. \right. \\ &\quad \left. \left. - b \left[\frac{1}{4h^2} (e^{-4h}(4h+1)-1) \right] \right] \right], \quad (\text{E-6}) \end{aligned}$$

where

$$a = \frac{1}{12} (m^2 - 1) \Delta\gamma^2 \quad (\text{E-6a})$$

and

$$b = \frac{(m+1)(2m+1)}{6m} \quad (E-6b)$$

Hence, from (E-4), (E-5) and (E-6), the narrow lobe diffuse power is found to be

$$\mathcal{P}_{d1} = \mathcal{R}_e \left[\sum_{v=0}^{\infty} e^{jv\omega't'} \frac{F_v^0}{4} e^{-\eta_v z'} \sum_{m=1}^M \frac{(W\alpha z')^m}{m!} \left[\frac{4}{hm\Delta\gamma^2} (1 - e^{-4h}) - \left(1 - \frac{\eta_v z'}{m+1} \right) \right. \right. \\ \left. \left. \cdot \left[\frac{1}{3} \frac{(m^2-1)}{m} \frac{1}{h} (e^{-4h}-1) + \frac{m+1}{m^2 \Delta\gamma^2} \frac{2m+1}{3} \frac{1}{h^2} (e^{-4h}(4h+1)-1) \right] \right] \right] \quad (E-7)$$

Appendix F. A Discussion of Simulated Annealing

The CT is conceptually similar to "simulated annealing", which is a stochastic computational viewpoint derived from statistical mechanics for finding near globally-minimum-cost solutions to large optimization problems. Kirkpatrick *et al* [15] were the first to propose and demonstrate the application of simulation techniques from statistical physics to problems of combinatorial optimization, specifically to problems of wire routing and component placement in VLSI designs.

Simulated annealing has been applied successfully to problems in computer design [16], image restoration and segmentation [17], combinatorial optimization such as the travelling salesman problem [15], phased-array antenna synthesis [18], neural networks [19,20] as well as IC layouts [21].

In general, finding the global minimum value of a cost function involves many possible choices, subject to conflicting constraints [22], because the cost function will tend to have many local minima. A procedure for solving this type of optimization problem should involve a high probability of finding a near-optimal solution and should also lend itself to efficient implementation. Over the past few years simulated annealing has emerged as a viable technique which meets these requirements. The following paragraphs summarize the concept of simulated annealing.

Simulated annealing originated from statistical mechanics which is the study of the behavior of very large systems of interacting particles. An example of one such system is atoms in a fluid in thermal

equilibrium at a finite temperature. Suppose that the configuration of the system is identified by a set of spatial positions of the particles. If the system is in thermal equilibrium at a given temperature T then the probability Π_s that the system is in a given state s depends upon the energy E_s of the state, which for some systems is given by the *Boltzmann distribution*,

$$\Pi_s = \frac{e^{-\frac{E_s}{kT}}}{\sum_s e^{-\frac{E_s}{kT}}} \quad , \quad (\text{F-1})$$

where k is the *Boltzmann* constant and the summation extends over all possible energy states.

One can simulate the behavior of a system of particles in thermal equilibrium at temperature T by using a stochastic relaxation technique developed by Metropolis *et al* [23]. Suppose that at time t , the system is in state r . A candidate s for the state at time $t + \Delta t$ is generated *randomly*. The criterion for selecting or rejecting state configuration s depends on the difference between the energies of state r and s . Specifically, one computes the ratio R of the probability of being in state s and the probability of being in state r ,

$$R = \frac{\Pi_s}{\Pi_r} = e^{-\frac{(E_r - E_s)}{kT}} \quad . \quad (\text{F-2})$$

Depending upon the selection of a value for R as a criterion, one either accepts or rejects the new configuration state s .

In studying such systems of particles, one often seeks to determine the nature of the low-energy states, for example, whether slow freezing

produces crystalline or glassy solids. Very low energy configurations are not common when considering the set of all configurations. However, at low temperatures they predominate because of the nature of the *Boltzmann* distribution. To achieve low-energy configurations, it is not sufficient to simply lower the temperature. One must use an *annealing* process where the temperature of the system is determined, and then gradually lowered, spending enough time at each temperature to reach thermal equilibrium. If insufficient time is spent at each temperature, especially near the freezing point, then the probability of attaining a very low energy configuration is greatly reduced. For example, defects in a crystalline structure might occur if the process of lowering the temperature is not done properly. As a result, the lower energy state would not be obtained.

The simulation of annealing as applied to optimization problems involves the following preparatory steps. First, one must identify analogies to the statistical physics concepts in the optimization procedure, *i.e.*, the energy function is chosen as the cost function, the configuration of particles becomes the configuration of the parameter values, finding a low-energy configuration becomes seeking a near-optimal solution, and temperature becomes the control parameter of the process. Second, one must select an annealing schedule consisting of a decreasing set of temperatures together with the amount of time to spend at each temperature. Third, one must have a way of generating and selecting new configuration states.

In CT, the cost function is taken to be the total error between experimental and numerical data which is minimized, and the schedule of lowering temperature is the allocation of standard deviations for the

parameters. For the allowable configuration state, a set of gaussian distributed random numbers is generated for minimizing the error.

4

[illegible]

```

C SOLUTION VS. FOURIER COMPONENTS OF INCIDENT
C GAUSSIAN PERIODIC PULSE.
C *****
C WRITE(6,*)
C WRITE(6,*) 'THIS ROUTINE REQUIRES PERIOD OF INPUT PULSE'
C WRITE(6,*) 'NORMALIZED PERIOD OF INPUT PULSE = 7 (EX: 2./10.)'
C WRITE(6,*)
C READ(6,*) PERIODNORM
C      1./ EXP(1) POINT
C PULSEAMP = 4.0 * SQRT(5.0)
C
C      ALPHA LOOP
C      ALPHA = ALPHA1(2)
C      WRITE(6,*)
C      WRITE(6,*) 'RUNNING FOR ALPHA ', ALPHA
C
C      ALBEDO LOOP
C      W = WI(1)
C      WRITE(6,*)
C      WRITE(6,*) 'RUNNING FOR ALBEDO ', W
C      READ(23,66) OUTPUT
C      FORMAT(A,6)
C      OPEN( UNIT= 24, FILE= OUTPUT, STATUS= 'NEW' )
C      WRITE(6,*) 'EIGENVALUES WILL BE SAVED IN ', OUTPUT
C
C      DO 485 INU = 1, MAXNU
C          EACH FREQUENCY COMPONENTS NU'S
C          REALNU = DFLQAT(INU) - 1.
C          COMCON = DCMPLX(1.0D00, (2.0*PI/PERIODNORM*REALNU))
C          WHAT = W * (1. - ALPHA)/( COMCON - W * ALPHA )
C          IF(INU.EQ.1) THEN
C              EPSILNU = 1.0
C              ENDIF
C          IF(INU.NE.1) THEN
C              EPSILNU = 2.0
C              ENDIF
C          FTNU(INU) = EPSILNU * DEXP(-(PI*REALNU/PULSEAMP)**2)
C          WRITE(35,*)
C          WRITE(35,*)
C          WRITE(35,*) 'NOW FREQUENCY = ', REALNU
C          WRITE(35,*)
C          IMSL ROUTINE IS USED FOR ZEROS OF
C          POLYNOMIAL EQUATION OF CHARACTERISTIC
C          FUNCTION
C          ERRORS = 1.E-20

```

```

C      ERRORS = 1.E-8
C      NKNOWN = 0
C      NNEW = NHALFM
C      NGUESS = NHALFM
C      ITHAX = 10000
C
C      INITIALIZE EIGENVALUES
C      IF( REALNU.EQ. 0.0 ) THEN
C          DO 312 IJ = 1, NHALFM-1
C              ZINIT(IJ) = DCMPLX( ( U( IJ + NHALFM ) + 1.D-5 ), 1.D-20 )
C              CONTINUE
C              ZINIT(NHALFM) = DCMPLX( 1.00001D00, 1.0D-20 )
C              ENDIF
C          IF( REALNU.NE. 0.0 ) THEN
C              DO 311 IJ = 1, NHALFM-1
C                  ZINIT(IJ) = DCMPLX( ( U( IJ + NHALFM ) + 1.D-5 ), 1.D00 )
C                  CONTINUE
C                  ZINIT(NHALFM) = DCMPLX( 1.00001D00, 1.0D00 )
C                  ENDIF
C          C
C          C      NEXT CALL FOR FINDING EIGENVALUES FOR
C          C      GIVEN ALPHA AND ALBEDO
C          C
C          CALL DZANLY(POL, ERRABS, ERRREL, NKNOWN, NNEW, NGUESS, ZINIT,
C              ITHAX, SIG, INFO)
C          C
C          C      NEXT LOOP FOR REARRANGING FOUND
C          C      EIGENVALUES IN ASCENDING ORDER OF
C          C      ITS REAL PART USING IMSL
C          DO 41 IS = 1, NHALFM
C              SIG(IS) = CDSORT(SIG(IS))
C              REALSIG(IS) = REAL( SIG( IS ) )
C          C
C          C      CONTINUE
C          CALL SVRGH( NHALFM, REALSIG, TEMP )
C          INCK = 1
C          DO 42 ISS = 1, NHALFM
C              INDEX = 0
C              DO 40 ISSS = 1, NHALFM
C                  IF( TEMP(ISS) .EQ. REALSIG(ISSS) ) THEN
C                      INDEX = ISSS
C                      ENDIF
C                  CONTINUE
C                  IF( INDEX.EQ. 0 ) THEN
C                      WRITE(6,*) 'NO MATCHING VALUE', ISS
C                      ENDIF
C                  SIGMA(ISS) = SIG(INDEX)
C                  WRITE(24,*) SIGMA(ISS)

```

RETURN
END

42 CONTINUE
C
C
C
C
ALL NECESSARY EIGHTH-POWERS CREATED
AND FILE POINTER WILL BE RESET TO
MORE CALCULATION

485 CONTINUE
CLOSE (UNIT-24)
49 CONTINUE
50 CONTINUE

CLOSE (UNIT-22)
CLOSE (UNIT-23)

STOP
END

C
C
C
C
C
THIS SUBROUTINE DESCRIBES THE POLYNOMIAL FORM OF CHARACTERISTIC EQ.

COMPLEX*16 FUNCTION POL(SIG)

PARAMETER(NDIM = 11, NTDIM = 22)
COMMON /OLD/ RMU(NTDIM), RNU, WHAT, PERIODNORM, PI, P(NTDIM)

COMPLEX *16 SIG, WHAT, FIRSTTERM, SECONDTERM, ADDTERM
REAL *8 RMU, WMRNU, RNU, PERIODNORM, PI, P
INTEGER N, NHALF, NHALFM, K19, K20, K21

WM = 2.*PI/PERIODNORM
WMRNU = WM * RNU
N = NTDIM-1
NHALF = (N+1)/2. + 1
NHALFM = NTDIM/2

FIRSTTERM = (1.0D00, 0.0D00)

DO 888 K19 = NHALF, N+1

FIRSTTERM = FIRSTTERM * (SIG - RMU(K19)**2)

888 CONTINUE

ADDTERM = (0.0D00, 0.0D00)

DO 889 K20 = NHALF, N+1

SECONDTERM = P(K20) * SIG

DO 890 K21 = NHALF, N+1

IF (K21 .NE. K20) THEN
SECONDTERM = SECONDTERM * (SIG - RMU(K21)**2)
ENDIF

890 CONTINUE

ADDTERM = ADDTERM + SECONDTERM

889 CONTINUE

POL = FIRSTTERM - WHAT * ADDTERM


```

C
C
      1./ EXP(1) POINT
PULSEALP = 4.0 * SQRT(5.0)
WRITE(6,*) ' CHOOSE TAU FOR INTENSITY CALCULATION'
DO 44444 I_TAU = 1, 15
  WRITE(6,*) I_TAU, TAU(I_TAU)
CONTINUE
44444 READ(6,*) K_TAU
WRITE(6,*) 'SELECTED TAU =', TAU(K_TAU)
  MAKE A LOOP (ALPHA) TO STATEMENT #50
C
C
  ALPHA = ALPHA(4)
  WRITE(6,*) 'NOW RUNNING FOR ALPHA =', ALPHA
  MAKE A LOOP (ALPHA) TO STATEMENT #49
C
C
  W = W(4)
  WRITE(6,*) 'NOW RUNNING FOR ALBEDO =', W
  READ(21,66) OUTPUT
  FORMAT(A,8)
  READ(22,66) INPUT
66
  WRITE(6,*) 'INPUT FILE = ', INPUT
  WRITE(6,*) 'OUTPUT FILE = ', OUTPUT
  OPEN(UNIT = 24, FILE = OUTPUT, STATUS = 'NEW')
  OPEN(UNIT = 25, FILE = INPUT, STATUS = 'OLD')
  EACH FREQUENCY COMPONENTS NU'S
C
  DO 486 INU = 1, MAXNU
    REALNU = DFLCAT(INU) - 1.
    COMECON = DCMPLX(1.0D00, (2.0*PI/PERIODNORM*REALNU))
    WHAT = W * (1. - ALPHA)/(COMECON - W * ALPHA)
    IF(INU.EQ.1) THEN
      EPSILNU = 1.0
      ENDIF
    IF(INU.NE.1) THEN
      EPSILNU = 2.0
      ENDIF
    FFNU(INU) = EPSILNU * DEXP(-(PI*REALNU/PULSEALP)**2)
    READ EIGENVALUES FROM FILE
C
    DO 777 KM = 1, NHALFM
      READ(25,*) SIGMA(KM)
777 CONTINUE
C

```

```

C
      VECTOR B_IJ = DELTA_IJ/P_J
DO 22 JI = 1, NHALFM
  B(JI) = 0.
  CONTINUE
  B(J-NHALFM) = 1./P(0)
C
C
  BUILD MATRIX FOR SOLUTION OF SYSTEM'S
  EQUATION( X = INVERSE a_ * b_ )
DO 25 JJ = 1, NHALFM
DO 25 KK = 1, NHALFM
  AMATX(JJ, KK) = 1./( 1. - U(JJ + NHALFM) / SIGMA(KK) )
25 CONTINUE
C
C
  CALL DLINCE( NHALFM, AMATX, NHALFM, CMATX, NHALFM )
C
C
  NEXT DO LOOP FOR CHECKING INVERSED MATRIX
DO 333 III = 1, NHALFM
DO 333 IIII = 1, NHALFM
  DMATX(III, IIII) = (0.0D00, 0.0D00)
  PP = (0.0D00, 0.0D00)
DO 333 IO = 1, NHALFM
  PP = CMATX( III, IO) * AMATX( IO, IIII )
  DMATX(III, IIII) = DMATX( III, IIII) + PP
333 CONTINUE
3333 CONTINUE
C
C
  NEXT STEP FOR ( INV a_ * b_ )
DO 444 IL = 1, NHALFM
  AMP(IL + NHALFM) = (0.0D00, 0.0D00)
  PPP = (0.0D00, 0.0D00)
DO 444 IK = 1, NHALFM
  PPP = CMATX( IL, IK ) * B( IK )
C
C
  SHIFTING FOR LATER MULTIPLICATION
  AMP( IL + NHALFM ) = AMP( IL + NHALFM ) + PPP
444 CONTINUE
DO 4445 ILT = 1, NHALFM
  PPP = (0.0D00, 0.0D00)
DO 445 IILT = 1, NHALFM
  PPP = PPP + AMATX( IILT, IILT ) * AMP( IILT+NHALFM )
C

```



```

1      DTGMS**2 * DFL0AT( MM**2 ) * GGBAR K(MM)**2 ) *
1      ( DEXP(-4.000*GGBAR_K(MM)) * (4.*GGBAR_K(MM)+1.0000)
1      - 1.0000 ) ) / 3.
      SUM = SUM + ( SUM0 + SUM_ADD ) * SUM_P
30      CONTINUE
      PWR2 = FFNU( INU ) * CDEXP( -TAU * COMECON / UP ) * SUM
      POWER2( INU ) = PWR2
      POWER #3 IS BACKGROUND PART OF
      DIFFUSED INTENSITY.
      PWR3 = P_nu
      SUM2 = 0.
      DO 35 K = NHALF, MM1
      SUM1 = 0.
      DO 37 N1 = 1, N1
      SUM1 = SUM1 + FN( UR( IV ), N1 ) / ( 1. - U( N1 )
      / SIGMA( K - NHALF ) )
37      CONTINUE
      SUM2 = SUM2 + AMP( K ) * CDEXP( - ( COMECON - W * ALPHA )
      * TAU / SIGMA( K - NHALF ) ) * SUM1
35      CONTINUE
      TERM = CDEXP( - ( COMECON - W * ALPHA ) * TAU / UP )
      * FN( UR( IV ), J ) / P( J )
      PWR3 = .5 * FFNU( INU ) * DTGMS**2 * ( SUM2 - TERM )
      POWER3( INU ) = PWR3
      ALL 3 INTENSITIES WILL BE ADDED
      TO FIND TOTAL (REDUCED AND DIFF.)
      INTENSITY. 2 DIMENSIONAL PWR3
      IS USED TO REDUCE LOOP NUMBERS
      PWR3V( INU, V ) = PWR1 + PWR2 + PWR3
      PWR_PART( INU, V ) = PWR1 + PWR3
487      CONTINUE
486      CONTINUE
      NEXT LOOP REPRESENTS FINAL SUMMATION
      WITH RESPECT TO TIME (INNER DO LOOP
      FOR DIFFERENT FREQUENCY VALUES)
      TOTAL PERIOD IS SET FOR 2 T' AND
      SAMPLING POINTS FOR MAXTIME.
      WHILE USING THESE DO LOOP, VALUE
      FOR TAU HAS TO BE SET FIXED.
      INDIVIDUAL POWERS GENERATED SEPARATELY

```

```

445      CONTINUE
4445      CONTINUE
      DIFFERENT ANGLE(PHI) OF RCVR ANTENNA
      PHIR = PHIR( 1 ) * PI
      DIFFERENT ANGLE(THETA) OF RCVR ANTENNA
      IV = 1
      CGAPR = DCOS( PHIR - PHIR ) * DSORT( ( 1. - UP**2 ) * ( 1. -
      UR( IV )**2 ) ) + UP * UR( IV )
      GGBAR = DBLE( DACOS( CGAPR ) )
      DIFFERENT OBSERVATION POSITION
      TAU = Z**
      TAU = TAU( K_TAU )
      POWER #1 IS REDUCED INTENSITY
      WHICH WILL DECREASE EXPONENTIALLY
      PWR1 = P_nu
      RED_INT1 = I_nu
      PWR1 = FFNU( INU ) * DEXP( - ( GGBAR / DTGMS ) **2 ) *
      CDEXP( -TAU * COMECON / UP )
      RED_INT = FFNU( INU ) * POINTING * CDEXP( -TAU * COMECON / UP )
      POWER( INU ) = PWR1
      TOT_INTEN1( INU ) = RED_INT
      POWER #2 IS STRONG FORWARD PART
      OF DIFFUSED INTENSITY WITH PULSE
      BROADENING EFFECT.
      SUM = 0.
      SUM0 = 1.
      SUM_ADD = 1.
      SUM_P = 1.
      FINITE SUMMATION OF FACTORIAL
      SUM0 : SUMMATION TERM OF ORIGINAL EQ.
      SUM_ADD : NEW ADDED SUMMATION
      SUM : TOTAL SUMMATION
      DO 30 MM = 1, M-1
      SUM_P : TERMS WITH M TH POWER AND FACTORIAL
      SUM_P = ALPHA * W * TAU / UP / DFL0AT(MM) * SUM_P
      NEXT LINE IS COMMENTED TO CHECK ZERO APPROXIMATION
      SUM0 = DTGMS**2 * GGBAR( GGBAR, MM )
      SUM0 = 4. / ( DFL0AT(MM) * DTGMS**2 ) * ( ( 1.0000 -
      DEXP( - 4.000 * GGBAR_K(MM) ) ) / GGBAR_K(MM) )
      SUM_ADD = - ( 1.0000 - TAU * COMECON / DFL0AT( MM + 1 ) ) *
      ( DFL0AT( MM**2 - 1 ) / ( DFL0AT( MM ) * GGBAR_K(MM) )
      * ( DEXP( - 4.0000 * GGBAR_K( MM ) ) - 1.000 ) +
      DFL0AT( ( MM + 1 ) * ( 2 * MM + 1 ) ) / (

```

```

C C C C C C C
TOTPNR = TOTAL POWER(P RI + P_STR + P_ISO)
TOT_INT1 = TOTAL INTENSITY
TOTPNR1 = P_RI
TOTPNR2 = P_STR
TOTPNR3 = P_ISO
DO 2222 ITIME = 1, MAXSAM
    TIMEDEL = 2. * PERIODNORM * DFLCAT( ITIME - 1 )
    / DFLCAT( MAXSAM )
    TOTPNR = (0.0000,0.0000)
    TOT_INT1 = (0.0000,0.0000)
    TOTPNR1 = (0.0000,0.0000)
    TOTPNR2 = (0.0000,0.0000)
    TOTPNR3 = (0.0000,0.0000)
    TOT_PART = (0.0000,0.0000)
    DO 2221 INU = 1, MAXNU
        REALNU = DFLCAT( INU ) - 1.
        COMPCON = DCEPLA( 1.0000, (2.0*PI/PERIODNORM*REALNU) )
        TOTPNR = TOTPNR + PWRCV( INU, K_TAU )
        * CDEXP((COMPCON - 1.000) * TIMEDEL)
        TOTPNR1 = TOTPNR1 + PWR1( INU )
        * CDEXP((COMPCON - 1.000) * TIMEDEL)
        TOT_INT1 = TOT_INT1 + TOT_INT1( INU )
        * CDEXP((COMPCON - 1.000) * TIMEDEL)
        TOTPNR2 = TOTPNR2 + PWR2( INU )
        * CDEXP((COMPCON - 1.000) * TIMEDEL)
        TOTPNR3 = TOTPNR3 + PWR3( INU )
        * CDEXP((COMPCON - 1.000) * TIMEDEL)
        TOT_PART = TOT_PART + PWR_PART( INU, K_TAU )
        * CDEXP((COMPCON - 1.000) * TIMEDEL)
    2221 CONTINUE
    Q = 10. * DLOG10( DREAL( TOTPNR ) )
    Q1 = 10. * DLOG10( DREAL( TOTPNR1 ) )
    WRITE(35, *) TIMEDEL, Q1
    IF ( TOTPNR2 .NE. 0.0000 ) THEN
        IF ( DREAL( TOTPNR2 ) .LE. 0.0000 ) THEN
            TOTPNR2 = DCEPLA( DREAL( TOTPNR2 ), DIMAG( TOTPNR2 ) )
            Q = 10. * DLOG10( DREAL( TOT_PART ) )
        ENDIF
    ENDIF

```

```

Q2 = 10. * DLOG10( DREAL( TOTPNR2 ) )
WRITE(36, *) TIMEDEL, Q2
ENDIF
Q3 = 10. * DLOG10( DREAL( TOTPNR3 ) )
WRITE(37, *) TIMEDEL, Q3
WRITE(24, *) TIMEDEL, Q
2222 CONTINUE
CLOSE(24)
CLOSE(25)
C ALBEDO LOOP
49 CONTINUE
C ALPHA LOOP
50 CONTINUE
CLOSE(UNIT=20)
STOP
END
REAL*8 FUNCTION FN( UI, NM )
    PARAMETER ( NDIH = 11, NTDIH = 22 )
    COMMON /OLD/ U(NTDIH), REALNU, W, PERIODNORM, FI, P(NTDIH)
    COMPLEX*16 W
    REAL*8 UI, U, REALNU, PERIODNORM, FI, P
    INTEGER NM
    INTRINSIC DABS
    FN = 0.
    N = NTDIH-1
    NHALF = (N+1)/2. + 1
    NHALFM = NTDIH/2
    IF (NM .EQ. 1 .OR. NM .EQ. N+1) GOTO 100
    IF (UI .LE. U(N+1) .OR. UI .GE. U(N+1)) RETURN
    FN = (U(N+1)-UI)/(U(N+1)-U(NM))
    IF (UI .LE. U(NM)) FN = (UI-U(N+1))/(U(NM)-U(N+1))
    RETURN
100 IF (NM .EQ. 1 .AND. UI .GE. U(2)) RETURN
    IF (NM .EQ. (N+1) .AND. UI .LE. U(N)) RETURN
    UI = DABS(UI)
    FN = (UI-U(N))/(1.-U(N))
    RETURN
END
C REAL*8 FUNCTION GBAR( GMAPR, MP )

```

```

COMMON /G4/ DLTCGR, DLTCGS
REAL *8 DELGAM, DLTCGR, DLTCGS, GMAPR
INTRINSIC DEXP
DELGAM = DLTCGR**2 + MP * DLTCGS**2
GMAPR = 4./DELGAM * DEXP (-GMAPR**2/DELGAM)
RETURN
END

C
REAL*8 FUNCTION GMAPR_K( MP )
COMMON /G4/ DLTCGR, DLTCGS
REAL *8 DELGAM, DLTCGR, DLTCGS, GMAPR
GMAPR_K = 1. / DLTCGR**2 + 1. / ( MP * DLTCGS**2 )
RETURN
END

```

C

?


```

995 FORMAT( 2X, 'INITIAL OPTIMUM ', I3, 'th ', 'X ', E22.15 )
996 FORMAT( 2X, 'OPTIMUM VALUE AFTER ', I3, ' ITERATION ',
997 E22.15 )
998 FORMAT( 2X, 'INITIAL GUESS FOR ', I3, 'th VARIABLE
999 (1) : TAU, (2) : ALBEDO, (3) : ALPHA' )
1000 FORMAT( 2X, 'TYPE STAN. DEV. FOR ', I3, 'th PARAMETER' )
1001 FORMAT( 2X, 'OPTIMUM ', I3, 'th ', 'X ', E22.15 )
1002
1003 STOP
1004 END
1005
1006 *****
1007 THIS SUBROUTINE GENERATES GAUSSIAN RANDOM NUMBERS WITH
1008 AVERAGE = 0.5 AND STANDARD DEVIATION = 0.04. THE ACTUAL
1009 VALUES RETURNED AS RANDOM VARIABLES WILL BE CHANGED SO
1010 THAT THE AVERAGE AND STANDARD DEVIATION BECOMES AS USER
1011 REQUESTS
1012 *****
1013
1014 SUBROUTINE GAUSSIAN( MED, STANDEV, NGR, ISEED, GR )
1015
1016 VARIABLE DECLARATION
1017 ISEED : SEED FOR RANDOM NUMBER
1018 NGR : NUMBER OF GAUSSIAN RANDOM VARIABLES TO BE GENERATED
1019 GR : ARRAY OF GAUSSIAN RANDOM NUMBERS
1020 UR : UNIFORM RANDOM NUMBERS
1021 SUM : VARIABLES USED FOR SUMMATION
1022 SSUM : VARIABLES USED FOR SUMMATION
1023 MED : AVERAGE
1024 STANDEV : STANDARD DEVIATION
1025
1026 PARAMETER( NUM_P = 3 )
1027
1028 INTEGER I, J, ISEED1, ISEED1, NGR
1029 REAL *8 UR( NUM_P ), SUM( NUM_P ), GR( NUM_P, 10000 ), LSUM,
1030 SSUM, MED( NUM_P ), STANDEV( NUM_P )
1031
1032 LOGICAL FOUND
1033
1034 ISEED1 = ISEED
1035 MAX_P = NUM_P
1036
1037 DO 9 K = 1, MAX_P
1038 SUM( K ) = 0.
1039 CONTINUE
1040
1041 DO 11 KK = 1, MAX_P
1042
1043 FOUND = .FALSE.
1044 I = 1
1045 DO 10 WHILE ( FOUND .EQ. .FALSE. )
1046
1047 DO 20 J = 1, 50
1048 UR( KK ) = RAN( ISEED1 )
1049 SUM( KK ) = UR( KK ) + SUM( KK )
1050 CONTINUE
1051
1052 GR( KK, I ) = ( STANDEV( KK ) / 0.04 ) * ( SUM( KK )
1053 / 50. - 0.5 ) + MED( KK )
1054 SUM( KK ) = 0.
1055
1056 I = I + 1
1057
1058 *****
1059 BOUNDED GAUSSIAN RANDOM NUMBER
1060 *****

```

```

C # 1 GAUSSIAN > 0.00001
IF( KK.EQ. 1 ) THEN
IF( GR( 1, I ) .GE. 1.0E-5 ) THEN
IF( ABS( GR( 1, I ) - MED( 1 ) ) .LT. STANDEV( 1 ) ) THEN
I = I + 1
ENDIF
ENDIF
ENDIF

C # 2 GAUSSIAN > 0.0 , AND < 0.95
IF( KK.EQ. 2 ) THEN
IF( GR( 2, I ) .GT. 0.0E00 .AND. GR( 2, I ) .LT.
9.5E-1 ) THEN
IF( ABS( GR( 2, I ) - MED( 2 ) ) .LT. STANDEV( 2 ) ) THEN
I = I + 1
ENDIF
ENDIF
ENDIF

C # 3 GAUSSIAN > 0.0 , AND < 0.95
IF( KK.EQ. 3 ) THEN
IF( GR( 3, I ) .GT. 0.0E00 .AND. GR( 3, I ) .LT.
9.5E-1 ) THEN
IF( ABS( GR( 3, I ) - MED( 3 ) ) .LT. STANDEV( 3 ) ) THEN
I = I + 1
ENDIF
ENDIF
ENDIF

IF( I.EQ. NGR+1 ) THEN
FOUND = .TRUE.
ENDIF

10 CONTINUE
11 RETURN
END

C NEXT FUNCTION IS OPTIMIZED WITH RESPECT TO X
REAL*8 FUNCTION COST_FUNC( X )
PARAMETER ( MAX = 3 )
COMMON // TWO PT
COMMON /DATA/ EXP_MEAS(500), ANG(500), MEAS_NUM
REAL*8 X( MAX ), TEMP, EXP_MEAS, ANG, TAU, ALBEDO, ALPHA
INTEGER MEAS_NUM
EXTERNAL ERROR_VALUE
MAX_PAR = MAX
TAU = X( 1 )
ALBEDO = X( 2 )
ALPHA = X( 3 )
COST_FUNC = 0.0
CALL ERROR_VALUE( TAU, ALBEDO, ALPHA, COST_FUNC )

```



```

IF (INU.EQ.1) THEN
  EPSILNU = 1.0
ENDIF
IF (INU.NE.1) THEN
  EPSILNU = 2.0
ENDIF
FTNU (INU) = EPSILNU * DEXP (- (PI*REALNU/FULSEALP)**2)
  WHAY = W * (1. - ALP) / ( COMECON - W * ALP )
  CALL EIGEN ( ALP, W, SIGMA )
  CALL INVERS ( TAU, ALP, W, LOOP PHI, COMECON, THETAP,
    MEAS_INT, SIGMA, ERROR_MEAN )
  CLOSE (UNIT-22)
  RETURN
END
*****
*** THIS FUNCTION REPRESENTS EACH OF MOMENT FOR BASIS FUNC. ***
*****
REAL*8 FUNCTION FN ( UI, NM )
  PARAMETER ( NDIH = 11, NTDIM = 22 )
  COMMON /OLD/ U (NTDIM), REALNU, W, PERIODNORM, FI, P (NTDIM)
  COMPLEX *16 W
  REAL *8 UI, U, REALNU, PERIODNORM, FI, P
  INTEGER NM
  INTRINSIC DABS
  FN = 0.
  N = NTDIM-1
  NHALF = (N+1)/2. + 1
  NHALFH = NTDIM/2
  IF (NM.EQ.1 .OR. NM.EQ.N+1) GOTO 100
  IF (UI.LE.U (NM-1) .OR. UI.GE.U (NM+1)) RETURN
  FN = (U (NM+1)-UI) / (U (NM+1)-U (NM))
  IF (UI.LE.U (NM)) FN = (UI-U (NM-1)) / (U (NM)-U (NM-1))
  RETURN
100
IF (NM.EQ.1 .AND. UI.GE.U (2)) RETURN
IF (NM.EQ.(N+1) .AND. UI.LE.U (N)) RETURN
IF (NM.EQ.1 .AND. UI.LX.U (2)) THEN
  FN = (U (2) - UI) / (U (2) + 1.)
ENDIF
IF (NM.EQ.(N+1) .AND. UI.GT.U (N)) THEN
  FN = (UI - U (N)) / (1. - U (N))
ENDIF
  RETURN

```

```

END
*****
*** THIS FUNCTION REPRESENTS BROADENING OF FORWARD LOBE. ***
*****
REAL FUNCTION CMBAR ( CMBAR, MP )
  COMMON /CM/ DLTGR,DLTGRS
  REAL *8 DELGAM,DLTGR,DLTGRS,CMBAR
  INTRINSIC DEXP
  DELGAM = DLTGR**2 + MP * DLTGRS**2
  CMBAR = 4./DELGAM * DEXP (-CMBAR**2/DELGAM)
  RETURN
END
*****
*** RETURNS MEAN ERROR CALCULATED FROM ANY ALBEDO, ALPHA, ***
*** AND SIGMA VALUE. ***
*****
SUBROUTINE INVERS ( TAU, ALPHA, W, LOOP PHI, COMECON,
  THETAP, MEAS_INT, SIGMA, ERROR_MEAN )
  PARAMETER ( NDIH = 11, NTDIM = 22, MAXNU = 11, MAXSAM = 200 )
  COMMON /CM/ DLTGR,DLTGRS
  COMMON /OLD/ U (NTDIM), REALNU, WHAY, PERIODNORM, FI, P (NTDIM), INU
  COMMON /INV/ TAU (15), UR (300)
  DIMENSION PHIRI (2), REALSIG (NDIM), TEMP (NDIM)
  COMPLEX *16 S (NTDIM), B (NTDIM), AMF (NTDIM), AMATX (NDIM,NDIM),
  DNATX (NDIM,NDIM), CHATX (NDIM,NDIM), SK, F, SMLNU,
  COMECON, CDABS, COREP, DCMPLX, SUM1, SUM2, SUM3,
  FMR1, FMR2, FMR3, SUM, SUMO, TAURAT, GUESS, SIG (NDIM),
  WHAY, ZINIT (NDIM), POL, DELTA, SIGMA (NDIM),
  FMRSCV (MAXNU,15), TOTEMP
  REAL *8
  DACOS, REALNU, PERIODNORM, EPSILNU, O, PI, CMBAR,
  FFNU (NDIM), CMAGNU, P, U, W, CMBAR, ALPHA,
  FULSEALP, ALPHAI (10), MI (10), ERRABS, ERRREL, PHIR,
  PHIP, UP, UR, TAU, PHIRI, TIMEDI, TAU, DLTGR,
  DLTGRS, FN, THET, TEMP, VALUE, TAU TEMP, DIGIT2,
  ALBEDO KNOWN, ALPHA KNOWN, Z KNOWN, ERROR_MEAN,
  MEAS_INT (300), UR_MEAS (300), CAL_INT (300), DIGIT1,
  ANG (300), WHOLE (300)
  INTEGER
  THETAP, V, INAX, NHALF, NHALFH, INFO (NDIM),
  ITMAX, NGUESS, NKNOWN, NNEW, IU, IP, IR, IA, IW,
  INU, IS, INCI, INDEX, ISS, ISSS, MAXTIME,
  LOOP PHI, Z_FIX
  CHARACTER *20 INFILE, OUT_FILE, FIX_Z, AA
  CHARACTER *2 CH_Z
  DATA PHIRI/0.,180./
  LOGICAL STOP
  EXTERNAL F, FN, CMBAR, POL, DZANLY, SRCH, SVRGN

```

```

INTRINSIC  DACOS, CDABS, CDEXP, DCMPLX, DBLE, DFLONT, DEXP,
+          DSORT, DABS, DATAN2, DIMAG, DREAL, DCOS, IIDINT,
+          CHAR, JIDINT
N          = NTDIN-1
NHALF     = (N+1)/2. + 1
NHALFM    = NTDIN/2.
N          = 30
PHIP      = 0.
ERROR_MEAN = 0.0
J         = THETAP
UP        = U(J) * SORT(5.0)
FULSEALP  = 4.0 * SORT(5.0)
INU = 1
IF (INU.EQ. 1) THEN
  EPSILAU = 1.0
  ENDOIF
IF (INU.NE. 1) THEN
  EPSILAU = 2.0
  ENDOIF
FTNU(INU) = EPSILAU * DEXP(-(PI*REALNU/FULSEALP)**2)
VECTOR B_IJ = DELTA_IJ/P_J
DO 22 JI = 1, NHALFM
  B(JI) = 0.
CONTINUE
B(J-NHALFM) = 2. * 1./P(J) * FTNU(INU)
BUILD MATRIX FOR SOLUTION OF SYSTEM'S
EQUATION( X = INVERSE a_ * b_ )
DO 25 JJ = 1, NHALFM
DO 25 KK = 1, NHALFM
  AMATX(JJ, KK) = 1./(( 1. - U(JJ + NHALFM) / SIGMA(KK) )
CONTINUE
CALL INSL LIBRARY FOR INVERSION
CALL DLINGC( NHALFM, AMATX, NHALFM, CHATX, NHALFM )
NEXT STEP FOR ( INV a_ * b_ )
DO 333 III = 1, NHALFM
DO 333 IIII = 1, NHALFM
  DMATX(III, IIII) = 0.0
  PP = 0.0
DO 333 IO = 1, NHALFM
  PP = CHATX( III, IO ) * AMATX( IO, IIII )
  DMATX(III, IIII) = DMATX( III, IIII ) + PP
CONTINUE
333
C

```

```

C
DO 444 IL = 1, NHALFM
  AMP(IL + NHALFM) = 0.0
  PPP = 0.0
DO 444 IK = 1, NHALFM
  PPP = CHATX( IL, IK ) * B( IK )
  SHIFTING FOR LATER MULTIPLICATION
  AMP( IL + NHALFM ) = AMP( IL + NHALFM ) + PPP
444 CONTINUE
  DIFFERENT ANGLE(PHI) OF RCVR ANTENNA
C
C
PHIR = PHIRI( 1 ) * PI
  DIFFERENT ANGLE(THETA) OF RCVR ANTENNA
C
C
DO 47 IV = 1, LOOP_PHI
  CGMAPR = DCOS( PHIP - PHIR ) * DSORT( ( 1. - UP**2 ) * ( 1. -
    UR( IV )**2 ) ) + UP * UR( IV )
  CHAPR = DBLE( DACOS( CGMAPR ) )
  POWER #1 IS REDUCED INTENSITY
  WHICH WILL DECREASE EXPONENTIALLY
  FWR1 = FTNU(INU) * DEXP( -( CHAPR / DLTCR )**2 ) *
    CDEXP( -TAU * COMCON / UP )
  POWER #2 IS STRONG FORWARD PART
  OF DIFFUSED INTENSITY.
  SUM = 0.
  SUMO = 1.
  FINITE SUMMATION OF FACTORIAL
DO 30 MM = 1, M-1
  SUMO = ALPHA * M * TAU / UP / DFLONT(MM) * SUMO
  SUM = SUM + SUMO*(CHAPR,MM)-CHAPR(CHAPR,MM)
CONTINUE
PWR2 = FTNU( INU ) * ( DLTCR / 2. )**2 * ( CDEXP( -TAU *
  COMCON / UP ) * ( SUM - CHAPR( CHAPR, M ) ) +
  CDEXP( -(COMCON-ALPHA*M)*TAU/UP ) * CHAPR(CHAPR, M) )
  POWER #3 IS ISOTROPIC PART OF
  DIFFUSED INTENSITY.
  SUM2 = 0.
DO 35 K = NHALF, N+1
  SUM1 = 0.
DO 37 N1 = 1, N+1
  SUM1 = SUM1 + FN( UR( IV ), N1 ) / ( 1. - U( N1 )
    / SIGMA( K - NHALFM ) )
CONTINUE
37
C

```



```

C      EACH FREQUENCY COMPONENTS NU'S
      COMPCOM = DCMPLX(1.0D00, (2.0*PI/PERIODNORM*REALNU))
      INU = 1
      IF (INU.EQ.1) THEN
        EPSILNU = 1.0
        ENDIF
      IF (INU.NE.1) THEN
        EPSILNU = 2.0
        ENDIF
      FFMU(INU) = EPSILNU * DEXP(-(PI*REALNU/PULSEALP)**2)
      ERRABS = 1.E-20
      ERRREL = 1.E-6
      MINCON = 0
      NNEW = NHALFM
      NGUESS = 11
      ITMAX = 10000
      IF (REALNU.EQ.0.0) THEN
        DO 312 IJ = 1, NHALFM-1
          XINIT(IJ) = DCMPLX( ( U( IJ + NHALFM ) + 1.D-5 ), 1.D-20 )
          CONTINUE
          XINIT(NHALFM) = DCMPLX( 1.00001D00, 1.0D-20 )
        ENDIF
      IF ( REALNU.NE.0.0 ) THEN
        DO 311 IJ = 1, NHALFM-1
          XINIT(IJ) = DCMPLX( ( U( IJ + NHALFM ) + 1.D-5 ), 1.D00 )
          CONTINUE
          XINIT(NHALFM) = DCMPLX( 1.00001D00, 1.0D00 )
        ENDIF
      NEXT LOOP FOR FINDING EIGENVALUES FOR
      GIVEN ALPHA AND ALBEDO "IMSL" ROUTINE
      CALL DEANLY(POL, ERRABS, ERRREL, NNEW, NNEW, NGUESS, XINIT,
        ITMAX, SIG, INFO)
      DO 41 IS = 1, NHALFM
        SIG(IS) = COSGT(SIG(IS))
        REALSIG(IS) = REAL( SIG( IS ) )
      CONTINUE
      CALL SVRCH( NHALFM, REALSIG, TEMP )
      INCX = 1
      DO 42 ISS = 1, NHALFM
        INDEX = 0
        DO 40 ISSS = 1, NHALFM
          IF ( TEMP(ISSS).EQ. REALSIG(ISSS) ) THEN
            INDEX = ISSS
          ENDIF
        CONTINUE
        IF ( INDEX.EQ.0 ) THEN
          WRITE(6,*) 'NO MATCHING VALUE', ISS
        ENDIF
      ENDIF

```

```

      SIGMA(ISS) = SIG(INDEX)
      DELTA = POL(SIGMA(ISS))
      42 CONTINUE
C      ALL NECESSARY EIGENVALUES CREATED
C      AND FILE POINTER WILL BE RESET TO
C      MORE CALCULATION
      485 CONTINUE
      49 CONTINUE
      50 CONTINUE
      RETURN
      END
C      *****
C      THIS SUBROUTINE WILL CHECK ACCURACY OF THE CALCULATED
C      SIGMA BY PLOTTING BACK INTO EQUATION.
C      *****
      COMPLEX*16 FUNCTION POL(SIG)
      PARAMETER( NDIM = 11, NTDIM = 22 )
      COMMON /OLD/ RNU(NTDIM), RNU, WHAT, PERIODNORM, PI, P(NTDIM)
      COMPLEX *16 SIG, WHAT, FIRSTTERM, SECONDTERM, ADDETERM
      REAL *8 RNU, WRNU, RNU, PERIODNORM, PI, P
      INTEGER N, NHALF, NHALFM, K19, K20, K21
      WW = 2.*PI/PERIODNORM
      WRNU = WW * RNU
      N = NTDIM-1
      NHALF = (N+1)/2. + 1
      NHALFM = NTDIM/2
      FIRSTTERM = (1.0D00, 0.0D00)
      DO 888 K19 = NHALF, N+1
        FIRSTTERM = FIRSTTERM * ( SIG - RNU(K19)**2)
      CONTINUE
      ADDETERM = (0.0D00, 0.0D00)
      DO 889 K20 = NHALF, N+1
        SECONDTERM = P(K20) * SIG
        DO 890 K21 = NHALF, N+1
          IF (K21.NE. K20) THEN
            SECONDTERM = SECONDTERM * (SIG - RNU(K21)**2)
          ENDIF
        CONTINUE
        ADDETERM = ADDETERM + SECONDTERM
      CONTINUE
      POL = FIRSTTERM - WHAT * ADDETERM
      RETURN
      END

```

References

- [1] E.J. Violette, R.H. Espeland, A.R. Mitz and F.A. Goodnight, *SHF-EHF Propagation Through Vegetation on Colorado East Slope*, US Army R&D Technical Report CECOM-81-CS020-F, Fort Monmouth, NJ, June 1981.
- [2] E.J. Violette and R.H. Espeland, *Vegetation Loss Measurement at 9.6, 28.8 and 57.6 GHz Through a Pecan Tree Orchard in Texas*, US Army R&D Technical Report CECOM-83-2, Fort Monmouth, NJ, March 1983.
- [3] R.A. Johnson and F. Schwering, *A Transport Theory of Millimeter Wave Propagation in Wood and Forests*, US Army R&D Technical Report CECOM-TR-85-1, Fort Monmouth, NJ, Feb. 1985.
- [4] S. Chandrasekhar, *Radiative Transfer*, Oxford University Press, London, 1950; also Dover Publications, New York, 1960.
- [5] M. N. Özisik, *Radiative Transfer and Interactions with Conduction and Convection*, A Wiley-Interscience Publication, New York, 1973.
- [6] A. Ishimaru, *Wave Propagation and Scattering in Random Media*, Academic Press, New York, 1978.
- [7] N. Cho, *Moment Method Solution of the Time-Dependent Transport Equation to Describe the Scattering of Gaussian Plane Wave Pulses by a Forest*, Master Thesis, New Jersey Inst. of Tech, NJ, 1982.
- [8] F. Schwering and R.A. Johnson, *A Transport Theory of Millimeter Wave Propagation in Woods and Forests*, J. of Wave-Material Interaction, Vol.1, No.2, pp205-236, April 1986.
- [9] N. J. McCormick, *Remote Characterization of a Thick Slab Target with a Pulsed Laser*, Opt. Soc. of Am., Vol.72, No.6, pp756-759, June 1982.
- [10] R. Sanchez and N.J. McCormick, *General Solutions to Inverse Transport Problems*, J. Math. Phys. Vol.22, No.4, pp847-855, April 1981.
- [11] D.A. Pierre, *Optimization Theory with Applications*, Dover, 1986
- [12] J.J. Duderstadt and W.R. Martin, *Transport Theory*, John Wiley & Sons, New York, 1979.
- [13] V.G. Jenson and G.V. Jeffreys, *Mathematical Methods in Chemical Engineering*, 2nd ed. Academic Press, London, 1977.
- [14] R.B. Bird, W.E. Stewart and E.N. Lightfoot, *Transport Phenomena*, John Wiley & Sons, Inc., New York, 1960.
- [15] S. Kirkpatrick, C.D. Gelatt, Jr. and M.P. Vecchi, *Optimization by Simulated Annealing*, Science Magazine, Vol.220, pp671-680, May 1983.
- [16] M.A. Breuer, *Design Automation of Digital Systems*, Prentice-Hall, Englewood Cliffs, NJ, 1972.

- [17] H.P.J. Haken, *Synergetics*, IEEE Circuits and Devices, pp3-7, Nov. 1988.
- [18] N.H. Farhat and B. Bai, *Phased-Array Antenna Pattern Synthesis by Simulated Annealing*, Proc. of IEEE, Vol.75, No.6, pp842-844, June 1987.
- [19] A. Lapedes and R. Farber, *Nonlinear Signal Processing Using Neural Networks: Prediction and System Modeling*, Submitted to Proceeding of IEEE.
- [20] R.P. Lippmann, *An Introduction to Computing with Neural Nets*, IEEE ASSP Magazine, pp4-22, April 1987.
- [21] R.A. Ruttenbar, *Simulated Annealing Algorithms: An Overview*, IEEE Circuits and Devices Magazine, pp19-26, Jan. 1989.
- [22] L. Davis, *Genetic Algorithms and Simulated Annealing*, Morgan Kaufman Publishers, Inc., Los Altos, Ca., 1987.
- [23] N. Metropolis, A.W. Rosenbluth, M.N. Rosenbluth, and A.H. Teller, *Equation of State Calculation by Fast Computing Machines*, J. Chem. Phys., Vol.21, pp1087-1092, June 1953.